Cyclometallates of Some Platinum Group Metal Ions with Aroylhydrazones Bearing Polycyclic Aryl Groups

A Thesis

Submitted for the Degree of

Doctor of Philosophy

By

A.R. BALAVARDHANA RAO

School of Chemistry

University of Hyderabad

Hyderabad 500 046

India

June 2014

CONTENTS

Chapter 1

Introduction

In this chapter, cyclometallates of platinum group metals and their importance in various areas of scientific research have been briefly discussed.

1.1. Cyclometallated Complexes of Platinum Group Metals: An Overview

Discovery of the first cyclometallated complex **I** [1] by Lleinman and Dubeck in 1963 laid a cornerstone to a class of organometallic species called cyclometallated compounds or cyclometallates. Very soon this chemistry was extended to platinum group metals. In 1965 Cope and Siekman have prepared cyclometallated complexes of palladium with azobenzene derivatives **II** [2] (Figure 1.1). Later it was extended to main group, transition and inner transition metals. However, till now the cyclometallation chemistry of platinum group metals (Ru, Os, Rh, Ir, Pd and Pt) has received the maximum attention. A variety

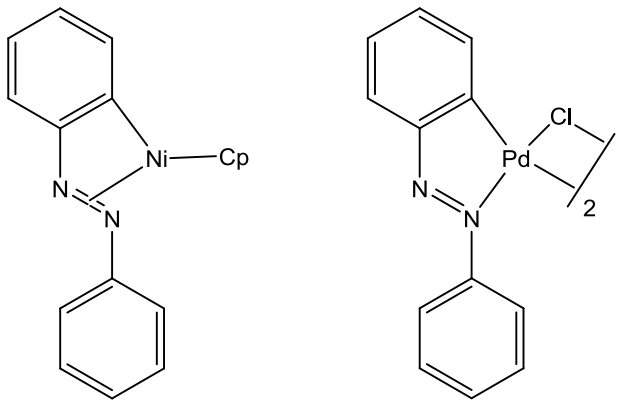

I **II**

Figure 1.1

of cyclometallated complexes of platinum group metals with various types of ligands such as bipyridines, imines, oxazoles, thiozoles, etc. are reported during the last few decades [3-20].

The immense interest in these platinum group cyclometallates is due to their applications in a wide range of research areas such as stabilization of reactive intermediates in organic synthesis, catalytic activation of C-H bonds, materials and devices, pharmaceutical chemistry and biology [21–40].

1.2. Applications

1.2.1. In Biology

Since the discovery of cisplatin as an anticancer agent many cisplatin analogs were reported and studied for their cytotoxic activity. Among these only three platinum based anticancer drugs (cisplatin, carboplatin and oxaliplatin) [41–43] were approved and widely used in the treatment. Cisplatin analogs have several limitations. The main limitation is their inactivation by small cellular molecules like glutathione and efflux out of the cell [44]. To overcome these limitations organometallic complexes such as cyclometallated complexes of platinum group metals are considered as alternatives for their enhanced stability and easily tunable activity by modification of the ligand scaffold. Many cyclometallated complexes of platinum group metals with various bidentate CN- and tridentate CNN-, CCN- and CNS-donor ligands with potential anticancer properties have been reported. Some of them are shown in Figure 1.2. Cyclometallated platinum(II) and palladium(II) complexes show better antitumor activity against breast, lung and leukemic tumor cells than the cisplatin analogs. In addition to anticancer application, luminescent rhodium(III) and iridium(III) cyclometallates have been frequently used as chemical and biological probes [45-50].

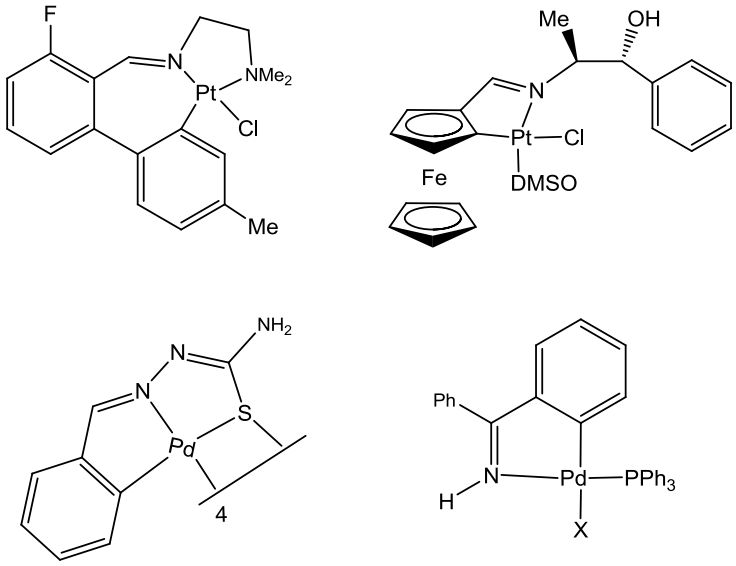

Figure 1.2

1.2.2. In Catalysis

Cyclometallated species of platinum group metals are the major intermediates in the corresponding metal catalyzed activation of unreactive bonds of saturated hydrocarbons. Apart from that, cyclometallated complexes themselves act as catalysts as well as pre-catalysts in many synthetic organic transformation reactions. The main advantage of the cyclometallated complex catalysts is their high thermodynamic stability, insensitivity to air etc.

Cross-coupling reactions catalyzed by palladium has become one of the important processes in synthetic organic chemistry for the formation of C–C and C–heteroatom bonds. Palladacycles have emerged as alternatives to the simple palladium salt catalysts such as $Pd(OAc)_2$, $PdCl_2$ etc. Catalytic activity of palladacycles was first studied by Lewis in 1986 for the hydrogenation of alkenes and alkynes with H_2 [51]. But catalytic activity of palladacycles in Heck and Suzuki-Miyaura cross-coupling reactions was first studied by Herrmann and Beller in 1995 [52–53]. During the last two decades a variety of palladacycles with bidentate phosphorus-, nitrogen-, sulfur-, oxygen-donor ligands as well as cyclopalladated complexes with pincer and pincer like PCP-, NCN-, PCS-, SCS-, CNN-, CNO- and CNS-donor ligands have been

studied for their activity as catalysts and pre-catalysts for Heck, Sonogashira, Suzuki-Miyaura, Stille and Kumada and Negishi cross coupling and Buchwald–Hartwig amination reactions [54–61]. The major advantages of palladacyles (Figure 1.3) are their high reactivity and stability achieved due to cyclometalation and commercially more viable low catalyst loading. Palladacyles are also very good catalysts for the olefination of the low reactive aryl bromides and chlorides.

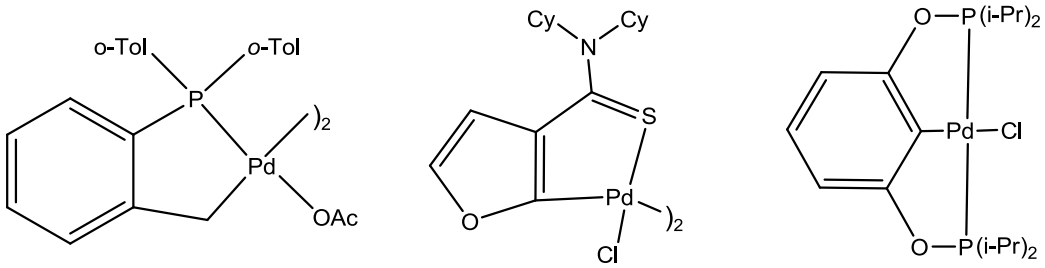

Figure 1.3

Cyclometallated complexes of rhodium and iridium are also used as catalysts in various synthetic transformation reactions such as transfer hydrogenation, asymmetric transfer hydrogenation of ketones, α,β-unsaturated carbonyl, unsaturated acids and esters and epoxides [62–72]. Several cyclometallated rhodium and iridium hydride complexes are known to catalyze CO_2 reduction [73–58]. Metallacyles are found as intermediates in various rhodium and iridium catalyzed reactions such as alkylation, carbonylation, aminaton etc. Synthesis of indole and isoquinoline derivatives by rhodium catalyzed oxidative cross-coupling between acetanilides or aldimines with alkynes are known to proceed through the rhodium cyclometallated compounds as an intermediate [78,79].

1.2.3. In Materials

Cyclometallated complexes play an important role in the development modern materials chemistry due to their potential applications in organic light-emitting diodes (OLEDs), solar photovoltaic cells and other electroluminescent technologies. In recent days, organic light-emitting diodes (OLEDs) have attracted great interest due to their viable use in low-cost, more-efficient display devices. Because of their short excited-state lifetime, high phosphorescence efficiency and colour tenability various cyclometallates of platinum group metals are being widely used as phosphorescent materials (Figure 1.4). Compared to the other organometallic compounds cyclometallates have very strong metal-ligand bonding. This strong metal–ligand bonding increases the d–d energy gap and affords low radiationless quenching [80–90].

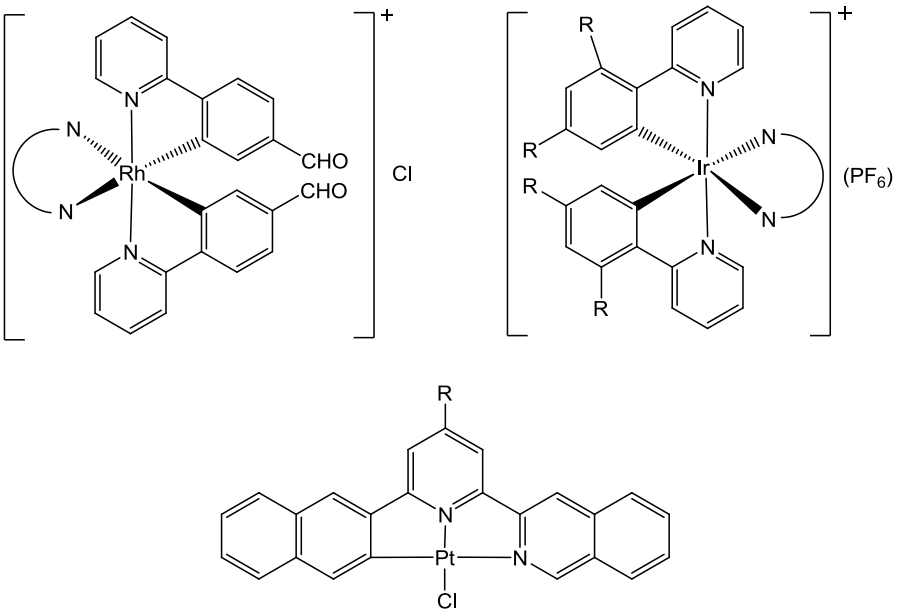

Figure. 1.4

1.3. Cyclometallated complexes with Schiff bases

In recent years cyclometallates with Schiff bases have attracted considerable attention. This is due to the relatively easy synthetic methods for the preparation of Schiff bases. The first cyclometallated complex with Schiff base was reported by Molnar and Orchin in 1969 [91]. The reaction of benzylideneaniline with bis(benzonitrile)palladium(II) dichloride results into the formation of the dichlorobis(benzy1ideneaniline) palladiurn(II) complex (Figure 1.5). At present a variety of cyclometallates with different classes of Schiff bases are available in the literature. Schiff bases for example oximes, semicarbazones, thiosemicarbazones, etc. are known to form cyclometallates with ring sizes varying from five to seven [92–103]. In general bidentate ligands are of CN-donor type, while different types of tridentate (such as CNO-, CNN-, CNS-, CNP-donor) Schiff bases are reported.

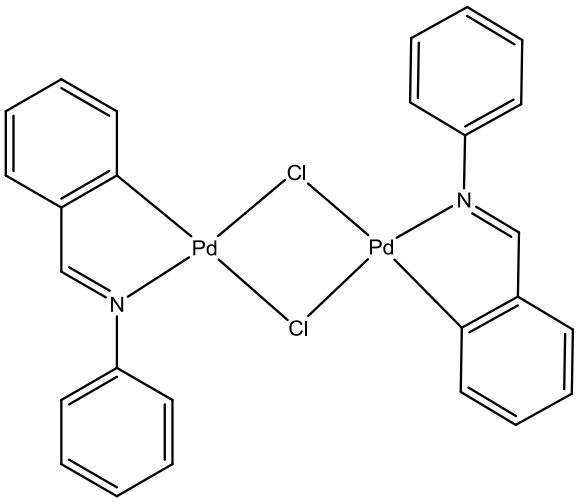

Figure 1.5

1.4. Regioselectivity in Cyclometallation

Regioselective cyclometallation is of particular interest in connection with the synthesis of tailor-made organic compounds as it provides the scope for functionalization of a specific site among various available. Such regioselectivity can play a decisive role in synthetic organic reactions. Regioselective cyclometallation of the polycyclic aryl moiety such as 1-naphthalenyl, 9-phenanthryl, 1-pyrenyl, 3-perilenyl and 3-indolyl (Figure 1.6) in the various bidentate and tridentate Schiff bases synthesized from the corresponding polycyclic aromatic aldehydes with platinum group metal ions have been reported. Generally for tridentate ligands either *ortho*- or *peri*-metallation occurs in a regioselective way, while only *ortho*-metallation takes place for the majority of the bidentate ligands except for few where both *ortho*- and *peri*-metallated products are isolated [104–115].

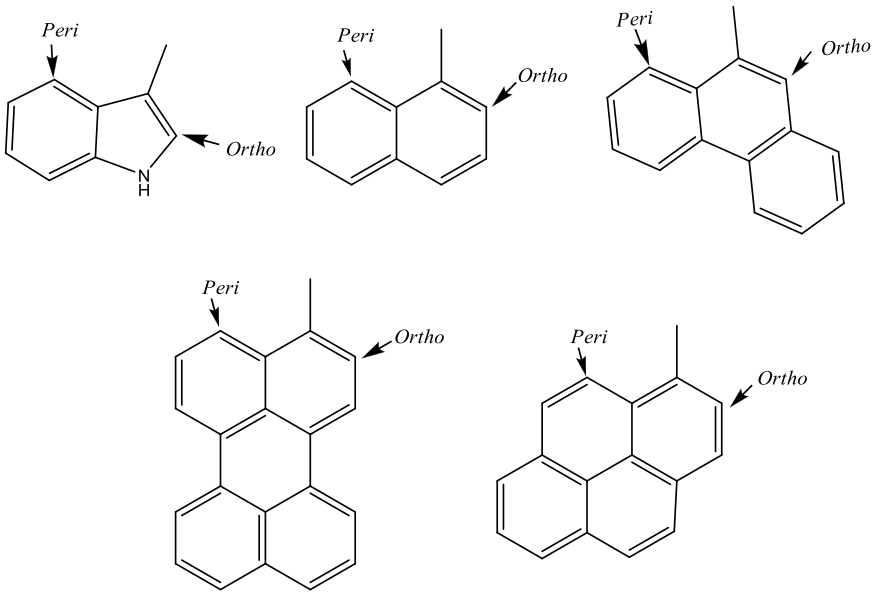

Figure 1.6

1.5. About the Present Investigation

In the preceding sections, we have briefly discussed about the chemistry of the cyclometallated complexes of platinum group metals with different classes of ligands and their potential applications in various research areas. We have also mentioned about the importance of regioselective cyclometallation reactions. In the present investigation, we have studied the cyclometallation chemistry of various aroylhydrazones of polycyclic aromatic aldehydes (Figure 1.7) using square-planar palladium(II) and platinum(II) and octahedral rhodium(III) and iridium(III). Our primary goal was to synthesize new cyclometallates and to explore if any regioselective metallation of the polycyclic aryl moiety occurs or not. Our observations in the above effort are described in the following chapters.

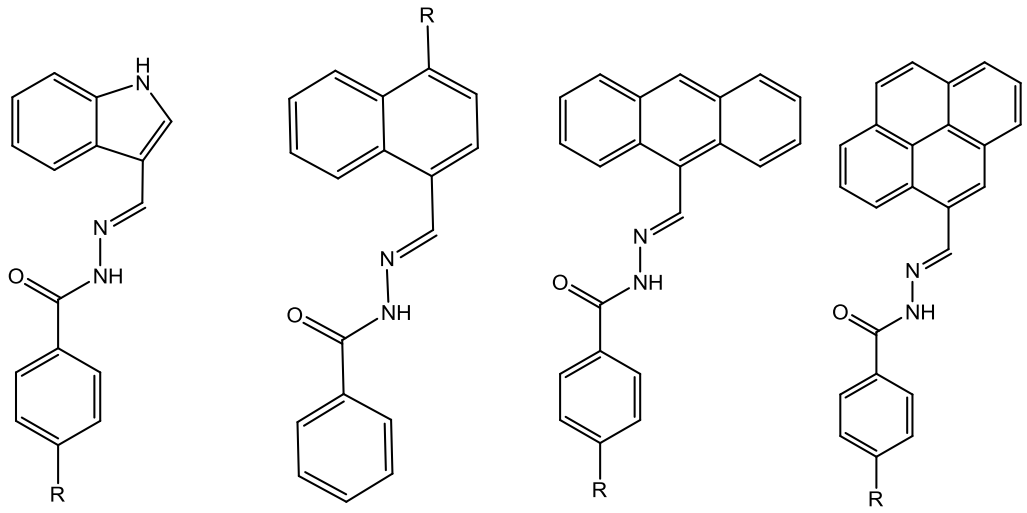

Figure 1.7

1.6. References

[1] J. P. Kleinman, M. Dubeck, *J. Am. Chem. Soc.* 85 (1963) 1544–1545.

[2] A. C. Cope, R.W. Siekman, *J. Am. Chem. Soc.* 87 (1965) 3272–3273.

[3] M. A. Stark, G. Jones, C. J. Richards, *Organometallics* 19 (2000) 1282-1291.

[4] Y. Motoyama, H. Narusawa, H. Nishiyama, *Chem. Commun.* (1999) 131–132.

[5] S. Ladouceur, D. Fortin, E. Z. –Colman, *Inorg. Chem.* 50 (2011) 11514−11526.

[6] V. K. Rai, M. Nishiura, M. Takimoto, S. Zhao, Y. Liu, Z. Hou, *Inorg. Chem.* 51 (2012) 822−835.

[7] L. Chen, H. You, C. Yang, D. Ma, J. Qin, *Chem. Commun.* (2007) 1352–1354.

[8] Y. Zheng, A. S. Batsanov, M. R. Bryce, *Inorg. Chem.* 50 (2011) 3354–3362.

[9] Z. Chen, Z. Bian, C. Huang, *Adv. Mater.* 22 (2010) 1534–1539.

[10] K. L. Garner, L. F. Parkes, J. D. Piper, J. A. G. Williams, *Inorg. Chem.* 49 (2010) 476–487.

[11] C. R. Baar, H. A. Jenkins, J. J. Vittal, G. P. A. Yap, R. J. Puddephatt, *Organometallics* 17 (1998) 2805–2818.

[12] C. R. Baar, H. A. Jenkins, M. C. Jennings, J. J. Vittal, G. P. A. Yap, R. J. Puddephatt, *Organometallics* 19 (2000) 4870–4877.

[13] W. Wu, J. Sun, S. Ji, W. Wu, J. Zhao, H. Guo, *Dalton Trans.*, 40 (2011) 11550–11561.

[14] N. Wang, B. Li, H. Song, S. Xu, B Wang, *Chem. Eur. J.* 19 (2013) 358–364.

[15] S. Leung, K.Y. Kwok, K.Y. Zhang, K. K. -W. Lo, *Inorg. Chem.* 49 (2010) 4984–4995.

[16] J. Moussa, M. N. Rager, L. M. Chamoreau, L. Ricard, H. Amouri, *Organometallics* 28 (2009) 397–404.

[17] S. Chen, Y. Li, J. Zhao, X. Li, Inorg. Chem. 48 (2009) 1198-1206.

[18] U. Mäder, A. V. Zelewsky, T. Jenny, *HCA* 69 (1986) 1085–1087.

[19] S. Paavola, K. Zetterberg, T. Privalov, I. Csöregh, C. Moberg, *Adv. Synth. Catal.* 346 (2004) 237–244.

[20] A. Moyano, M. Rosol, R. M. Moreno, C. López, M. A. Maestro, *Angew. Chem. Int. Ed.* 44 (2005) 1865 –1869.

[21] A. D. Ryabov, *Chem. Rev.* 90 (1990) 403–424.

[22] A. J. Canty, G. van Koten, *Acc. Chem. Res.* 28 (1995) 406−413.

[23] J. Dupont, C. S. Consorti, J. Spencer, *Chem. Rev.* 105 (2005) 2527−2572.

[24] J. P. Djukic, J. B. Sortais, L. Barloy, M. Pfeffer, *Eur. J. Inorg. Chem.* (2009) 817−853.

[25] M. Albrecht, *Chem. Rev.* 110 (2010) 576–623.

[26] I. P. Beletskaya, A. V. Cheprakov, *J. Organomet. Chem.* 689 (2004) 4055–4082.

[27] N. Selander, K. J. Szabó, *Chem. Rev.* 111 (2011) 2048–2076.

[28] D. Gelman, S. Musa, *ACS Catal.* 2 (2012) 2456−2466.

[29] M. Pfeffer, *Pure Appl. Chem.* 64 (1992) 335−342.

[30] J. Cámpora, P.Palma, E. Carmona, *Coord. Chem. Rev.* 193–195 (1999) 207–281.

[31] I. Omae, *Coord. Chem. Rev.* 248 (2004) 995−1023.

[32] A. Steffen, R. M. Ward, W. D. Jones, T. B. Marder, *Coord. Chem. Rev.* 254 (2010) 1950–1976.

[33] M. Albrecht, G. van Koten, *Angew. Chem. Int. Ed.* 40 (2001) 3750−3781.

[34] Q. Zhao, C. Huang, F. Li, *Chem. Soc. Rev.* 40 (2011) 2508–2524.

[35] G. Zhou, W. –Y. Wong, X. Yang, *Chem. Asian J.* 6 (2011) 1706−1727.

[36] Y. You, W. Nam, *Chem. Soc. Rev.* 41 (2012) 7061–7084.

[37] P. G. Bomben, K. C. D. Robson, B. D. Koivisto, C. P. Berlinguette, *Coord. Chem. Rev.* 256 (2012) 1438–1450.

[38] K. K. –W. Lo, K. Y. Zhang, S. P. –Y. Li, *Pure Appl. Chem.* 83 (2011) 823–840.

[39] N. Cutillas, G. S. Yellol, C. de Haro, C. Vicente, V. Rodríguez, J. Ruiz, *Coord. Chem. Rev.* 257 (2013) 2784–2797.

[40] D. Ashen-Garry, M. Selke, *Photochem. Photobiol.* 90 (2014) 257–274.

[41] F. Muggia, *Gynecol. Oncol*. 112 (2009) 275–281.

[42] M. A. Fuertes, J. Castilla, C. Alonso, J. M. Pérez, Curr. *Med. Chem*. 10 (2003) 257–266.

[43] S. J. Berners-Price, *Angew. Chem. Int. Ed*. 50 (2011) 804–805.

[44] A. Gautier, F. Cisnetti, *Metallomics* 4 (2012) 23–32.

[45] D. Talancón, C. López, M. Font-Bardía, T. Calvet, J. Quirante, C. Calvis, R. Messeguer, R. Cortés, M. Cascante, L. Baldomà, J. Badia, *J. Inorg. Biochem*. 118 (2013) 1–12.

[46] R. Cortés, M. Crespo, L. Davin, R. Martín, J. Quirante, D. Ruiz, R. Messeguer, C. Calvis, L. Baldomà, J. Badia, M. Font-Bardía, T.Calvet, M. Cascante, *Eur. J. Med.Chem.* 54 (2012) 557–566.

[47] C. -H. Leung, H. -J. Zhong, H. Yang, Z. Cheng, D. S. -H. Chan, V. P. -Y. Ma, R. Abagyan, C. -Y. Wong, D. -L. Ma, *Angew. Chem. Int. Ed.* 51 (2012) 9010–9014.

[48] C. -H. Leung, H. Yang, V. P. -Y. Ma, D. S. -H. Chan, H. -J. Zhong, Y. -W. Li, W. -F. Fong, D. -L. Ma, Med. *Chem. Commun*. 3 (2012) 696–698.

[49] J. Kuil, P. Steunenberg, P. T. K. Chin, J. Oldenburg, K. Jalink, A. H. Velders, F. W. B. van Leeuwen, *ChemBioChem* 12 (2011) 1897–1903.

[50] N. Cutillas, G. S. Yellol, C. de Haro, C. Vicente, V. Rodríguez, J. Ruiz, *Coord. Chem. Rev.* 257 (2013) 2784−2797.

[51] L. N. Lewis, *J. Am. Chem. Soc.* 108 (1986) 743–749.

[52] W. A. Herrmann, C. Brossmer, K. Öfele, C. -P. Reisinger, T. Priermeier, M. Beller, H. Fischer, *Angew. Chem. Int. Ed.* 34 (1995) 1844 –1848.

[53] M. Beller, H. Fischer, W. A. Herrmann, *Angew. Chem. Int. Ed.* 34 (1995) 1848 –1849.

[54] M. Ohff, A. Ohff, M. E. van der Boom, D. Milstein, *J. Am. Chem. Soc*. 119 (1997) 11687–11688.

[55] E. D. -Barra, J. Guerra, V. Hornillos, S. Merino, J. Tejeda, *Organometallics* 192 (2003) 4610–4612.

[56] M. -T. Chen, C. -A. Huang, C. -T. Chen, *Eur. J. Inorg. Chem*. (2006) 4642–4648.

[57] D. E. Bergbreiter, P. L. Osburn, J. D. Frels, *Adv. Synth. Catal.* 347 (2005) 172–184.

[58] R. B. Bedford, C. S. J. Cazin, *Chem. Commun.* (2001) 1540–1541.

[59] J. Louie, J. F. Hartwig, *Angew. Chem. Int. Ed.* 35 (1996) 2359–2361.

[60] D. A. Alonso, C. Nájera, M. C. Pacheco, *Organic Letters* 2 (2000) 1823–1826.

[61] D. Zim, S. L. Buchwald, *Organic Letters* 5 (2003) 2413–2415.

[62] Y. Himeda, N. O. -Komatsuzaki, H. Sugihara, H. Arakawa, K. Kasuga, J. Mol. *Catal. A: Chem.* 195 (2003) 95–100.

[63] G. Zassinovich, G. Mestroni, S. Gladiali, *Chem. Rev.* 92 (1992) 1051-1009.

[64] T. Ikariya, A.J. Blacker, *Acc. Chem. Res.* 40 (2007) 1300–1308.

[65] M. Albrecht, R. H. Crabtree, J. Mata, E. Peris, *Chem. Commun*. (2002) 32–33.

[66] K. Murata, T. Ikariya, *J. Org. Chem*. 64 (1999) 2186-2187.

[67] O. Prakash, K. N. Sharma, H. Joshi, P. L. Gupta, A. K. Singh, *Organometallics* 33 (2014) 983−993.

[68] A. M. Kalsin , T. A. Peganova, V. V. Novikov, A. I. Zhamoytina, L. Gonsalvi, M. Peruzzini, Chem. Eur. J. 20 (2014) 846–854.

[69] M. Aydemir, N. Meric, A. Baysal, *J. Organomet. Chem*. 720 (2012) 38–45.

[70] R. Spogliarich. A. Tencich, J. Kaspar, M. Graziani, *J. Organomet. Chem*. 240 (1982) 453-459.

[71] D. Beaupere, P. Bauer, L. Nadjo, R. Uzan, *J. Organomet. Chem*. 238 (1982) C12–C14.

[72] B. Ding, Z. Zhang, Y. Liu, M. Sugiya, T. Imamoto, W. Zhang, *Organic Letters*. 15 (2013) 3690–3693.

[73] W. Wang, P. Gu, Y. Wang, H. Wei, *Organometallics* 33 (2014) 847−857.

[74] S. Gruber, M. Neuburger, A. Pfaltz, *Organometallics* 32 (2013) 4702−4711.

[75] S. Sato, T. Morikawa, T. Kajino, O. Ishitani, *Angew. Chem. Int. Ed*. 52 (2013) 988 –992.

[76] T. J. Schmeier, G. E. Dobereiner, R. H. Crabtree, N. Hazari, *J. Am. Chem. Soc*. 133 (2011) 9274–9277.

[77] S. Sanz, M. Benı´tez, E. Peris, *Organometallics* 29 (2010) 275–277.

[78] D. R. Stuart, M. B. Laperle, K. M. N. Burgess, K. Fagnou, *J. Am. Chem. Soc.* 130 (2008) 16474–16475.

[79] N. Guimond, K. Fagnou, *J. Am. Chem. Soc*. 131 (2009) 12050–12051.

[80] Y. Chi, P. -T. Chou, *Chem.Soc.Rev*. 39 (2010) 638–655.

[81] J. Kalinowski, V. Fattori, M. Cocchi, J.A.G. Williams, *Coord. Chem. Rev*. 255 (2011) 2401–2425.

[82] J. A. G. Williams, S. Develay, D. L. Rochester, L. Murphy, *Coord. Chem. Rev*. 252 (2008) 2596–2611.

[83] R. Wang, D. Liu, H. Ren, T. Zhang, H. Yin, G. Liu, J. Li, *Adv. Mater*. 23 (2011) 2823–2827.

[84] L. He, J. Qiao, L. Duan, G. Dong, D. Zhang, L. Wang, Y. Qiu, *Adv. Funct. Mater*. 19 (2009) 2950–2960.

[85] C. L. Ho, W. Y. Wong, G. J. Zhou, B. Yao, Z. Xie, L. Wang, *Adv. Funct. Mater*. 17 (2007) 2925–2936.

[86] Z. Chen, Z. Bian, C. Huang, *Adv. Mater*. 22 (2010) 1534–1539.

[87] S. C. Lo, R. N. Bera, R. E. Harding, P. L. Burn, I. D. W. Samuel, *Adv. Funct. Mater*. 18 (2008) 3080–3090.

[88] R. Wang, D. Liu, R. Zhang, L. Deng, J. Li, *J. Mater. Chem*. 22 (2012) 1411–1417.

[89] R. Wang, D. Liu, H. Ren, T. Zhang, X. Wang, J. Li, *J. Mater. Chem.* 21 (2011) 15494–15500.

[90] K. K. –W. Lo, C. –K. Li, K. –W. Lau, N. Zhu, *Dalton Trans.* (2003) 4682 – 4689.

[91] S. P. Molnar, M. Orchin, *J. Organomet. Chem.* 16 (1969) 196-200.

[92] I. Omae, *Chem. Rev.* 79 (1979) 287–321.

[93] D. Pou, C. López, S. Pérez, X. Solans, M. F. Bardía, P. W. N. M. van Leeuwen, G. P. F. van Strijdonck, *Eur. J. Inorg. Chem*. (2010) 1642–1648.

[94] L. Adrio, J. M. Antelo, J. M. Ortigueira, J. J. Fernández, A. Fernández, M. T. Pereira, J. M. Vila, *J. Organomet. Chem*. 694 (2009) 1273–1282.

[95] A. Ferna´ndez, D. V. -García, J. J. Fernández, M. L. -Torres, A. Suárez, J. M. Vila, *J. Organomet. Chem*. 690 (2005) 3669–3679.

[96] J. Albert, M. Crespo, J. Granell, J. Rodríguez, J. Zafrilla, T. Calvet, M. F. Bardia, X. Solans, *Organometallics* 29 (2010) 214–225.

[97] J. Albert, R. M. Ceder, M. Gómez, J. Granell, J. Sales, *Organometallics* 11 (1992) 1536-1541.

[98] I. Pal, S. Dutta, F. Basuli, S. Goverdhan, S. -M. Peng, G. -H. Lee, S. Bhattacharya, *Inorg. Chem*. 42 (2003) 4338−4345.

[99] S. Basu, S. Dutta, M. G. B. Drew, S. Bhattacharya, *J. Organomet. Chem*. 691 (2006) 3581–3588.

[100] R. Acharyya, F. Basuli, R. -Z. Wang, T. C. W. Mak, S. Bhattacharya, *Inorg. Chem.* 43 (2004) 704−711.

[101] S. Basu, R. Acharyya, F. Basuli, S. -M. Peng, G. -H. Lee, G. Mostafa, S. Bhattacharya, *Inorg. Chim. Acta* 363 (2010) 2848–2856.

[102] C. Andersona, M. Crespo, M. F. -Bardía, A. Klein, X. Solans, *J. Organomet. Chem*. 601 (2000) 22–33.

[103] P. Ramírez, R. Contreras, M. Valderrama, D. Carmona, F. J. Lahoz, A.I. Balana, *J. Organomet. Chem*. 693 (2008) 349–356.

[104] Y. –F. Han, H. Li, P. Hu, G. –X. Jin, *Organometallics* 30 (2011) 905–911.

[105] S. Tollari, G. Palmisano, F. Demartin, M. Grassi, S. Magnaghi, S. Cenini, *J. Organomet. Chem*. 488 (1995) 79–83.

[106] R. Annunziata, S. Cenini, F. Demartin, G. Palmisano, S. Tollari, *J. Organomet. Chem*. 496 (1995) C1–C3.

[107] M. Crespo, M. Font-Bardia, S. Perez, X. Solans, *J. Organomet. Chem.* 642 (2002) 171–178.

[108] Y. Li, K.–H. Ng, S. Selvaratnam, G. –K. Tan, J. J. Vittal, P. –H. Leung, *Organometallics* 22 (2003) 834–842.

[109] R. Bhawmick, P. Das, D. N. Neogi, P. Bandyopadhyay, *Polyhedron* 25 (2006) 1177–1181.

[110] S. Lentijo, J. A. Miguel, P. Espinet, *Organometallics* 30 (2011) 1059–1066.

[111] S. Lentijo, J. A. Miguel, P. Espinet, *Dalton Trans.* 40 (2011) 7602–7609.

[112] A. N. Biswas, P. Das, S. Sengupta, A. Choudhury, P. Bandyopadhyay, *RSC Advances* 1 (2011) 1279–1286.

[113] A. N. Biswas, P. Das, V. Bagchi, A. Choudhury, P. Bandyopadhyay, *Eur. J. Inorg. Chem*. (2011) 3739–3748.

[114] D. N. Neogi, A. N. Biswas, P. Das, R. Bhawmick, P. Bandyopadhyay, *J. Organomet. Chem*. 724 (2013) 147□154.

[115] A. Mercier, S. Wagschal, L. Guénée, C. Besnard, E. P. Kündig, *Organometallics* 32 (2013) 3932–3942.

Chapter 2

Cyclopalladation of 4-*R*-N′-(9-anthracenylidene)-benzohydrazides: Synthesis, properties and structures[§]

Reactions of equimolar amounts of Li_2PdCl_4, 4-*R*-N′-(9-anthracenylidene)-benzohydrazides (H_2L^n; n = 1 and 2 for *R* = H and NMe_2, respectively) and $CH_3COONa{\cdot}3H_2O$ in methanol produce the cyclopalladated complexes with the formula $[Pd(HL^n)Cl]$ (**1** (*R* = H) and **2** (*R* = NMe_2)). Reactions of $[Pd(HL^n)Cl]$ (**1** and **2**) with two mole equivalents of PPh_3 in acetone provide the complexes of formula $[Pd(L^n)(PPh_3)]$ (**3** (*R* = H) and **4** (*R* = NMe_2)). Complexes **1**−**4** have been characterized by elemental analysis and spectroscopic (IR, UV-Vis, fluorescence and NMR) measurements. Molecular structures of **1**−**4** have been confirmed by X-ray crystallography. In $[Pd(HL^n)Cl]$ (**1** and **2**), the C,N,O-donor $(HL^n)^-$ and the chloride form a CNOCl square-plane around the metal centre, while $(L^n)^{2-}$ and the PPh_3 assemble a CNOP square-plane around the metal centre in $[Pd(L^n)(PPh_3)]$ (**3** and **4**).

2.1. Introduction

A common strategy to generate metallacycles is the metallation of a pendant aromatic ring of the coordinated ligand. In literature *ortho*-metallation of pendant phenyl ring is more prevalent than the metallation of hetero cyclic rings and fused aromatic rings. Our group has been working for quite some time now on *ortho*-metallated species with C,N,O-donor Schiff bases derived from acid hydrazides and benzaldehyde or its substituted derivatives [1−4]. In view of the very few reports on cyclopalladated complexes involving anthracene [5−8], in the present work we have explored the palladium(II) chemistry with Schiff bases (H_2L^n) prepared from 4-*R*-

[§] This work has been published in *J. Organomet. Chem.* 701 (2012) 62–67.

benzoylhydrazines (*R* = H and NMe_2) and 9-anthraldehyde. In this effort, we have isolated two types of *peri*-palladates [$Pd(HL^n)Cl$] and [$Pd(L^n)(PPh_3)$] (Scheme 2.1). In the following account, we have described the synthesis, properties and X-ray structures of these complexes.

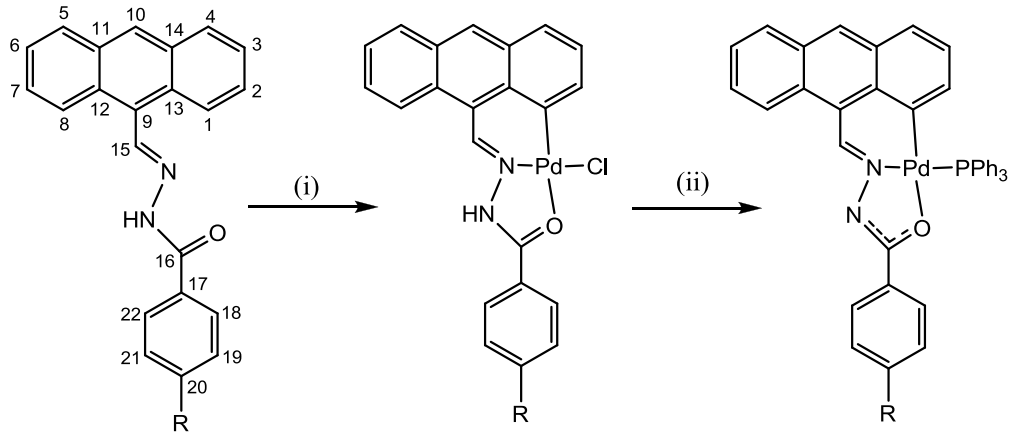

H_2L^n
R = H (n = 1) and NMe_2 (n = 2)

1 (*R* = H)
2 (*R* = NMe_2)

3 (*R* = H)
4 (*R* = NMe_2)

Scheme 2.1. (i) Li_2PdCl_4 and $CH_3COONa{\cdot}3H_2O$ (equimolar amounts of each in methanol), (ii) PPh_3 (2 mole equivalent in acetone).

2.2. Experimental

2.2.1. Materials

All the chemicals used in this work were of analytical grade available commercially and were used as received. The solvents used were purified by standard methods [9].

2.2.2. Physical measurements

Microanalytical (C, H, N) data were obtained with a Thermo Finnigan Flash EA1112 series elemental analyzer. IR spectra in KBr pellets were recorded on a Jasco-5300 FT-IR spectrophotometer. A Shimadzu LCMS 2010 liquid chromatograph mass spectrometer was used for the purity verification of H_2L^1 and H_2L^2. Solution electrical conductivities were measured with a Digisun DI-909 conductivity meter. A Perkin-Elmer Lambda 35 UV/vis

spectrophotometer was used to collect the electronic spectra. The fluorescence spectra were recorded using a Horiba Jobin Yvon Fluoromax-4 spectrofluorometer. The NMR spectra were recorded with the help of Bruker 400 and 500 MHz NMR spectrometers.

2.2.3. Synthesis of H_2L^1

9-anthraldehyde (206 mg, 1mmol) and a few drops of acetic acid were added to an ethanol solution of benzoylhydrazine (136 mg, 1 mmol). The mixture was boiled under reflux for 3 h. The pale yellow solid separated was collected by filtration, washed with ethanol and then dried in air. Yield: 265 mg (82%). Mass in Me_2NCHO: m/z = 325.

H_2L^2 was prepared in 83% yield from equimolar amounts of 9-anthraldehyde and 4-dimthylaminobenzoylhydrazine in presence of acetic acid using the same procedure as described for H_2L^1. Mass in Me_2NCHO: m/z = 368.

2.2.4. Synthesis of [Pd(HL^1)Cl] (1)

A mixture of $PdCl_2$ (178 mg, 1.0 mmol) and LiCl (86 mg, 2.0 mmol) was taken in methanol (20 ml) and boiled with stirring under reflux for 1 h. It was then cooled to room temperature and filtered. The filtrate was added drop-wise with stirring to a methanol solution (20 ml) of H_2L^1 (324 mg, 1.0 mmol) and $CH_3COONa{\cdot}3H_2O$ (136 mg, 1.0 mmol). The mixture was stirred at room temperature for 48 h. The complex precipitated as orange solid was collected by filtration, washed with methanol and finally dried in air. Yield: 290 mg (62%).

The red [Pd(HL^2)Cl] (**2**) was synthesized in 65% yield by following a procedure very similar to that described for **1** using H_2L^2 instead of H_2L^1.

2.2.5. Synthesis of [Pd(L^1)(PPh_3)] (3)

Solid PPh_3 (131 mg, 0.5 mmol) was added to a suspension of [Pd(HL^1)Cl] (**1**) (116 mg, 0.25 mmol) in acetone (10 ml) and the mixture was stirred at room temperature for 24 h. The complex [Pd(L^1)(PPh_3)] (**3**) separated as an orange solid was collected by filtration, washed with acetone and finally dried in air. Yield: 104 mg (60%). ^{31}P NMR in $(CD_3)_2SO$: δ (ppm) = 25.51.

[Pd(L^2)(PPh_3)] (**4**) was synthesized as an orange-red solid in 65% yield from one mole equivalent of [Pd(HL^2)Cl] (**2**) and two mole equivalents of PPh_3 using a very similar procedure described above. ^{31}P NMR in $(CD_3)_2SO$: δ (ppm) = 25.53.

2.2.6. X-ray crystallography

Single crystals of [Pd(HL^n)Cl] (**1** and **2**) were grown by dithethyl ether vapor diffusion into their corresponding dimethylformamide solutions, while that of [Pd(L^n)(PPh_3)] (**3** and **4**) were obtained by slow evaporation of their corresponding acetonitrile solutions. Both **1** and **2** crystallize as [Pd(HL^n)Cl]·Me_2NCHO (**1**·Me_2NCHO and **2**·Me_2NCHO). Complex **3** crystallizes as **3**·CH_3CN, while complex **4** crystallizes as it is. A Bruker-Nonius SMART APEX CCD single crystal diffractometer, equipped with a graphite monochromator and a Mo $K\alpha$ fine-focus sealed tube (λ = 0.71073 Å) was used to determine the unit cell parameters and intensity data collection at 298 K for **1**·Me_2NCHO and **4**. The SMART and the SAINT-Plus packages [10] were used for data acquisition and data extraction, respectively. The SADABS program [11] was used for absorption corrections. Determination of the unit cell parameters and the intensity data collection at 298 K for each of **2**·Me_2NCHO and **3**·CH_3CN were performed on an Oxford Diffraction Xcalibur Gemini single crystal X-ray diffractometer using graphite monochromated Mo $K\alpha$ radiation (λ = 0.71073 Å). The CrysAlisPro software [12] was used for data collection, reduction and absorption correction. The structures of all four complexes were solved by direct method and refined on

Table 2.1. Selected crystallographic data

Complex	**1**·Me_2NCHO	**2**·Me_2NCHO	**3**·MeCN	**4**
Empirical formula	$PdC_{25}H_{22}N_3O_2Cl$	$PdC_{27}H_{27}N_4O_2Cl$	$PdC_{42}H_{32}N_3OP$	$PdC_{42}H_{34}N_3OP$
Formula weight	538.34	581.41	732.13	734.15
Crystal system	Triclinic	Monoclinic	Monoclinic	Monoclinic
Space group	$P\bar{1}$	$P2_1/c$	$P2_1/n$	$P2_1/c$
a (Å)	9.1279(7)	10.7700(4)	12.300(4)	10.3624(6)
b (Å)	11.3041(8)	30.1455(11)	13.354(3)	14.4229(8)
c (Å)	11.9347(9)	8.0191(4)	21.260(8)	22.6557(13)
α (°)	65.176(1)	90	90	90
β (°)	77.392(1)	105.383(4)	104.35(4)	96.096(1)
γ (°)	75.122(1)	90	90	90
V (Å^3)	1071.60(14)	2510.26(18)	3383.1(2)	3366.9(3)
Z	2	4	4	4
ρ (g cm^{-3})	1.668	1.538	1.437	1.448
μ (mm^{-1})	1.020	0.878	0.634	0.637
Reflections collected	10272	10588	12407	31774
Reflections unique	3762	4412	5947	5926
Reflections ($I \geq 2\sigma(I)$)	3622	3413	3489	5491
Parameters	294	323	434	435
$R1$, $wR2$ ($I \geq 2\sigma(I)$)	0.0239, 0.0619	0.0529, 0.1094	0.0405, 0.0820	0.0297, 0.0742
$R1$, $wR2$ (all data)	0.0249, 0.0626	0.0745, 0.1144	0.0796, 0.0892	0.0323, 0.0759
GOF (F^2)	1.080	1.151	0.871	1.068
Largest peak and hole (e Å^{-3})	0.647 and −0.336	0.736 and −0.675	0.552 and −0.867	0.353 and −0.333

F^2 by full-matrix least-squares procedures. All non-hydrogen atoms were refined anisotropically. The hydrogen atom of the amide functionality of the tridentate ligand in each of **1**·Me_2NCHO and **3**·CH_3CN was located in a difference map and refined with $U_{iso}(H) = 1.2U_{iso}(N)$. The remaining hydrogen atoms of **1**·Me_2NCHO and **3**·CH_3CN and all the hydrogen atoms of **2**·Me_2NCHO and **4** were included in the structure factor calculation at idealized positions by using a riding model. The SHELX-97 programs [13] available in the WinGX package [14] were used for structure solution and refinement. The ORTEX6a [15] and Platon [16] packages were used for molecular graphics. All the crystallographic data (except for the structure factors) are deposited with the Cambridge Crystallographic Data Centre. The deposition numbers are CCDC 847010–847013 for **1**·Me_2NCHO, **2**·Me_2NCHO, **3**·MeCN and **4**, respectively. Selected crystallographic data are summarized in Table 2.1.

2.3. Results and discussion

2.3.1. Synthesis and characterization

The Schiff bases H_2L^n (n = 1 and 2) [17] were synthesized in slightly more than 80% yields by condensation of 9-anthraldehyde and 4-*R*-benzoylhyrazines (*R* = H and NMe_2) in presence of a few drops of acetic acid in ethanol. Elemental analysis and spectroscopic (IR, ^{1}H NMR and mass) measurements were used to characterize these Schiff bases. Reactions of equimolar amounts H_2L^n, $CH_3COONa·3H_2O$ and Li_2PdCl_4 (generated in situ using $PdCl_2$ and LiCl in 1:2 mole ratio) in methanol produce $[Pd(HL^n)Cl]$ (**1** (*R* = H) and **2** (*R* = NMe_2)**)** in 62 and 65% yields. Reactions of $[Pd(HL^n)Cl]$ (**1** and **2**) with PPh_3 in 1:2 mole ratio in acetone provide the complexes $[Pd(L^n)(PPh_3)]$ (**3** (*R* = H) and **4** (*R* = NMe_2)**)** in 60 and 65% yields. Presumably the excess PPh_3 provides a mild basic environment to facilitate the deprotonation of the amide functionality of $(HL^n)^-$ and the formation of **3** and **4**. All the four complexes are orange to red in color and they are diamagnetic.

The elemental analysis data of **1**–**4** are in good agreement with their corresponding molecular formula (Table 2.2). Complexes **1** and **2** are highly soluble in dimethylformamide and dimethylsulfoxide and sparingly soluble in acetone and acetontrile. The solubility behaviors of **3** and **4** are very similar to that of **1** and **2**, except for their high solubility in halogenated solvents such as chloroform and dichloromethane. In solution, they behave as nonelectrolyte.

Table 2.2. Elemental analysis data

Compound	Found (calc) (%)		
	C	H	N
H_2L^1	81.45 (81.23)	4.97 (4.78)	8.65 (8.47)
H_2L^2	78.44 (78.26)	5.76 (5.69)	11.44 (11.32)
[Pd(HL1)Cl]	56.80 (56.95)	3.25 (3.33)	6.02 (6.12)
[Pd(HL^2)Cl]	56.71 (56.58)	3.97 (3.91)	8.27 (8.36)
[Pd(L^1)(PPh_3)]	69.52 (69.31)	4.23 (4.32)	4.05 (3.91)
[Pd(L^2)(PPh_3)]	68.71 (68.49)	4.67 (4.74)	5.72 (5.57)

2.3.2. Infrared spectral properties

IR spectra of all the compounds display a large number of bands in the frequency range 400−1650 cm^{-1} and a few bands within 3000−3220 cm^{-1} of various intensities. A representative spectrum is shown in Figure 2.1. We have only attempted to assign a few characteristic bands by comparing with the spectra of similar compounds reported earlier [1−4,17−19]. The free Schiff bases (H_2L^n) show the medium intensity N–H stretching band at ~3210 cm^{-1}. The strong band at ~1645 cm^{-1} and the following overlapping medium intensity band at ~1615 cm^{-1} are assigned to the C=O and C=N stretches, respectively. In the spectra of **1** and **2**, a weak band observed at ~3200 cm^{-1} is possibly due to the N–H stretch of the ligand $(HL^n)^-$. Two strong bands

observed at ~1610 and ~1570 cm^{-1} are attributed to the coordinated C=O and C=N groups of $(HL^n)^-$, respectively. The spectra of **3** and **4** do not display any band assignable to the N–H and C=O stretches. Thus the amide functionality of the tridentate $(L^n)^{2-}$ in **3** and **4** is in iminolate form (Scheme 1). The strong and sharp band observed at ~1600 cm^{-1} for these two complexes is very likely to be due to the conjugated C=N–C=N fragment of $(L^n)^{2-}$.

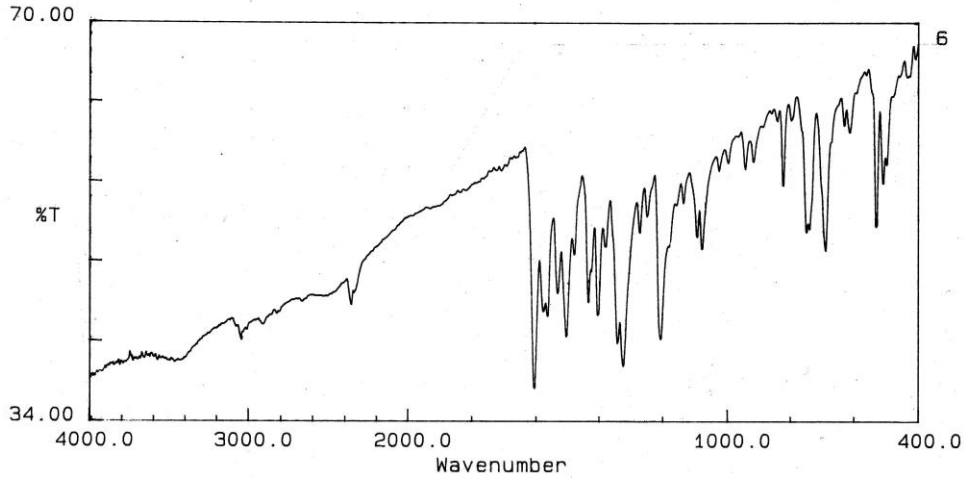

Figure 2.1. Infrared spectrum of $[Pd(L^2)(PPh_3)]$ (**4**)

2.3.3. Electronic and emission spectral properties

Dimethylformamide solutions of the Schiff bases (H_2L^1 and H_2L^2) and the corresponding complexes **1**−**4** with them were used to record the electronic absorption spectra. Spectroscopic data are listed in Table 2.3 and representative spectra is shown in Figure. 2.2. The spectral profiles of all the four complexes and the free Schiff bases (H_2L^n) are very similar. Interestingly except for the highest energy band all the spectra resemble that of pure anthracene [17,20,21]. Thus the absorptions in **1**−**4** are by and large due to ligand centred transitions only. However, there is a gradual red-shift of the band positions from anthracene to the Schiff bases to the complexes. This type of red-shift of π−π* absorption bands due to alteration of the π-energy levels and thus the decrease of the π−π* gap caused by substituent on the

Table 2.3. Electronic and emission spectroscopic[a] data

Complex	Absorption λ_{max} (nm) ($10^{-3} \times \varepsilon$ (M^{-1} cm^{-1}))	Emission λ_{max} (nm) (excitation at λ nm))
H_2L^1	438sh (10.3), 390 (52.4), 374 (47.5), 350[b] (27.4), 334[b] (15.5), 300[b] (33.9).	480 (390)
H_2L^1	440[b] (22.3), 417[b] (49.2), 398 (54.9), 370[b] (39.3), 314 (71.1)	700 and 490 (415)
1	512 (13.9), 482 (15.9), 453 (11.2), 424[b] (9.1), 390 (9.8), 368[b] (8.5), 323[b] (12.8), 288 (26.6)	570 (510)
2	524 (15.2), 490 (16.0), 461 (9.8), 381[b] (11.2), 314[b] (23.4), 287 (29.2)	645 (460)
3	515 (17.7), 485 (21.2), 460 (15.1), 425sh (6.8), 388 (5.2), 368[b] (4.5), 292 (25.2)	585 (510)
4	523 (20.0), 491 (21.4), 460[b] (12.6), 431[b] (6.3), 370[b] (13.2), 284 (44.9)	660 (460)

[a] In dimethylformamide

[b] Shoulder.

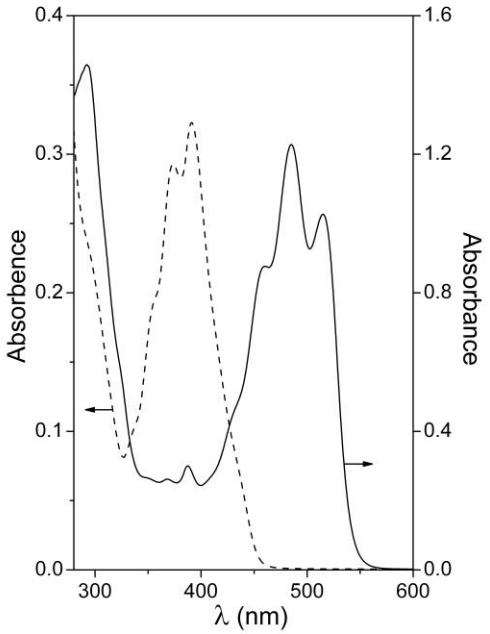

Figure 2.2. Electronic spectra of H_2L^1 (----) (0.6166 X 10^{5-}M) and [Pd(L^1)(PPh_3)] (**3**) (—) (0.5788 X 10^{4-}M) in dimethylformamide.

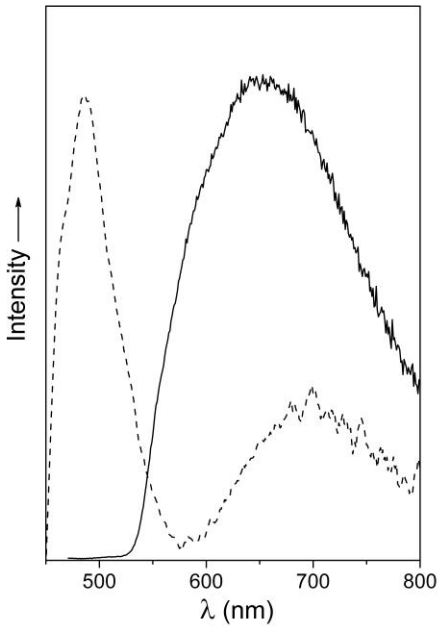

Figure 2.3. Emission spectra of H_2L^2 (----) (0.5443 X 10^{3-}M) and [Pd(HL^2)Cl] (**2**) (—) (0.5901 X 10^{3-}M) in dimethylformamide.

arene and also by metal coordination to aromatic heterocycle is documented before [21−23]

Emission spectra of both Schiff bases (H_2L^1 and H_2L^2) and complexes **1**−**4** were collected using their corresponding dimethylformamide solutions. Spectroscopic data are listed in Table 2.3 and representative spectra is shown in Figure. 2.3. All the compounds are emissive in nature. On excitation at 390 nm H_2L^1 shows a broad emission band centred at 480 nm. On excitation at 510 nm complexes **1** and **3** with H_2L^1 also display a similar broad emission band centred at 570 and 585 nm, respectively. In contrast to H_2L^1, H_2L^2 displays dual fluorescence property. On excitation at 410 nm, it shows two emission bands at 490 and 700 nm (Figure 2.3). Presumably after excitation the strong donor group NMe_2 on the aroyl moiety of H_2L^2 induces a conformational change and hence it exhibits two emission bands from two conformational isomers of the excited state [24,25]. However, dual fluorescence has not been observed for the complexes with H_2L^2. On excitation at 460 nm **2** and **4** display a broad emission band at 645 and 660 nm, respectively (Figure 2.3). Perhaps in these cases metal ion coordination causes stabilization of only one conformation of the excited state.

2.3.4. NMR spectral properties

^{1}H NMR spectra of H_2L^1, H_2L^2, and complexes **1**−**4** with them were recorded in dimethylsulfoxide-d6. Chemical shift values are summarized in Table 2.4 and representative spectra are shown in Figures 2.4 and 2.5. The spectra of **1** and **2** show all the protons of $(HL^n)^-$, whereas for **3** and **4** except for a few the remaining aromatic protons of $(L^n)^{2-}$ could not be clearly assigned due to the PPh_3 phenyl ring protons. The Schiff bases and **1** and **2** display the resonance corresponding to the N–H proton as a singlet in the range δ 11.81−13.70. As expected, **3** and **4** do not display any such signal due to the iminolate form of the amide functionality in $(L^n)^{2-}$ (Scheme 2.1). The methyl protons of NMe_2 in H_2L^2, **2** and **4** appear as singlet within δ 3.02−3.09.

Table 2.4. ^{1}H NMR data[a] of H_2L^{1-2} and **1**–**4**

Compound	δ (ppm) (J (Hz))
H_2L^1	12.12 (s, 1H, NH), 9.69 (s, 1H, H^{15}), 8.79 (s, 1H, H^{10}), 8.77 (5) (d, 2H, H^1, H^8), 8.19 (8) (d, 2H, H^4, H^5), 8.05 (7) (d, 2H, H^{18}, H^{22}), 7.66 (m, 3H, H19, H20, H21), 7.61 (m, 4H, H^2, H^3, H^6, H^7).
H_2L^2	11.81 (s, 1H, NH), 9.61 (s, 1H, H^{15}), 8.78 (s, 1H, H^{10}), 8.73 (14) (d, 2H, H^1, H^8), 8.16 (8) (d, 2H, H^4, H^5), 7.91 (8) (d, 2H, H^{18}, H^{22}), 7.61 (m, 4H, H^2, H^3, H^6, H^7), 6.81 (9) (d, 2H, H^{19}, H^{21}), 3.02 (s, 6H, NMe_2).
1	12.11 (s, 1H, NH), 10.11 (s, 1H, H^{15}), 8.98 (s, 1H, H^{10}), 8.76 (8) (d, 1H, H^8), 8.63 (br, s, 1H, H^4), 8.27 (8) (d, 1H, H^5), 8.14 (7) (d, 2H, H^{18}, H^{22}), 8.02 (8) (d, 1H, H^2), 7.86 (8) (t, 1H, H^{20}), 7.70 (m, 4H, H^6, H^7, H^{19}, H^{21}), 7.41 (8) (t, 1H, H^3).
2	13.70 (s, 1H, NH), 10.10 (s, 1H, H^{15}), 8.96 (s, 1H, H^{10}), 8.78 (9) (d, 1H, H^8), 8.61 (br, s, 1H, H^4), 8.26 (8) (d, 1H, H^5), 8.02 (8) (d, 1H, H^2), 7.98 (9) (d, 2H, H^{18}, H^{22}), 7.85 (8) (t, 1H, H^7), 7.68 (8) (t, 1H, H^6), 7.40 (8) (t, 1H, H^3), 6.90 (6) (d, 2H, H^{19}, H^{20}), 3.09 (s, 6H, NMe_2).
3	10.06 (s, 1H, H^{15}), 8.92 (s, 1H, H^{10}), 8.87 (br, s, 1H, H^8), 8.24 (8) (d, 1H, H^5), 7.65 (m, 24H, H^2, H^4, H^6, H^7, H^{18-22}, Hs of PPh_3), 6.78 (br, s, 1H, H^3).
4	10.28 (s, 1H, H^{15}), 8.98 (s, 1H, H^{10}), 8.75 (br, s, 1H, H^8), 8.27 (8) (d, 1H, H^5), 7.95 (7) (d, 1H, H^4), 7.87 (8) (t, 1H, H^7), 7.65 (m, 19H, H^2, H^6, H^{18}, H^{22}, and Hs of PPh_3), 6.81 (br, s, 1H, H^3), 6.76 (br, s, 2H, H^{19}, H^{21}), 3.04 (s, 6H, NMe_2).

[a] In dmso-d6.

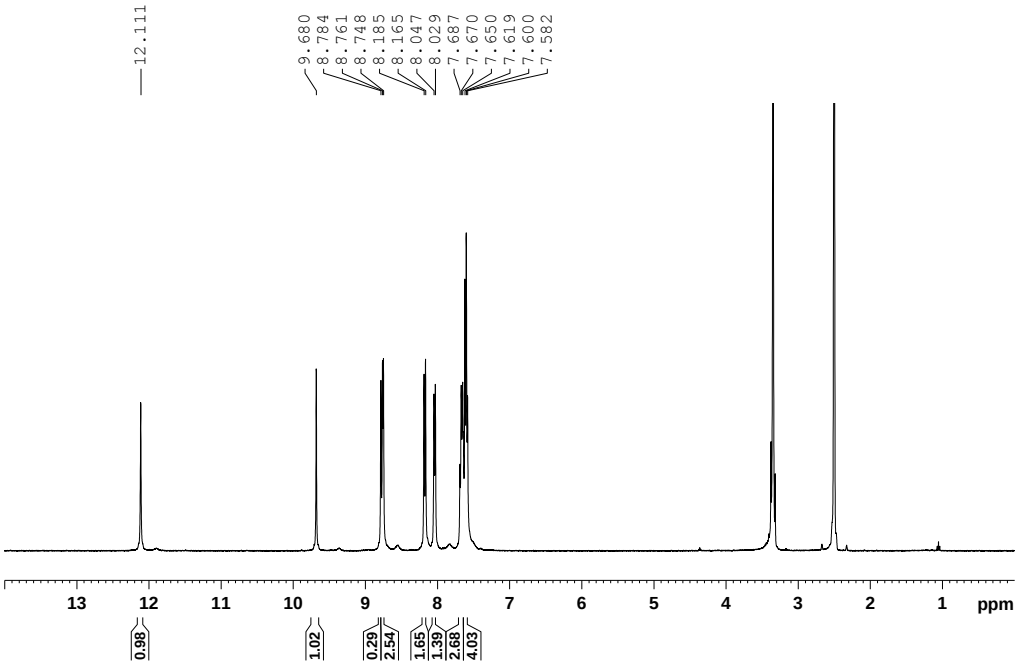

Figure 2.4. ^{1}H NMR spectrum of HL^{1}

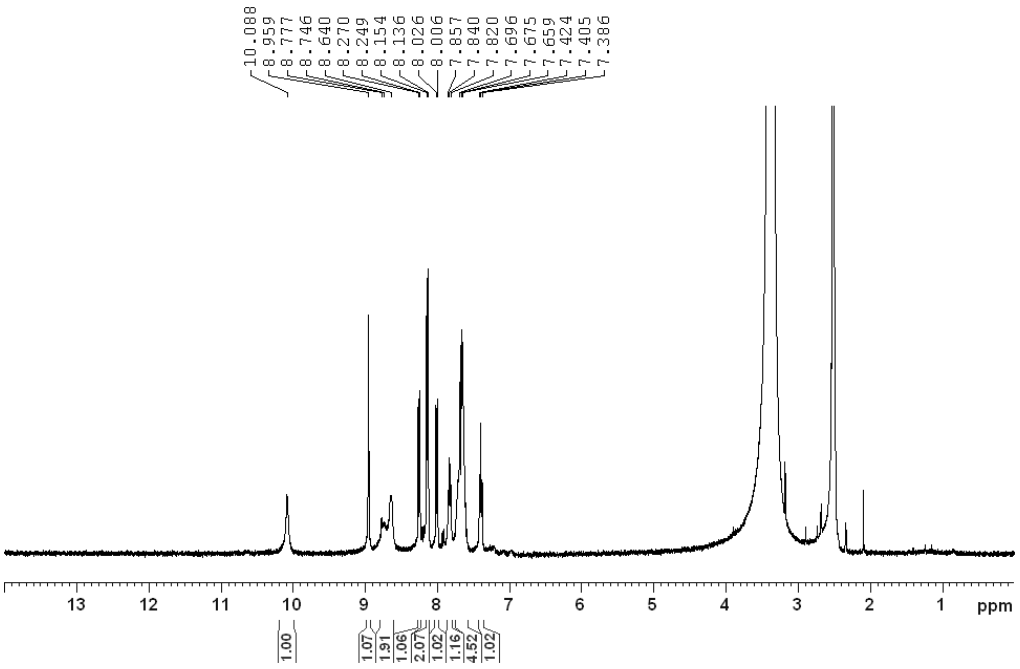

Figure 2.5. ^{1}H NMR spectrum of [Pd(HL^{1})Cl]

The H^1 and H^8 protons resonate together as a doublet at δ 8.77 and 8.73 in H_2L^1 and H_2L^2, respectively. In contrast, **1**−**4** display a doublet or a broad singlet in the same range (δ 8.75−8.87) corresponding to a single proton (H^8) due to the metallation at C_1 position. By and large, there is a downfield shift of the H^2 and H^4 protons and an upfield shift of the H^3 proton in the complexes compared to the free Schiff bases. These shifts further substantiate the metallation at C_1 position in **1**−**4**. Generally the resonances corresponding to H^{2-4} and H^{18-22} are upfield shifted in **3** and **4** compared to that in free Schiff bases and the chloro complexes (**1** and **2**) due to the shielding effects of the PPh_3 phenyl rings. The ^{31}P NMR spectra of **3** and **4** have been also examined. The spectrum of **3** is illustrated in Figure 2.6. A signal around δ 25.5 confirms the phosphine coordination in **3** and **4**.

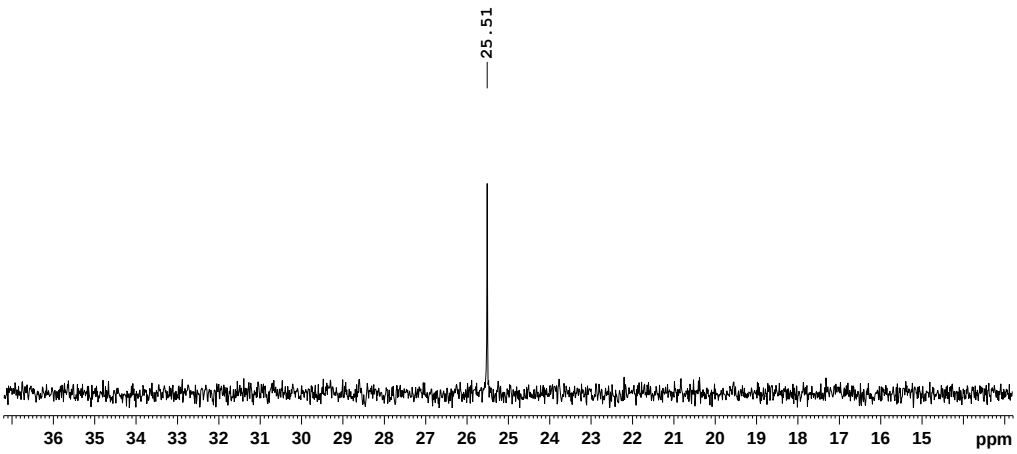

Figure 2.6. ^{31}P NMR spectrum of [Pd(L^1)(PPh_3)] (**3**)

2.3.5. Description of X-ray structures

The molecular structures of [Pd(HL^n)Cl] (**1** and **2**) and [Pd(L^n)(PPh$_3$)] (**3** and **4**) determined by X-ray crystallography are illustrated in Figures 2.7–2.10. Selected bond parameters associated with the metal ion for **1**−**4** are listed in Table 2.5. The metal centres are in distorted square-planar environment in all the complexes. The anthracenyl *peri*-C, the azomethine-N and the amide-O atom donor planar (HL^n)$^-$ and the chloride form a CNOCl square-plane around the metal centres in **1** and **2**. On the other hand, the anthracenyl *peri*-C, the azomethine-N and the iminolate-O atom donor (L^n)$^{2-}$ and the PPh$_3$ assemble a CNOP square-plane around the metal centres in **3** and **4**. In both type of complexes the tridentate ligands form 6,5-membered fused chelate rings. Each chelate ring is satisfactorily planar (rms deviations 0.01−0.13 Å). The values of the dihedral angle between the two fused chelate rings in **1** and **2** are 1.0(1) and 3.1(2)^o, respectively, while that in **3** and **4** are 12.3(2) and 6.00(3)^o, respectively. This relatively more non-coplanarity of the two chelate rings in **3** and **4** is most likely due to the bulky PPh$_3$. In **1** and **2**, the C(16)–O(1) bond length is shorter and the C(16)–N(2) bond length is longer compared to the corresponding bond lengths in **3** and **4** (Table 2.5). This difference is in agreement with the protonated form of the amide functionality in **1** and **2** and the iminolate form of the amide functionality in **3** and **4** [1−4,18]. The iminolate-O is expected to have better σ-bonding ability and hence better *trans* directing ability than the protonated amide O-atom. As a consequence the Pd−O(1) bond length is shorter and the Pd–C(1) bond length is longer in **3** and **4** compared to the corresponding bond lengths in **1** and **2** (Table 2.5). Significantly longer Pd−N(1) bond length in **3** and **4** than that in **1** and **2** is due to the superior *trans* effect of PPh$_3$ compared to that of chloride. Within [Pd(HL^n)Cl] (**1** and **2**), the Pd−O(1) bond length in **1** is longer than that in **2**. Similarly in [Pd(L^n)(PPh$_3$)] (**3** and **4**), the Pd−O(1) bond length in **3** is longer than that in **4**. The strong electron donating ability of the substituent NMe$_2$ at *para* to the aroyl group makes the amide-O of (HL^2)$^-$ and the

iminolate-O atom of $(L^2)^{2-}$ a better donor compared to the corresponding O-atoms in $(HL^1)^-$ and $(L^1)^{2-}$, respectively and hence the Pd−O(1) bond lengths turn out to be different in **1** and **2** and in **3** and **4**. Overall the Pd–C, Pd–N, Pd−O, Pd–Cl and Pd–P bond lengths and the bond angles observed in **1**−**4** are comparable with the values reported for cyclopalladated complexes with similar ligands [1,2,5−8,18,26,27].

Table 2.5. Selected bond lengths (Å) and angles (°) for **1**·Me_2NCHO, **2**·Me_2NCHO, **3**·MeCN and **4**

Complex	**1**·Me_2NCHO	**2**·Me_2NCHO	**3**·MeCN	**4**
Pd–C(1)	1.980(2)	1.994(5)	2.005(4)	2.001(2)
Pd–N(1)	1.959(2)	1.961(4)	1.990(3)	1.989(2)
Pd–O(1)	2.141(2)	2.123(3)	2.108(2)	2.070(2)
Pd–Cl/P	2.3256(6)	2.3146(16)	2.2876(11)	2.2927(6)
C(16)–O(1)	1.243(3)	1.252(5)	1.292(4)	1.280(3)
C(16)–N(2)	1.354(3)	1.348(6)	1.329(5)	1.321(3)
C(1)–Pd–N(1)	91.57(8)	91.76(18)	91.10(14)	92.28(9)
C(1)–Pd–O(1)	171.26(8)	171.60(17)	167.63(12)	169.86(8)
C(1)–Pd–Cl/P	99.00(7)	98.26(15)	97.36(11)	98.93(7)
N(1)–Pd–O(1)	79.69(6)	79.90(14)	78.76(11)	78.43(7)
N(1)–Pd–Cl/P	169.38(5)	169.91(12)	167.67(10)	165.94(5)
O(1)–Pd–Cl/P	89.74(4)	90.10(10)	93.81(8)	90.87(4)

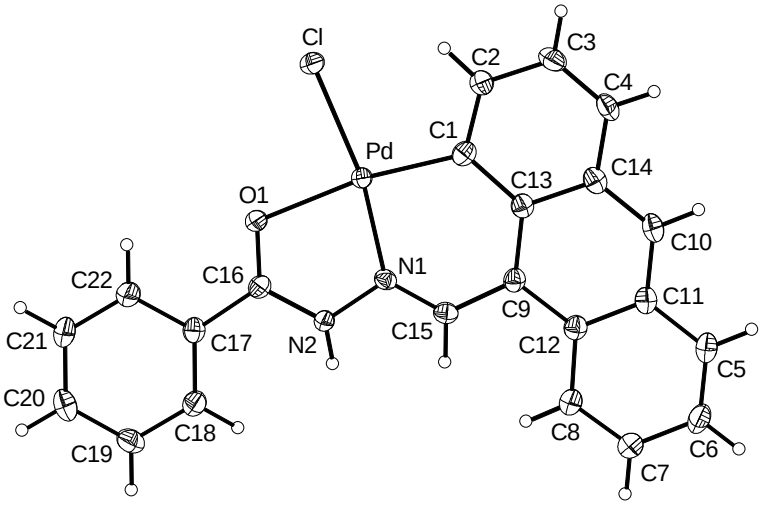

Figure 2.7. Molecular structures of [Pd(HL[1])Cl] (**1**) with the atom labeling schemes. All non-hydrogen atoms are represented by their 50% probability thermal ellipsoids.

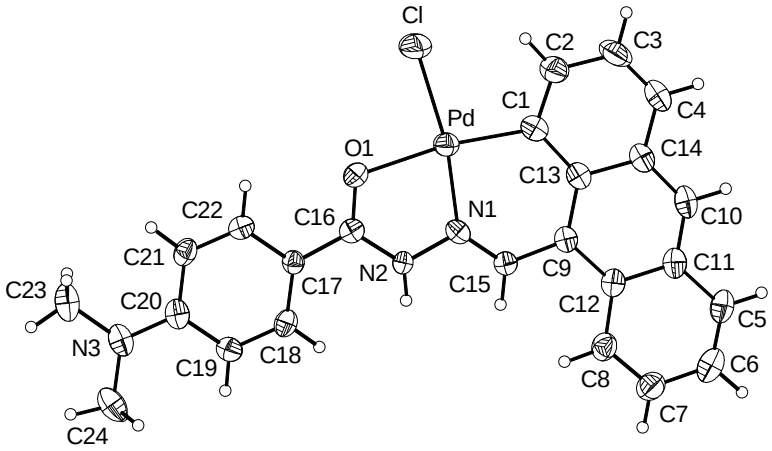

Figure 2.8. Molecular structures of [Pd(HL[2])Cl] (**2**) with the atom labeling schemes. All non-hydrogen atoms are represented by their 50% probability thermal ellipsoids.

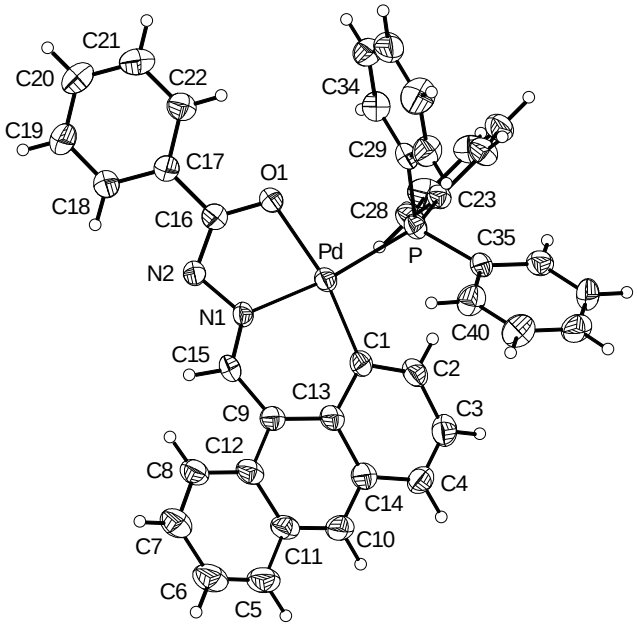

Figure 2.9. Molecular structures of [Pd(L^1)(PPh_3)] (**3**) with the atom labeling schemes. All non-hydrogen atoms are represented by their 50% probability thermal ellipsoids.

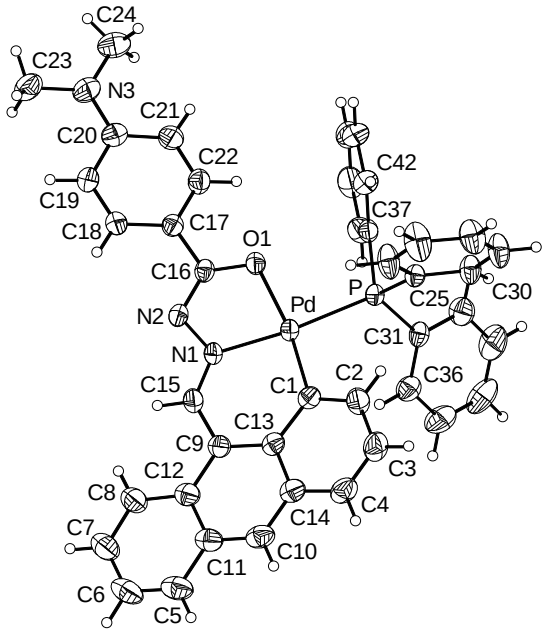

Figure 2.10. Molecular structures of [Pd(L^2)(PPh_3)] (**4**) with the atom labeling schemes. All non-hydrogen atoms are represented by their 50% probability thermal ellipsoids.

Among **1**−**4** only [Pd(L^2)(PPh_3)] (**4**) crystallizes without any solvent molecule. [Pd(HL^n)Cl] (**1** and **2**) crystallize as [Pd(HL^n)Cl]·Me_2NCHO (**1**·Me_2NCHO and **2**·Me_2NCHO) from dimethylformamide-diethylether. In each case, the solvent molecule is hydrogen bonded to the complex molecule. The O-atom of the Me_2NCHO is connected to the adjacent amide N−H and metal coordinated polarized azomethine C−H groups of the ligand $(HL^n)^-$. The N(2)···O(2) distances and the N(2)−H···O(2) angles are 2.762(2) Å and 168(3)^o and 2.765(5) Å and 162(5)^o for **1**·Me_2NCHO and **2**·Me_2NCHO, respectively. The C(15)···O(2) distances and the C(15)−H···O(2) angles are 3.120(3) Å and 145^o and 3.115(6) Å and 144^o for **1**·Me_2NCHO and **2**·Me_2NCHO, respectively. [Pd(L^1)(PPh_3)] (**3**) crystallizes from acetonitrile as **3**·CH_3CN. However, no significant interaction between the acetonitrile and the complex molecule could be detected here.

2.4. Conclusions

Cyclopalladated complexes [Pd(HL^n)Cl] (**1** and **2**) and [Pd(L^n)(PPh_3)] (**3** and **4**) with the Schiff bases 4-*R*-N′-(9-anthracenylidene)benzohydrazides (H_2L^n, *R* = H (n = 1) and NMe_2 (n = 2)) have been synthesized. The deprotonation of the amide functionality in [Pd(HL^n)Cl] occurs in presence of excess PPh_3 with the formation of [Pd(L^n)(PPh_3)]. Elemental analysis and various spectroscopic measurements have been used for the characterization of the complexes. X-ray crystal structures show that the $(HL^n)^-$ acts as the anthracenyl *peri*-C, the azomethine-N and the amide-O donor, while $(L^n)^{2-}$ acts as the anthracenyl *peri*-C, the azomethine-N and the iminolate-O donor. Both $(HL^n)^-$ and $(L^n)^{2-}$ form 6,5-membered fused chelate rings. Except for the red-shift the electronic spectra of **1**−**4** are very similar with the spectra of the Schiff bases (H_2L^1 and H_2L^2) and anthracene. Both H_2L^1, H_2L^2 and the complexes **1**−**4** are emissive. The Schiff base H_2L^2 having strong electron donor substituent *R* = NMe_2 displays dual fluorescence but not the complexes (**2** and **4**) with it.

2.5. References

[1] S. Das, S. Pal, *J. Organomet. Chem.* 689 (2004) 352–360.

[2] S. Das, S. Pal, *J. Organomet. Chem.* 691 (2006) 2575–2583.

[3] R. Raveendran, S. Pal, *J. Organomet. Chem.* 692 (2007) 824–830.

[4] R. Raveendran, S. Pal, *J. Organomet. Chem.* 694 (2009) 1482–1486.

[5] J. Albert, R. Bosque, J. Granell, R. Tavera, *J. Organomet. Chem.* 595 (2000) 54–58.

[6] J. Zhou, Q. Wang, H. Sun, *Acta Crystallogr*. E64 (2008) m688.

[7] C. M. Anderson, M. Crespo, J. M. Tanski, *Organometallics* 29 (2010) 2676−2684.

[8] J. Zhou, X. Li, H. Sun, *J. Organomet. Chem.* 695 (2010) 297−303.

[9] D. D. Perrin, W. L. F. Armarego, D. P. Perrin, *Purification of Laboratory Chemicals* 2nd ed., Pergamon, Oxford, 1983.

[10] *SMART version 5.630 and SAINT-plus version 6.45* Bruker-Nonius Analytical X-ray Systems Inc., Madison, WI, USA, 2003.

[11] G. M. Sheldrick, *SADABS, Program for Area Detector Absorption Correction* University of Göttingen, Göttingen, Germany, 1997.

[12] *CrysAlisPro version 1.171.33.55* Oxford Diffraction Ltd., Abingdon, Oxfordshire, UK, 2007.

[13] G. M. Sheldrick, *XHELX-97, Structure Determination Software* University of Göttingen, Göttingen, Germany, 1997.

[14] L. J. Farrugia, *J. Appl. Crystallogr*. 32 (1999) 837−838.

[15] P. McArdle, *J. Appl. Crystallogr*. 28 (1995) 65.

[16] A. L. Spek, *Platon, A Multipurpose Crystallographic Tool* Utrecht University, Utrecht, The Netherlands, 2002.

[17] Z. Bedlovičová, J. Imrich, P. Kristian, I. Danihel, S. Böhm, D. Sabolová, M. Kožurková, H. Paulíková, K.D. Klika, *Heterocycles* 80 (2010) 1047−1066.

[18] S. Tollari, G. Palmisano, F. Dematrin, M. Grassi, S. Magnaghi, S. Cenini, *J. Organomet. Chem*. 488 (1995) 79−83.

[19] N. R. Sangeetha, S. Pal, *J. Chem. Cryst*. 29 (1999) 287−293.

[20] H. Du, R. A. Fuh, J. Li, L. A. Corkan, J. S. Lindsey, *Photochem. Photobiol*. 68 (1998) 141−142.

[21] R. N. Jones, *Chem. Rev*. 41 (1947) 353−371.

[22] L. Cuffe, R. D. A. Hudson, J. F. Gallagher, S. Jennings, C. J. McAdam, R. B. T. Connelly, A. R. Manning, B. H. Robinson, J. Simpson, *Organometallics* 24 (2005) 2051−2060.

[23] Y. –Y. Liu, M. Grzywa, M. Tonigold, G. Sastre, T. Schüttrigkeit, N. S. Leeson, D. Volkmer, *Dalton Trans*. 40 (2011) 5926–5938.

[24] T. Soujanya, G. Saroja, A. Samanta, *Chem. Phys. Lett*. 236 (1995) 503−509.

[25] Z. R. Grabowski, K. Rotkiewicz, *Chem. Rev*. 103 (2003) 3899−4031.

[26] J. M. Vila, T. Pereira, J. M. Ortigueira, M. López-Torres, A. Castiñeiras, D. Lata, J. J. Fernández, A. Fernández, *J. Organomet.Chem.* 556 (1998) 21−30.

[27] A. Fernández, M. López-Torres, A. Suárez, J. M. Ortigueira, T. Pereira, J. J. Fernández, J. M. Vila, H. Adams, *J. Organomet. Chem.* 598 (2000) 1−12.

Chapter 3

Regioselective cyclopalladation of 4-*R*-N′-(3-indolylidene)benzohydrazides [§]

Reactions of $PdCl_2$, LiCl, 4-*R*-N′-(3-indolylidene)benzohydrazides (H_2L^n; n = 1, 2, 3 and 4 for *R* = H, Cl, OMe and NMe_2, respectively) and $CH_3COONa{\cdot}3H_2O$ (68 mg, 0.5 mmol) in 1:2:1:1 mole ratio in methanol produce the cyclopalladated species of general formula $[Pd(HL^n)Cl]$ in 65−85% yields. The complexes have been characterized with the help of elemental analysis and spectroscopic (infrared, electronic and NMR) measurements. The proton NMR spectra of the complexes suggest palladation at the peri position of the indole moiety in $(HL^n)^-$. Molecular structure of a representative complex determined by X-ray crystallography confirms the *peri*-palladation and formation of a distorted CNOCl square-plane around the metal centre by the tridentate $(HL^n)^-$ and the chloride.

3.1. Introduction

In the previous chapter, we have explored the *peri*-palladates of general formulas $[Pd(HL^n)Cl]$ and $[Pd(L^n)(PPh_3)]$ with 4-*R*-N′-(9-anthracenylidene)benzohydrazides. As we stated in the earlier chapter metallation of fused heterocyclic and aromatic rings are rare. In this chapter, we report the cyclopalladation of 4-*R*-N′-(3-indolylidene)benzohydrazides (H_2L^n, 2 H represent the dissociable protons from the amide functionality and indole ring). These ligands offer either of the two positions namely 2 or *ortho* and 4 or *peri* of the indole moiety for cyclometallation and as C,N,O-donor it can form either 5,5- or 6,5-membered fused chelate rings (Chart 3.1). It may also be noted that in recent time's indole containing ligands and their metal

[§] This work has been published in *J. Organomet. Chem.* 696 (2011) 2660–2664.

complexes are receiving considerable attention for their biological and clinical relevance [1−4]. There are only two reports on X-ray structurally characterized cyclometallated complexes with such ligands. These ligands are bidentate alkaloids gramine and tryptamine and (S)-triptophan methyl ester [5] and the tridentate Schiff bases prepared by condensation of indole-3-carboxaldehyde with semicarbazide, ethyl hydrazinecarboxylate and acetylhydrazine [6]. We have tried to synthesize cylcopalladated species with H_2L^n to find out regioselectivity of the metallation. Herein we describe the synthesis, structure and properties of a family of *peri*-metallated complexes having the general formula [Pd(HL^n)Cl].

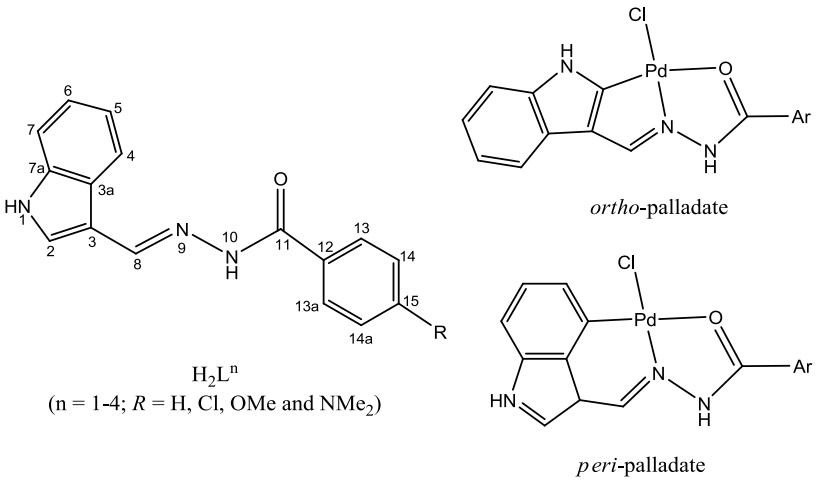

Chart 3.1. Indole-3-carboxaldehyde aroylhydrazone and possible cyclopalladates.

3.2. Experimental

3.2.1. Materials

Purification of solvents was performed by standard methods [7]. All the chemicals used in this work were of analytical grade available commercially and were used without further purification.

3.2.2. Physical measurements

A Thermo Finnigan Flash EA1112 series elemental analyzer was used to collect the elemental (C, H, N) analysis data. A Shimadzu LCMS 2010

liquid chromatograph mass spectrometer was used for the purity verification. Solution electrical conductivities were measured with a Digisun DI-909 conductivity meter. Infrared spectra were recorded on a Jasco-5300 FT-IR spectrophotometer by using KBr pellets. A Perkin-Elmer Lambda 35 UV/vis spectrophotometer was used to collect the electronic spectra. The proton NMR spectra were recorded with the help of a Bruker 400 MHz NMR spectrometer.

3.2.3. Synthesis of [Pd(HL^1)Cl] (1)

A mixture of $PdCl_2$ (89 mg, 0.5 mmol) and LiCl (43 mg, 1 mmol) was taken in 15 ml of dry methanol and refluxed with stirring for 1 h. It was then cooled to room temperature and filtered. H_2L^1 (132 mg, 0.5 mmol) and $CH_3COONa{\cdot}3H_2O$ (68 mg, 0.5 mmol) were added to the filtrate and the mixture was stirred at room temperature for 12 h. The complex separated as a green solid was collected by filtration, washed with cold methanol and finally dried in air. Yield: 170 mg (84%).

The other three complexes namely [Pd(HL^2)Cl] (**2** (*R* = Cl)), [Pd(HL^3)Cl] (**3** (*R* = OMe)) and [Pd(HL^4)Cl] (**4** (*R* = NMe_2)) were synthesized from $PdCl_2$, LiCl, the corresponding Schiff base (H_2L^n) and $CH_3COONa{\cdot}3H_2O$ in 65–85% yields by following procedures very similar to that described above for **1** (*R* = H).

3.2.4. X-ray crystallography

A Bruker-Nonius SMART APEX CCD single crystal diffractometer, equipped with a graphite monochromator and a Mo $K\alpha$ fine-focus sealed tube (λ = 0.71073 Å) was used for determination of unit cell parameters and intensity data collection at 298 K. The SMART and the SAINT-Plus packages [8] were used for data acquisition and data extraction, respectively. The absorption correction was performed with the help of SADABS program [9]. The structure was solved by direct method and refined on F^2 by full-matrix

Table 3.1. Selected crystallographic data.

Chemical formula	$PdC_{18}H_{15}N_4OCl$
Formula weight	445.22
Crystal system	Triclinic
Space group	$P\bar{1}$
a (Å)	9.3308(10)
b (Å)	10.4842(11)
c (Å)	10.6176(11)
α	66.404(2)
β (º)	84.781(2)
γ	66.675(2)
V (Å^3)	871.23(16)
Z	2
ρ (g cm^{-3})	1.697
μ (mm^{-1})	1.232
Reflections collected	8421
Reflections unique	3053
Reflections [$I \geq 2\sigma(I)$]	2854
Parameters	227
$R1$, $wR2$ [$I \geq 2\sigma(I)$]	0.0318, 0.0717
$R1$, $wR2$ [all data]	0.0352, 0.0730
GOF on F^2	1.105
Largest diff. peak and hole (e Å^{-3})	0.500, –0.272

least-squares procedures. All non-hydrogen atoms were refined anisotropically. The hydrogen atoms were included in the structure factor calculation at idealized positions by using a riding model. The SHELX-97 programs [10] were used for structure solution and refinement. The ORTEX6a [11] and Platon packages [12] were used for molecular graphics. All the crystallographic data (except for the structure factors) have been deposited with the Cambridge Crystallographic Data Centre. The deposition number is CCDC 811956 for **1**·CH_3CN. Selected crystallographic data are summarized in Table 3.1.

3.3. Results and discussion

3.3.1. Synthesis and characterization

The Schiff bases (H_2L^n) were prepared in 75–90% yields by condensation reactions of equimolar amounts of indole-3-carboxaldehyde and the corresponding 4-*R*-benzoylhydrazine (*R* = H, Cl, OMe and NMe_2) in presence of a few drops of acetic acid in ethanol [21]. Their molecular formulae and structures were confirmed with the help of elemental analysis (Table 3.2) and spectroscopic (mass and proton NMR) measurements. Reactions of H_2L^n and $CH_3COONa·3H_2O$ with Li_2PdCl_4 (generated in situ from one mole equivalent of $PdCl_2$ and two mole equivalents of LiCl) in dry methanol provide the cyclometallated species in moderate to good yields. The elemental analysis data (Table 3.2) of the complexes (**1**−**4**) are consistent with the general formula [Pd(HL^n)Cl]. As expected for palladium(II) species, **1**−**4** are diamagnetic. The solubility of all four complexes in polar acetone, acetonitrile, dimethylformamide and dimethylsulfoxide is moderate to high, while they are slightly soluble in relatively much less polar halogenated solvents such as dichloromethane and chloroform. In solution, **1**−**4** behave as non-electrolyte. Thus the chloride is coordinated to the metal centre in each complex.

Table 3.2. Elemental analysis and electronic spectroscopic[a] data.

Complex	Found (calc.) (%)			λ_{max} (nm) (10^{-4} x ε (M^{-1} cm^{-1}))
	C	H	N	
1	47.55 (47.21)	2.99 (3.05)	10.40 (10.55)	407 (5.92), 386 (7.89), 370 (5.92), 350[b] (3.38), 293[b] (2.53)
2	43.81 (43.54)	2.53 (2.38)	9.58 (9.35)	410 (5.78), 390 (7.84), 373 (5.87), 354[b] (3.43), 297[b] (2.48)
3	47.03 (47.12)	3.25 (3.36)	9.68 (9.59)	406 (6.40), 386 (8.18), 369 (5.97), 348[b] (3.41), 315[b] (2.36)
4	48.34 (48.03)	3.83 (3.72)	12.53 (12.37)	412 (7.06), 391 (8.77), 373 (6.32), 354[b] (3.84), 311 (4.56)

[a] In dimethylformamide.

[b] Shoulder.

3.3.2. Infrared spectral properties

Infrared spectra of **1**−**4** display the two N−H and the C=O stretches in the frequency ranges 3195−3605 and 1597−1615 cm^{-1}, respectively [6,13]. The C=O stretches in **1**−**4** are about 15−25 cm^{-1} lower than the C=O stretches displayed by the free Schiff bases (H_2L^n). A strong band observed in the range 1600−1612 cm^{-1} for H_2L^n is attributed to the C=N stretch. The corresponding band for **1**−**4** appears at a lower frequency range of 1560−1580 cm^{-1} [14−17,6]. The lowering of both C=O and C=N stretches indicates that the ligand $(HL^n)^-$ coordinates to the metal centre through the azomethine N-atom and the protonated amide functionality O-atom forming a five-membered chelate ring. A representative infrared spectrum is shown in Figure 3.1.

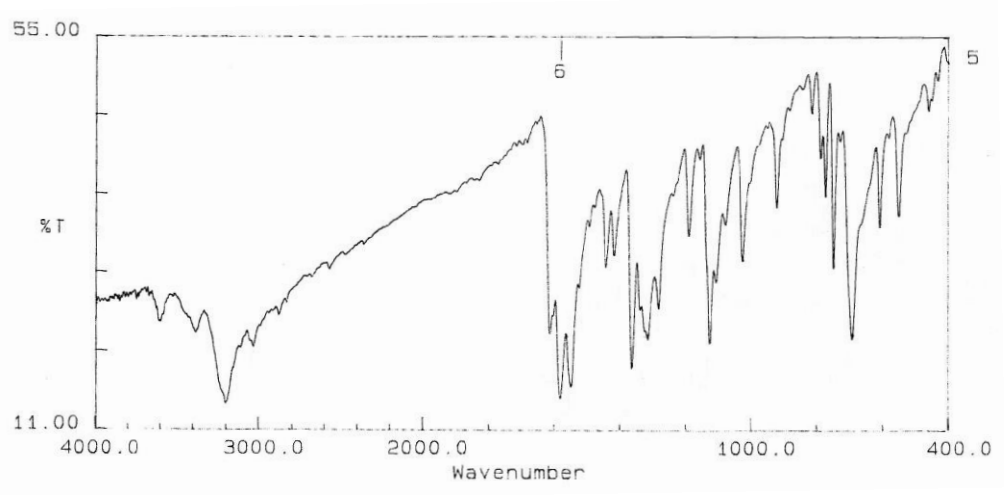

Figure 3.1. Infrared spectrum of $[Pd(HL^1)Cl]$ (**1**).

3.3.3. Electronic spectral properties

The electronic spectra of **1**−**4** were collected in dimethylformamide. The spectral data are listed in Table 3.2 and a representative spectrum is shown in Figure 3.2. The spectral profiles of **1**−**4** are very similar except for some small shifts in the band positions. They display three strong peaks in the wave length range 412−369 nm. These are followed by two shoulders within

354−293 nm for **1**−**3** and a shoulder and a peak at 354 and 311 nm, respectively for **4** (Table 3.2). The free Schiff bases in dimethylformamide show only two absorptions in the ranges 333−323 and 289−268 nm. Thus the longer and the shorter wavelength absorptions displayed by **1**−**4** are due to charge transfer and ligand centred transitions, respectively [14,15,18,19].

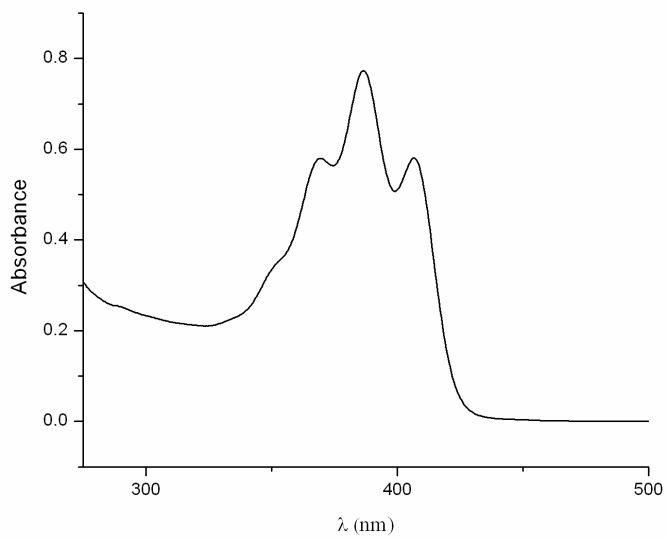

Figure 3.2. Electronic spectrum of [Pd(HL^1)Cl] (**1**).

3.3.4. NMR spectral properties

The proton NMR spectra of the complexes and the free Schiff bases were recorded in dmso-d6. The data for the complexes are listed in Table 3.3. The ^{1}H NMR spectrum of **1** is shown in Figure 3.3. The H^4 proton observed as a doublet within δ 7.77−7.84 for the free Schiff bases is absent in the spectra of the complexes. The absence of this resonance indicates *peri*-metallation of the indole moiety in **1**−**4**. In general, the resonances in the complexes show a downfield shift compared to the corresponding resonances observed for the free Schiff bases. However, the downfield shift by δ 0.5−0.6 of the H^5 is significantly larger compared to that (δ 0.1−0.2) of the other C−H protons. This large shift of H^5 corroborates *peri*-metallation of the indole ring in **1**−**4**. The singlets corresponding to indole N−H (H^1 δ 11.52−11.60) and the amide N−H (H^{10} δ 11.22−11.60) protons are very closely spaced for the free Schiff

bases. On the other hand, these signals are well separated in the spectra of **1**−**4** due to disproportionate downfield shift of both. The indole N−H (H^1) appears within δ 12.08−12.20, while amide N−H (H^{10}) appears in the range δ 13.31−13.93. The much larger downfield shift of the latter indicates coordination of the azomethine N-atom adjacent to the amide N−H and hence formation of a six-membered metallacycle in each of **1**−**4** (Chart 3.1). In the aroyl fragment, the *meta* protons (H^{13}, H^{13a}) with respect to the substituent (*R*) resonate as a doublet within δ 7.87−8.04. The *ortho* protons appear as a triplet for **1** (*R* = H), broad singlet for **2** (*R* = Cl) and doublet for **3** (*R* = OMe) and **4** (*R* = NMe_2) in the range δ 6.82−7.71. The methyl protons of *R* in **3** and **4** appear as singlet at δ 3.87 and 3.03, respectively; while, the proton (H^{15}) at the same position in **1** appears as a triplet at δ 7.72.

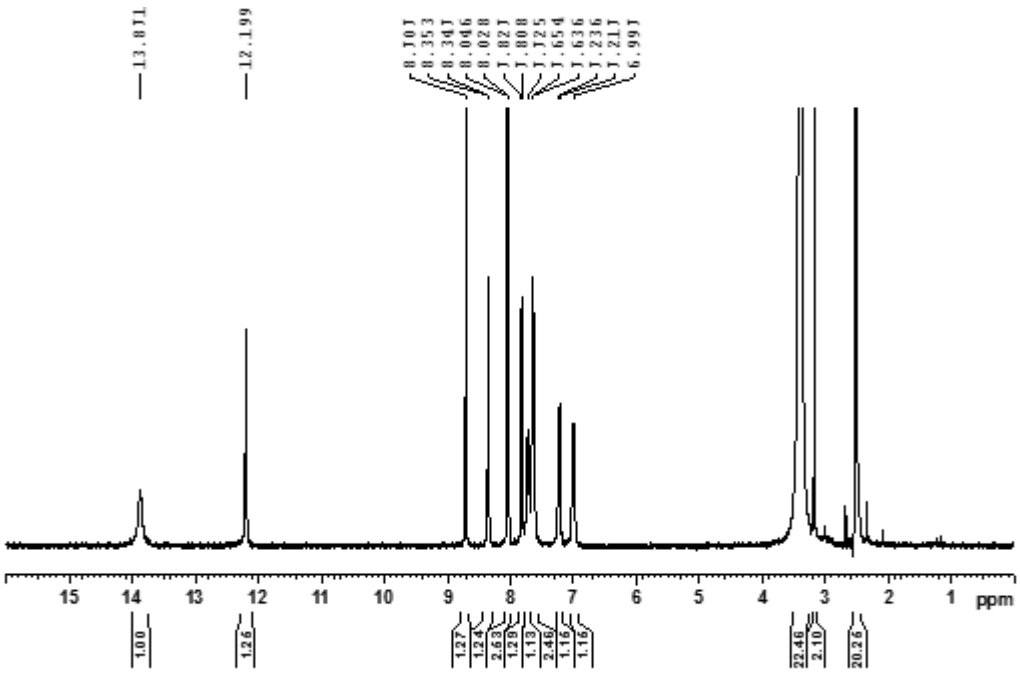

Figure 3.3. ^{1}H NMR spectrum of [Pd(HL^1)Cl] (**1**).

Table 3.3. ^{1}H NMR data[a] (δ (ppm) (J (Hz))) for complexes **1**−**4**.

Complex	H(1)	H(2)	H(5)	H(6)	H(7)	H(8)	H(10)	H(13,13a)	H(14,14a)	R
1 (*R* = H)	12.18 (s)	8.34 (d) (2)	7.80 (d) (8)	6.98 (br,s)	7.21 (d) (7)	8.69 (s)	13.86 (s)	8.02 (d) (7)	7.63 (t) (7)	7.72 (t) (6)
2 (*R* = Cl)	12.20 (s)	8.33 (br,s)	7.80 (d) (7)	6.99 (br,s)	7.21 (br,s)	8.68 (s)	13.93 (s)	8.04 (d) (8)	7.71 (br,s)	−
3 (*R* = OMe)	12.14 (s)	8.30 (d) (3)	7.79 (d) (8)	6.98 (br,s)	7.20 (d) (7)	8.66 (s)	13.63 (s)	8.00 (d) (9)	7.16 (d) (8)	3.87 (s)
4 (*R* = NMe_2)	12.08 (s)	8.27 (d) (2)	7.78 (d) (8)	6.96 (br,s)	7.19 (d) (6)	8.64 (s)	13.31 (s)	7.87 (d) (9)	6.82 (d) (9)	3.03 (s)

[a] In dmso-d6.

The comparable spectral characteristics suggest that **1**−**4** have similar molecular structures. The coordination of the chloride to the square-planar bivalent palladium centre is confirmed by their non-electrolytic and diamagnetic nature. Thus it becomes apparent that the deprotonated Schiff base $(HL^n)^-$ acts as a tridentate indole *peri*-C, azomethine-N and amide-O donor ligand to form a 6,5-membered fused chelate rings system and together with the chloride constitutes a CNOCl square-plane around the metal centre in **1**−**4**.

3.3.5. Description of X-ray structures

To confirm the above molecular structure we have tried to grow single crystals of all the complexes. X-ray quality crystals could be grown for only **1** by slow evaporation of its acetonitrile solution. The complex crystallizes as **1**·CH_3CN in the space group $P\bar{1}$. The asymmetric unit contains one molecule each of the complex and acetonitrile. The structure of **1** is illustrated in Figure 3.4. Selected bond parameters are listed in Table 3.4. As expected $(HL^n)^-$ is indole *peri*-C, azomethine-N and amide-O donor and the fourth coordination site of the square-planar metal centre is satisfied by the chloride. The C−O and C−N bond lengths in the –C(=O)−NH− fragment in $(HL^1)^-$ clearly indicate the protonated state of the amide functionality [14,6,13,20,21]. The Pd−C, Pd−N and Pd−O bond lengths are within the range reported for bivalent palladium having similar coordinating atoms [14,15,6,20−22]. The Pd−Cl bond length is unexceptional [14,22−24]. The PdCNOCl square-plane is not ideal with respect to the bond parameters associated with the metal centre. The C(1)−Pd−N(2) angle in the six-membered ring is 94.54(12)°, while the O(1)−Pd−N(2) angle in the five-membered ring is 78.26(9)°. However, the CNOCl square-plane including the metal centre is perfectly planar (mean deviation 0.01 Å). In fact except for the phenyl ring C(11)−C(16) rest of the molecule lie in a single plane (Figure 3.4). The maximum and the minimum deviations from the mean plane constituted by Pd, Cl, O(1), N(1)−N(3) and

C(1)−C(10) are 0.077 and 0.003 Å, respectively. The phenyl ring plane (mean deviation 0.006 Å) is slightly twisted along the C(10)−C(11) bond. The dihedral angle between the phenyl ring plane and the plane containing remaining atoms of **1** is 19.6(1)^{o}.

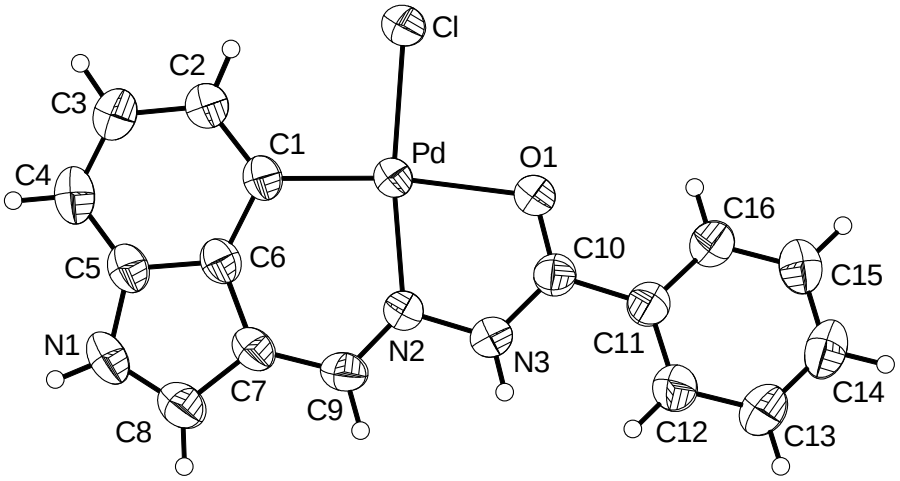

Figure 3.4. Molecular structure of [Pd(HL^{1})Cl] (**1**) with the atom labeling scheme. All non-hydrogen atoms are represented by their 50% probability thermal ellipsoids.

Table 3.4. Selected bond lengths (Å) and angles (^{o}) for **1**·CH_3CN.

Pd−C(1)	1.972(3)	Pd−O(1)	2.156(2)
Pd−N(2)	2.016(3)	Pd−Cl	2.299(1)
C(10)−O(1)	1.240(4)	C(10)−N(3)	1.342(4)
C(1)−Pd−O(1)	172.57(11)	C(1)−Pd−N(2)	94.54(12)
C(1)−Pd−Cl	94.08(10)	O(1)−Pd−N(2)	78.26(9)
O(1)−Pd−Cl	93.18(6)	N(2)−Pd−Cl	171.25(7)

We have scrutinized the X-ray structure of **1**·CH_3CN for possible intermolecular non-covalent interactions to explore its self-assembly pattern and the packing in the crystal lattice. Two types of intermolecular hydrogen bonds are found. These involve the indole N(1)−H(1) and the amide N(3)−H(3) as donors and palladium bound Cl and acetonitrile-N, respectively as acceptors. The N(1)···Cl distance is 3.220(3) Å and N(1)−H(1)···Cl angle is 150^o while, the N(3)···N(4) distance is 3.033(5) Å and N(3)−H(3)···N(4) angle is 152^o. The amide-NH···N(acetonitrile) interaction connects the complex with the acetonitrile and the indole-NH···Cl interaction leads to a one-dimensional linear assembly of the **1**·CH_3CN units in the crystal lattice (Figure 3.5).

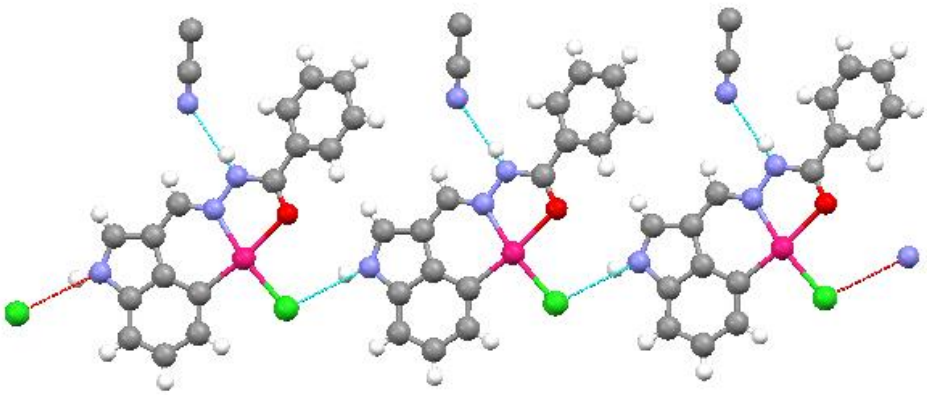

Figure 3.5. One-dimensional ordering of N−H···N connected [Pd(HL^1)Cl]·CH_3CN (**1**·CH_3CN) via N−H···Cl hydrogen bonds.

3.4. Conclusions

Synthesis and characterization of a new series of cyclopalladated complexes, [Pd(HL^n)Cl], with the tridentate Schiff bases 4-*R*-N′-(3-indolylidene)benzohydrazides (H_2L^n, *R* = H, Cl, OMe and NMe_2) have been reported. The deprotonated Schiff bases can act as C,N,O-donor ligands due to the accessibility of either the *ortho*- or the *peri*-C of their indole fragment for cyclometallation. In [Pd(HL^n)Cl], *peri*-metallation with the formation of

6,5-membered fused chelate rings is preferred over *ortho*-metallation and formation of 5,5-membered fused chelate rings (Chart 3.1).

3.5. References

[1] Z. Huang, S. Li, R. Korngold, *Peptide Science* 43 (1997) 367−382.

[2] Y. Shimazaki, T. Yajima, M. Takani, O. Yamauchi, *Coord. Chem. Rev*. 253 (2009) 479−492.

[3] H. Shirinzadeh, A. D. Yilmaz, M. Gumustas, S. Suzen, S. Ozden, S. A. Ozkan, *Comb. Chem. High Throughput Screen*. 13 (2010) 619−627.

[4] G. Gurkok, N. Altanlar, S. Suzen, *Chemother*apy. 55 (2009) 15−19.

[5] R. Annuunziata, S. Cenini, F. Demartin, G. Palmisano, S. Tollari, *J. Organomet. Chem*. 496 (1995) C1−C3.

[6] S. Tollari, G. Palmisano, F. Dematrin, M. Grassi, S. Magnaghi, S. Cenini, *J. Organomet. Chem*. 488 (1995) 79−83.

[7] D. D. Perrin, W. L. F. Armarego, D. P. Perrin, *Purification of Laboratory Chemicals* 2nd ed., Pergamon, Oxford, 1983.

[8] *SMART version 5.630 and SAINT-plus version 6.45* Bruker-Nonius Analytical X-ray Systems Inc., Madison, WI, USA, 2003.

[9] G. M. Sheldrick, *SADABS, Program for area detector absorption correction* University of Göttingen, Göttingen, Germany, 1997.

[10] G. M. Sheldrick, *SHELX-97, Structure Determination Software* University of Göttingen, Göttingen, Germany, 1997.

[11] P. McArdle, *J. Appl. Crystallogr*. 28 (1995) 65.

[12] A. L. Spek, *PLATON, A multipurpose Crystallographic Tool* Utrecht University, Utrecht, The Netherlands, 2002.

[13] N. R. Sangeetha, S. Pal, *J. Chem. Cryst*. 29 (1999) 287−293.

[14] S. Das, S. Pal, *J. Organomet. Chem*. 689 (2004) 352−360.

[15] S. Das, S. Pal, *J. Organomet. Chem*. 691 (2006) 2575−2583.

[16] R. Raveendran, S. Pal, *J. Organomet. Chem*. 692 (2007) 824−830.

[17] R. Raveendran, S. Pal, *J. Organomet. Chem*. 694 (2009) 1482−1486.

[18] H. Jude, J. A. K. Bauer, W. B. Connick, *Inorg. Chem*. 41 (2002) 2275−2281.

[19] E. V. Ivanova, M. V. Puzyk, K. P. Balashev, *Russ. J. Gen. Chem*. 79 (2009) 2096−2101.

[20] J. M. Vila, T. Pereira, J. M. Ortigueira, M. López-Torres, A. Castiñeiras, D. Lata, J. J. Fernández, A. Fernández, *J. Organomet.Chem*. 556 (1998) 21−30.

[21] A. Fernández, M. López-Torres, A. Suárez, J. M. Ortigueira, T. Pereira, J. J. Fernández, J. M. Vila, H. Adams, *J. Organomet. Chem*. 598 (2000) 1−12.

[22] N. H. Kiers, B. L. Feringa, H. Kooijman, A. L. Spek, P. W. N. M. van Leeuwen, *J. Chem. Soc., Chem. Commun*. (1992) 1169−1170.

[23] A. Onoda, K. Kawakita, T. Okamura, H. Yamamoto, N. Ueyama, *Acta Crystallogr*. E59 (2003) m291−m293.

[24] D. Li, D. Liu, *J. Chem. Crystallogr*. 33 (2003) 989−991.

Chapter 4

Regioselective cyclopalladation of N′-(4-*R*-1-naphthylidene)benzohydrazide[§]

Reactions of Li_2PdCl_4, N′-(4-*R*-1-naphthylidene)benzohydrazide (H_2L^n; n = 1 and 2 for *R* = H and OMe, respectively) and $CH_3COONa{\cdot}3H_2O$ in 1:1:1 mole ratio in methanol provide the cyclopalladated complexes with the general formula [Pd(HL^n)Cl] (**1** (*R* = H) and **2** (*R* = OMe)). Treatment of one mole equivalent of [Pd(HL^n)Cl] (**1** and **2**) with two mole equivalents of PPh_3 in acetone results in the deprotonation of the O-coordinated amide functionality and the replacement of the metal coordinated chloride with PPh_3 leading to the formation of [Pd(L^n)(PPh_3)] (**3** and **4**). All the complexes have been characterized with the help of elemental analysis and spectroscopic (IR, UV-Vis and ^{1}H NMR) measurements. NMR spectra indicates the *peri*-metallation of the 1-naphthalenyl fragment of the tridentate ligand in **1**–**4**. Molecular structures determined by X-ray crystallography confirm the regioselective *peri*-metallation in each of **2**, **3** and **4**.

4.1. Introduction

In the preceding two chapters, we have reported some *peri*-palladates with 4-*R*-benzoylhydrazones derived from 9-anthraldehyde and indole-3-carboxaldehyde. It may be noted that in the case of 3-indolyl both *ortho* and *peri* positions are available for metallation, while in the case of 9-anthraldehyde only *peri* position is available for metallation. Cyclometallated complexes with various bidentate and tridentate ligands containing polycyclic aromatic fragments such as 3-indolyl, 1-naphthalenyl, 9-phenanthryl, 1-pyrenyl and 3-perilenyl are available in literature [1–17]. Among the bidentate ligands, majority produce exclusively *ortho*-metallated species [1−7], while

[§] This work has been published in *J. Organomet. Chem.* 731 (2013) 67–72.

few give both *ortho*- and *peri*-metallated complexes [8−10]. On the other hand, the tridentate ligands produce exclusively either *peri*-metallated [11−14,18] or *ortho*-metallated species [5,15−17]. The dominance of *ortho* metallation over *peri* metallation in bidentate ligands is attributed to more stable 5-membered than less stable 6-membered cyclometallated ring formation [9,12]. In this chapter, we have studied the chemistry of palladium with the potentially tridentate C,N,O-donor N′-(4-*R*-1-naphthylidene)-benzohydrazide (H_2L^n, n = 1 and 2 for *R* = H and OMe, respectively) and found regioselective *peri* metallation of the 1-naphthalenyl fragment of the ligands (Scheme 4.1). Herein, we describe syntheses, characterization and X-ray crystal structures of these *peri*-metallated complexes.

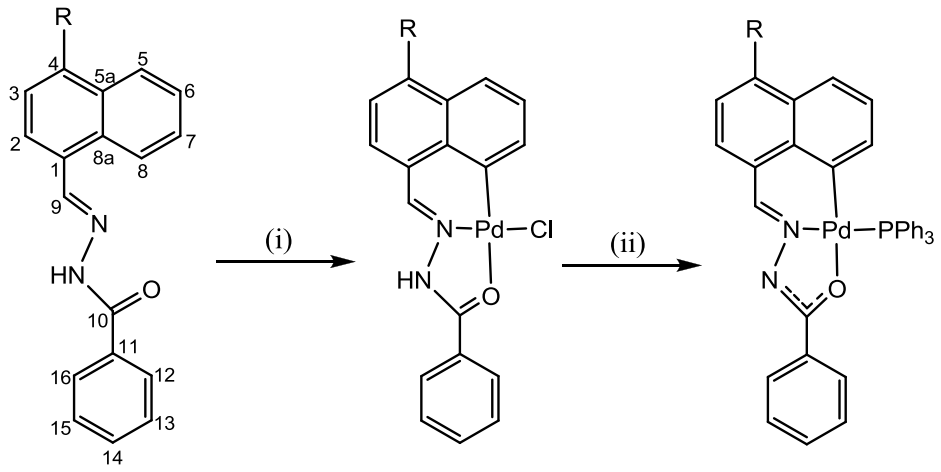

H_2L^n
R = H (n = 1) and OMe (n = 2)

1 (*R* = H)
2 (*R* = OMe)

3 (*R* = H)
4 (*R* = OMe)

Scheme 4.1. (i) Li_2PdCl_4 and $CH_3COONa{\cdot}3H_2O$ (equimolar amounts of each in methanol), (ii) PPh_3 (2 mole equivalents in acetone).

4.2. Experimental

4.2.1. Materials

All chemicals used in this work were of analytical grade available commercially and were used as received. The solvents used were purified by standard methods [19].

4.2.2. Physical measurements

Elemental analysis data were obtained with a Thermo Finnigan Flash EA1112 series elemental analyzer. Jasco-5300 and Thermo Scientific Nicolet 380 FT-IR spectrophotometers were used to record the infrared spectra. Purity verifications of H_2L^1 and H_2L^2 were performed with a Shimadzu LCMS 2010 liquid chromatograph mass spectrometer. Solution electrical conductivities were measured with a Digisun DI-909 conductivity meter. Electronic spectra were collected on Perkin-Elmer Lambda 35 UV/Vis and Shimadzu UV3600 UV-Vis-NIR spectrophotometers. The NMR spectra were recorded with the help of Bruker 400 and 500 MHz NMR spectrometers.

4.2.3. Synthesis of H_2L^1

1-naphthaldehyde (468 mg, 3 mmol) and a few drops of acetic acid were added to an ethanol solution (50 ml) of benzoylhydrazine (408 mg, 3 mmol). The mixture was boiled under reflux for 3 h. The white crystalline solid separated was collected by filtration, washed with ethanol and then dried in air. Yield: 660 mg (80%). Mass in Me_2NCHO: m/z = 274.

H_2L^2 was prepared in 85% yield from equimolar amounts of 4-methoxy-1-naphthaldehyde and benzoylhydrazine in presence of acetic acid using the same procedure as described for H_2L^1. Mass in Me_2NCHO: m/z = 304.

4.2.4. Synthesis of [Pd(HL^1)Cl] (1)

A mixture of $PdCl_2$ (178 mg, 1 mmol) and LiCl (86 mg, 2 mmol) was taken in methanol (20 ml) and boiled with stirring under reflux for 1 h. It was then cooled to room temperature and filtered. The filtrate was added drop-wise with stirring to a methanol solution (20 ml) of H_2L^1 (275 mg, 1 mmol) and $CH_3COONa{\cdot}3H_2O$ (136 mg, 1 mmol). The mixture was stirred at room temperature for 48 h. The complex precipitated as yellowish-green solid was collected by filtration, washed with methanol and finally dried in air. Yield: 332 mg (80%).

The yellowish-green [Pd(HL^2)Cl] (**2**) was synthesized in 80% yield from $PdCl_2$, LiCl, $CH_3COONa{\cdot}3H_2O$ and H_2L^2 (1:2:1:1 mole ratio) by following a procedure very similar to that described for **1**.

4.2.5. Synthesis of [Pd(L^1)(PPh$_3$)] (3)

Solid PPh_3 (131 mg, 0.5 mmol) was added to a suspension of [Pd(HL^1)Cl] (**1**) (104 mg, 0.25 mmol) in acetone (10 ml) and the mixture was stirred at room temperature for 24 h. The complex [Pd(L^1)(PPh$_3$)] (**3**) separated as a yellowish-green solid was collected by filtration, washed with acetone and finally dried in air. Yield: 110 mg (68%). ^{31}P NMR in $(CD_3)_2SO$: δ (ppm) = 25.51.

The yellowish-green [Pd(L^2)(PPh$_3$)] (**4**) was synthesized in 68% yield from one mole equivalent of [Pd(HL^2)Cl] (**2**) and two mole equivalents of PPh_3 using a very similar procedure described above. ^{31}P NMR in $(CD_3)_2SO$: δ (ppm) = 25.49.

4.2.6. X-ray crystallography

Single crystals of **2** were grown by diethyl ether vapor diffusion into its dimethylformamide solution, while single crystals of **3** and **4** were obtained by slow evaporation of their corresponding acetonitrile solutions. Complex **2** crystallizes as $[Pd(HL^2)Cl]\cdot Me_2NCHO$ (**2**·Me_2NCHO). On the other hand, complexes **3** and **4** crystallize as it is without any solvent molecule. Determination of unit cell parameters and intensity data collection at 298 K for **2**·Me_2NCHO and **4** were performed with the help of a Bruker-Nonius SMART APEX CCD single crystal diffractometer using graphite monochromated Mo $K\alpha$ radiation (λ = 0.71073 Å). The SMART and the SAINT-Plus packages [20] were used for data acquisition and data extraction, respectively. The SADABS program [21] was used for absorption corrections. Unit cell parameters and the intensity data at 298 K for **3** were obtained using graphite monochromated Mo $K\alpha$ radiation (λ = 0.71073 Å) on an Oxford Diffraction Xcalibur Gemini single crystal X-ray diffractometer. The CrysAlisPro software [22] was used for data collection, reduction and absorption correction. The structures of all three complexes were solved by direct method and refined on F^2 by full-matrix least-squares procedures. All non-hydrogen atoms were refined anisotropically. The hydrogen atom of the N−H group of $(HL^2)^-$ in **2**·Me_2NCHO was located in a difference map and refined isotropically with restrained thermal parameter. The remaining hydrogen atoms in **2**·Me_2NCHO and all the hydrogen atoms in **3** and **4** were included at ideal positions for structure factor calculation by using a riding model. The SHELX-97 programs [23] available in the WinGX package [24] were used for structure solution and refinement. The Platon [25] and Mercury [26] packages were used for molecular graphics. All the crystallographic data (except for the structure factors) have been deposited with the Cambridge Crystallographic Data Centre. The deposition numbers are CCDC 916284–916286 for **2**·$(CH_3)_2NCHO$, **3** and **4** respectively. Selected crystallographic data are summarized in Table 4.1.

Table 4.1. Selected crystallographic data.

Complex	**2**· Me_2NCHO	**3**	**4**
Chemical formula	$PdC_{22}H_{22}N_3O_3Cl$	$PdC_{36}H_{27}N_2OP$	$PdC_{37}H_{29}N_2O_2P$
Formula weight	518.28	640.97	670.99
Crystal system	Monoclinic	Monoclinic	Monoclinic
Space group	*C*2/c	$P2_1/n$	$P2_1/c$
a (Å)	21.487(3)	16.0972(5)	24.8618(14)
b (Å)	8.9400(12)	15.4471(4)	15.7887(9)
c (Å)	23.968(4)	23.2869(7)	15.4990(9)
β (º)	111.397(5)	102.977(3)	101.218(1)
V (Å^3)	4286.8(11)	5642.5(3)	5967.7(6)
Z	8	8	8
ρ (g cm^{-3})	1.606	1.509	1.494
μ (mm^{-1})	1.019	0.748	0.713
Reflections collected	19917	27787	42467
Reflections unique	3779	9937	10515
Reflections [$I \geq 2\sigma(I)$]	2952	6511	8226
Parameters	274	739	775
*R*1, *wR*2 [$I \geq 2\sigma(I)$]	0.0560, 0.1107	0.0398, 0.0913	0.0380, 0.0878
*R*1, *wR*2 [all data]	0.0762, 0.1192	0.0694, 0.0998	0.0539, 0.0943
GOF on F^2	1.098	0.907	1.023
Largest diff. peak and hole (e Å^{-3})	0.586, −0.315	1.953, −0.612	0.575, −0.260

4.3. Results and discussion

4.3.1. Synthesis and characterization

The Schiff bases (H_2L^n) were synthesized in 80−90% yields by condensation of the corresponding 4-*R*-1-naphthaldehyde and benzoylhydrazine in 1:1 mole ratio in presence of a few drops of acetic acid in ethanol. The elemental analysis, LCMS and ^{1}H NMR spectra of H_2L^1 and H_2L^2 are consistent with their structures. Treatment of one mole equivalent each of H_2L^n and $CH_3COONa{\cdot}3H_2O$ with Li_2PdCl_4 (generated in situ from $PdCl_2$ and LiCl in 1:2 mole ratio) in methanol afforded the complexes of formula $[Pd(HL^n)Cl]$ in very good yields (80%). Reaction of $[Pd(HL^n)Cl]$ (**1** and **2)** with PPh_3 in 1:2 mole ratio in acetone produced $[Pd(L^n)(PPh_3)]$ (**3** and **4**) in ~70% yields (Scheme 4.1). The elemental analysis data of each of **1**–**4** support the corresponding molecular formula (Table 4.2). All the complexes are yellowish-green and diamagnetic. Both **1** and **2** are sparingly soluble in halogenated solvents like dichloromethane and chloroform, moderately soluble in acetonitrile and acetone and highly soluble in dimethylsulfoxide and dimethylformamide. Solubility behavior of **3** and **4** is very similar to that of **1** and **2** except for their high solubility in dichloromethane and chloroform also. In solution, all the complexes behave as non-electrolyte.

Table 4.2. Elemental analysis data.

Compound	Found (calc) (%)		
	C	H	N
H_2L^1	78.96 (78.81)	5.21 (5.14)	10.11 (10.21)
H_2L^2	74.81 (74.98)	5.21 (5.30)	9.36 (9.20)
$[Pd(HL^1)Cl]$	52.15 (52.07)	3.08 (3.16)	6.85 (6.75)
$[Pd(HL^2)Cl]$	51.36 (51.26)	3.51 (3.40)	6.15 (6.29)
$[Pd(L^1)(PPh_3)]$	67.58 (67.45)	4.15 (4.25)	4.26 (4.37)
$[Pd(L^2)(PPh_3)]$	66.38 (66.23)	4.41 (4.36)	4.07 (4.17)

4.3.2. Infrared spectral properties

Infrared spectra of the Schiff bases (H_2L^1 and H_2L^2) and the corresponding complexes (**1**–**4**) have been collected using KBr pellets. The spectrum of **1** is depicted in Figure 4.1. The Schiff bases display two medium intensity bands at ~3223 and ~3062 cm^{-1} due to the amide N–H and the aromatic C−H stretches, respectively. The amide C=O stretch appears as a strong band at 1645 and 1651 cm^{-1} for H_2L^1 and H_2L^2, respectively. The strong band observed at 1576 and 1580 cm^{-1} for H_2L^1 and H_2L^2, respectively is attributed to the C=N stretch [18,27–31]. As observed for H_2L^1 and H_2L^2, both **1** and **2** also display two bands at ~3180 and ~3040 cm^{-1} due to the amide N–H and the aromatic C−H stretches, respectively. The O-coordinated amide C=O and N-coordinated C=N stretches of the tridentate ligand $(HL^n)^-$ in **1** and **2** appear at ~1600 and ~1560 cm^{-1}, respectively. Both **3** and **4** do not display any band assignable to the N–H or C=O indicating the deprotonation of the amide functionality. The band observed at ~3050 cm^{-1} for **3** and **4** is because of the aromatic C−H moieties of the ligands. Both complexes display a strong band at ~1550 cm^{-1} due to the conjugated C=N−N=C fragment of the tridentate $(L^n)^{2-}$ [27–31].

4.3.3. Electronic spectral properties

Electronic spectra of the Schiff bases (H_2L^1 and H_2L^2) and the complexes (**1**–**4**) were recorded using their dimethylformamide solutions. Spectroscopic data are listed in Table 4.3 and representative spectra are illustrated in Figure 4.2. The spectra of H_2L^1 and H_2L^2 are very similar and exhibit an intense absorption at 336 and 350 nm, respectively. This absorption is flanked by two shoulders at 355 and 320 nm and 370 and 335 nm for H_2L^1 and H_2L^2, respectively. Thus there is a red-shift of the band positions from the unsubstituted H_2L^1 to the substituted H_2L^2. The spectral profiles of **1–4** are also very similar. All of them display closely spaced three sharp absorptions followed by two shoulders in the wavelength range 438−345 nm (Fig. 4.2).

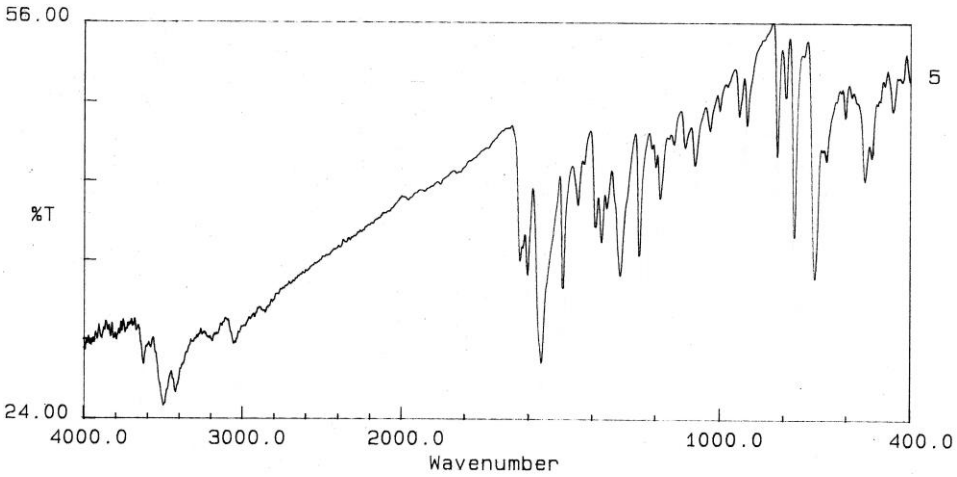

Figure 4.1. Infrared spectrum of [Pd(HL^1)Cl] (**1**).

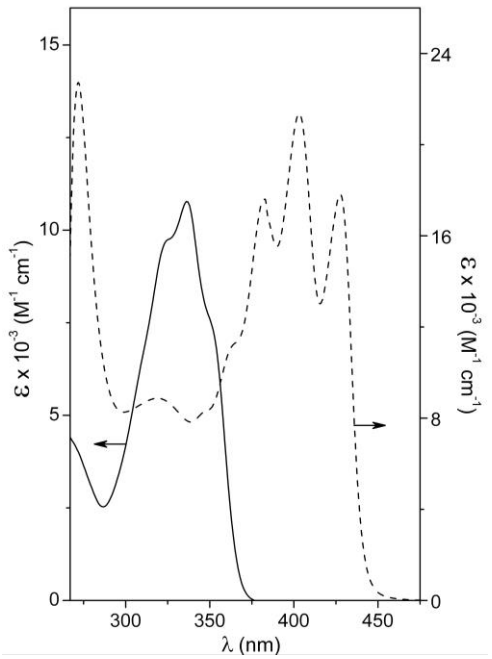

Figure 4.2. Electronic spectra of H_2L^1 (—) and [Pd(L^1)(PPh_3)] (**3**) (----) in dimethylformamide.

In addition to this group of five absorptions, each complex shows two more absorption at ~318 and ~271 nm. It may be noted that the spectrum reported for naphthalene in cyclohexane shows a similar group of absorptions centred at ~275 nm and a high energy shoulder at ~225 nm [32]. Thus the absorption bands of **1–4** are primarily due to ligand centred transitions only. As observed for the Schiff bases, here also the absorption features of **2** and **4** are red-shifted compared to those of **1** and **3**. The spectral profiles and the red-shift of band positions observed for H_2L^1, H_2L^2 and the complexes **1**–**4** strongly resemble the spectral characteristics of the corresponding 9-anthracenyl analogues [31]. Alteration of the π-π* energy gaps and hence red-shift of arene absorption bands due to introduction of substituent and also metal coordination is reported in literature [31,33−35].

Table 4.3. Electronic spectroscopic[a] data.

Complex	Absorption λ_{max} (nm) ($10^{-3} \times \varepsilon$ (M^{-1} cm^{-1}))
H_2L^1	355[b] (7.1), 336 (10.8), 320[b] (9.5)
H_2L^1	370[b] (13.6), 350 (22.3), 335[b] (20.9), 280[b] (6.8)
1	428 (15.8), 403 (17.6), 382 (13.5), 360[b] (8.0), 350[b] (6.5), 320 (8.0), 271 (17.3)
2	436 (15.9), 412 (20.3), 391 (16.8), 370[b] (10.8), 350[b] (6.9), 315 (7.8), 270 (16.3)
3	428 (17.8), 403 (21.4), 383 (17.6), 360[b] (11.0), 345[b] (8.2), 319 (8.9), 272 (22.7)
4	438 (14.0), 415 (20.8), 394 (17.8), 370[b] (11.4), 355[b] (6.9), 315[b] (7.2), 271 (21.2)

[a] In dimethylformamide

[b] Shoulder.

4.3.4. NMR spectral properties

Dimethylsulphoxide-d6 solutions of H_2L^1, H_2L^2 and the complexes **1**−**4** were used to record the proton NMR spectra. Chemical shift values are summarized in Table 4.4 and representative spectra are shown in Figures 4.3 and 4.4. The spectra of **1** and **2** display all the protons of $(HL^n)^-$, while in the spectra of **3** and **4** some of the aromatic protons of $(L^n)^{2-}$ could not be assigned due to the overlapping signals of the PPh_3 phenyl ring protons. The H^8 proton of H_2L^1 and H_2L^2 resonates as a doublet at δ 7.97 and δ 7.87, respectively. The absence of any such signal in the spectra of **1**–**4** indicates metallation at C8. The signal corresponding to the N−H proton of H_2L^1 and H_2L^2 is observed at δ 11.99 and δ 11.83, respectively. A broad weak signal exhibited by **1** and **2** at δ 14.05 and δ 14.17, respectively is assigned to the N–H proton of $(HL^n)^-$. No such signal in the spectra of **3** and **4** indicates the deprotonation of the amide functionality and the dianionic form ($(L^n)^{2-}$) of the ligand. A singlet observed in the range δ 4.05–4.11 for H_2L^2, **2** and **4** is attributed to the methyl protons of the –OMe substituent. The singlet corresponding to the azomethine proton (H^9) resonates at δ 9.16 and δ 9.00 for H_2L^1 and H_2L^2, respectively, and within δ 8.88−9.07 for **1**–**4**. There is an upfield shift of H^2, H^6 and H^9 protons of the complexes when compared with the corresponding protons of the free Schiff bases. On the other hand, H^3 and H^7 protons of the complexes are shifted downfield and H^5 does not show any significant change. In the benzoyl fragment of **1**–**4**, *ortho* protons (H^{12} and H^{16}) are slightly downfield shifted, while no shift is observed in case of *meta* and *para* protons (H^{13}, H^{14} and H^{15}). ^{31}P NMR spectra of **3** and **4** display a singlet at δ ~25.5 indicating PPh_3 coordination to the metal centre.

Table 4.4. ^{1}H NMR data[a] of H_2L^{1-2} and **1**–**4**.

Compound	δ (ppm) (J (Hz))
H_2L^1	11.99 (s, 1H, NH), 9.16 (s, 1H, H^9), 8.91 (8) (d, 1H, H^2), 8.03 (m, 4H, H^4, H^5, H^{12}, H^{16}), 7.97 (7) (d, 1H, H^8), 7.70 (8) (t, 1H, H^{14}), 7.63 (m, 3H, H^3, H^{13}, H^{15}), 7.58 (8) (t, 2H, H^6, H^7).
H_2L^2	11.83 (s, 1H, NH), 9.02 (8) (d, 1H, H^2), 9.00 (s, 1H, H^9), 8.28 (8) (d, 1H, H^5), 7.99 (7) (d, 2H, H^{12}, H^{16}), 7.87 (8) (d, 1H, H^8), 7.71 (8) (t, 1H, H^{14}), 7.62 (7) (d, 2H, H^{13}, H^{15}), 7.57 (8) (t, 2H, H^6,H^7), 7.11 (8) (d, 1H, H^3) 4.05 (s, 3H, OMe).
1	14.05 (s, 1H, NH), 8.92 (s, 1H, H^9), 8.63 (br.s, 1H, H^2), 8.23 (8) (d, 1H, H^4), 8.13 (6) (d, 1H, H^5), 8.08 (7) (d, 2H, H^{12}, H^{16}), 7.82 (8) (d, 1H, H^7), 7.72 (8) (t, 1H, H^{14}), 7.67 (8) (t, 1H, H^3), 7.63 (m, 2H, H^{13}, H^{15}), 7.35 (8) (t, 1H, H^6).
2	14.17 (s, 1H, NH), 8.76 (s, 1H, H^9), 8.68 (br.s, 1H, H^2), 8.12 (8) (d, 2H, H^5, H^7), 8.06 (7) (d, 2H, H^{12}, H^{16}), 7.71 (br.s, 1H, H^{14}), 7.62 (br.s, 2H, H^{13}, H^{15}), 7.31 (8) (t, 1H, H^6), 7.20 (8) (d, 1H, H^3), 4.11 (s, 3H, OMe).
3	9.07 (s, 1H, H^9), 8.65 (br, s, 1H, H^2), 8.20 (br, s, 2H, H^{12}, H^{16}), 7.56 (m, 22H, H^3, H^4, H^5, H^7, H^{13-15}, Hs of PPh_3), 6.77 (br, s, 1H, H^6).
4	8.88 (s, 1H, H^9), 8.69 (br.s, 1H, H^2), 8.16 (8) (d, 2H, H^5, H^7), 8.01 (6.4) (d, 2H, H^{12}, H^{16}), 7.73 (br.s, 4H, H^{14}, *para* ^{1}Hs of PPh_3), 7.63 (m, 2H, H^{13}, H^{15}), 7.45 (m, 12H, *o*,*m* ^{1}Hs of PPh_3), 7.21 (8.4) (d, 1H, H^3), 6.71 (br, s, 1H, H^6), 4.11 (s, 3H, OMe).

[a] In dmso-d6.

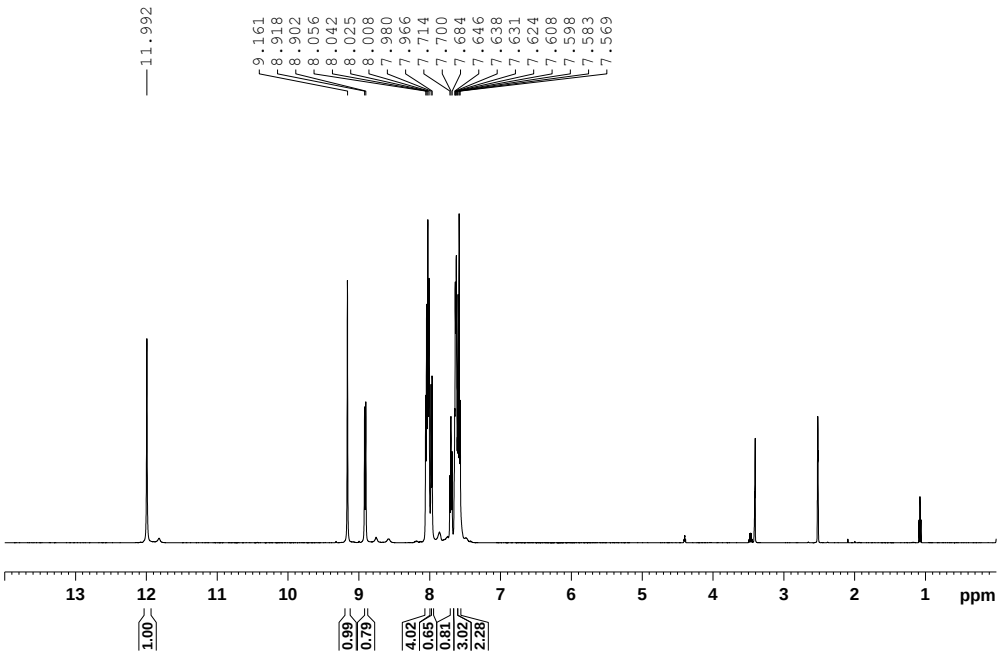

Figure 4.3. ^{1}H NMR spectrum of HL^{1}.

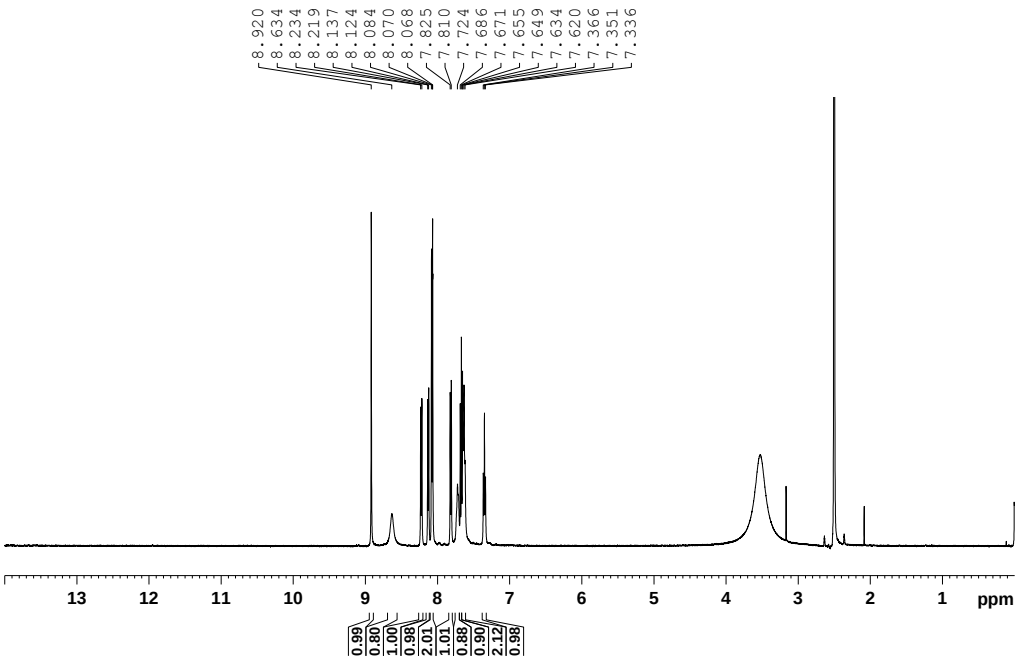

Figure 4.4. ^{1}H NMR spectrum of [Pd(HL^{1})Cl] (**1**).

4.3.5. Description of X-ray structures

The molecular structures of **2**, **3** and **4** are confirmed by single crystal X-ray crystallography. Despite our best attempts X-ray quality crystals of **1** could not be grown. The asymmetric unit of **2** contains one complex molecule and one dimethylformamide molecule, while that of each of **3** and **4** contains two complex molecules. The bond parameters involving the metal centre for all three structures are listed in Tables 4.5 and 4.6. There is no significant variation in the bond parameters of the two molecules present in the asymmetric unit of each of **3** and **4**. The solvated **2**·Me_2NCHO unit dimerises due to two types of hydrogen bonding. These hydrogen bonds are between the tridentate ligand N−H and the solvent amide-O and between the solvent C−H and the coordinated Cl. In these N−H···O and C−H···Cl interactions, N···O and C···Cl distances are 2.709(6) and 3.620(8) Å, respectively and N−H···O and C−H···Cl angles are 163(5) and 146°, respectively. The structure of **2** and the dimer of the solvate **2**·Me_2NCHO are illustrated in Figures 4.5 and 4.6, respectively. For each of **3** and **4**, the structure of only one of the two molecules present in the corresponding asymmetric unit is shown in Figure 4.7. The $(HL^2)^-$ binds the metal atom through the 1-naphthalenyl *peri*-C, the azomethine-N and the amide-O atoms in **2**, while the metal atom is coordinated to the 1-naphthalenyl *peri*-C, the azomethine-N and the amidate-O atoms of $(L^n)^{2-}$ in each of **3** and **4**. The fourth coordination site in **2** is occupied by a Cl-atom, whereas that in each of **3** and **4** is occupied by the P-atom of a PPh_3 molecule. In each of the three complexes, the four coordinating atoms form a satisfactory square-plane (mean deviation 0.05−0.13 Å) around the metal centre and there is essentially no deviation (0.01−0.04 Å) of the metal centre from this square-plane. The tridentate ligand forms 6,5-fused chelate rings in each of **2**, **3** and **4**. The two chelate rings are slightly folded along the metal and azomethine-N bond (Figures 4.5–4.7). The fold angles are within 3.1(2)−6.5(1)°. The C−O and C−N bond lengths of the amide

fragment of the tridentate ligand in **2** are 1.241(6) and 1.341(6) Å, respectively, while in **3** and **4** they are within 1.293(4)−1.298(4) and 1.298(4)−1.311(4) Å, respectively. Thus the amide functionality in **2** is protonated and that in **3** and **4** is deprotonated and the negative charge is delocalized over OCN fragment [27−31]. This is also reflected in the significantly longer Pd−O bond length in **2** than that in both **3** and **4** (Tables 4.5 and 4.6). The Pd−N bond length in **4** is longer compared to that in **2** due to the better *trans* directing ability of PPh_3 than chloride. The Pd−C bond lengths (2.004(3)−2.021(4) Å) in **3** and **4** are also longer than that (1.975(5) Å) in **2**. It is very likely that this difference in Pd−C bond lengths is the result of larger *trans* effect of amidate-O in **3** and **4** than the *trans* effect of amide-O in **2** [31]. The Pd−Cl (in **2**) and the Pd−P (in **3** and **4**) bond lengths are unexceptional. In general, all the bond lengths associated with the metal atom in each of **2**, **3** and **4** are within the ranges observed for Pd(II) complexes having similar coordinating atoms [6,9−11,13, 18,27,28, 31, 36].

Table 4.5. Selected bond lengths (Å) and angles (°) for **2**·Me_2NCHO.

Complex **2**			
Pd(1)−C(1)	1.975(5)	Pd(1)−N(1)	1.963(4)
Pd(1)−O(1)	2.132(3)	Pd(1)−Cl(1)	2.3090(15)
C(1)−Pd(1)−N(1)	93.12(19)	C(1)−Pd(1)−O(1)	171.09(17)
C(1)−Pd(1)−Cl(1)	98.06(15)	N(1)−Pd(1)−O(1)	78.58(15)
N(1)−Pd(1)−Cl(1)	168.59(13)	O(1)−Pd(1)−Cl(1)	90.38(10)

Table 4.6. Selected bond lengths (Å) and angles (°) for **3** and **4**.

Complex **3**			
Molecule 1			
Pd(1)−C(1)	2.020(4)	Pd(1)−N(1)	2.008(3)
Pd(1)−O(1)	2.082(3)	Pd(1)−P(1)	2.2997(10)
C(1)−Pd(1)−N(1)	92.59(14)	C(1)−Pd(1)−O(1)	169.15(12)
C(1)−Pd(1)−P(1)	98.14(11)	N(1)−Pd(1)−O(1)	78.33(11)
N(1)−Pd(1)−P(1)	168.43(9)	O(1)−Pd(1)−P(1)	91.41(7)
Molecule 2			
Pd(2)−C(37)	2.021(4)	Pd(2)−N(3)	2.006(3)
Pd(2)−O(2)	2.078(2)	Pd(2)−P(2)	2.2952(10)
C(37)−Pd(2)−N(3)	92.78(13)	C(37)−Pd(2)−O(2)	169.78(12)
C(37)−Pd(2)−P(2)	97.75(10)	N(3)−Pd(2)−O(2)	78.00(11)
N(3)−Pd(2)−P(2)	168.96(9)	O(2)−Pd(2)−P(2)	91.74(7)
Complex **4**			
Molecule 1			
Pd(1)−C(1)	2.004(3)	Pd(1)−N(1)	1.998(2)
Pd(1)−O(1)	2.077(2)	Pd(1)−P(1)	2.2923(8)
C(1)−Pd(1)−N(1)	93.00(11)	C(1)−Pd(1)−O(1)	168.48(10)
C(1)−Pd(1)−P(1)	99.02(9)	N(1)−Pd(1)−O(1)	78.18(9)
N(1)−Pd(1)−P(1)	166.16(8)	O(1)−Pd(1)−P(1)	90.69(6)
Molecule 2			
Pd(2)−C(38)	2.010(3)	Pd(2)−N(3)	1.997(2)
Pd(2)−O(3)	2.087(2)	Pd(2)−P(2)	2.2905(8)
C(38)−Pd(2)−N(3)	93.05(12)	C(38)−Pd(2)−O(3)	169.68(10)
C(38)−Pd(2)−P(2)	97.52(9)	N(3)−Pd(2)−O(3)	77.82(10)
N(3)−Pd(2)−P(2)	166.97(8)	O(3)−Pd(2)−P(2)	92.19(6)

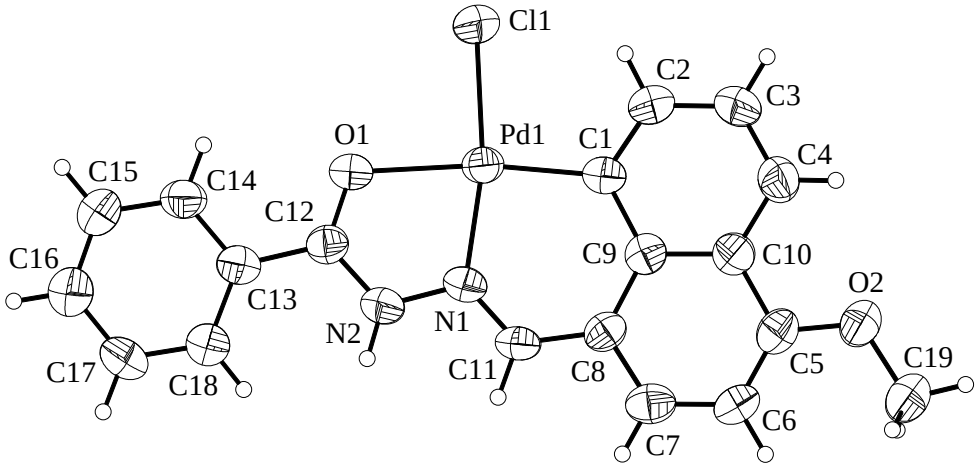

Figure 4.5. Molecular structure of **2** with the atom labeling scheme. All non-hydrogen atoms are represented by their 50% probability thermal ellipsoids.

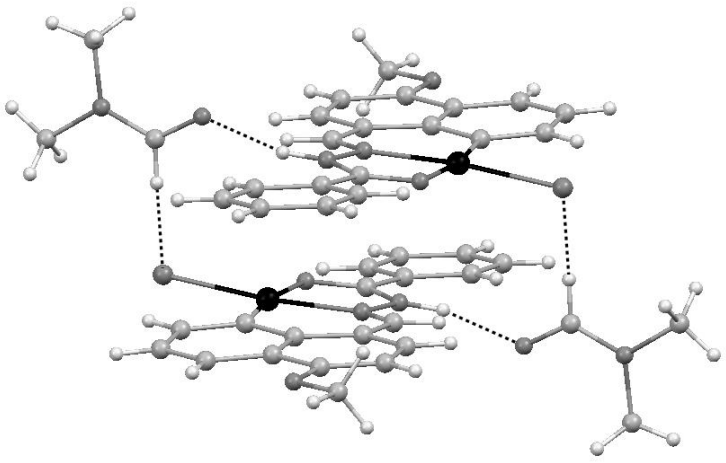

Figure 4.6. Ball and stick diagram of the hydrogen bonded dimer of **2**·Me_2NCHO.

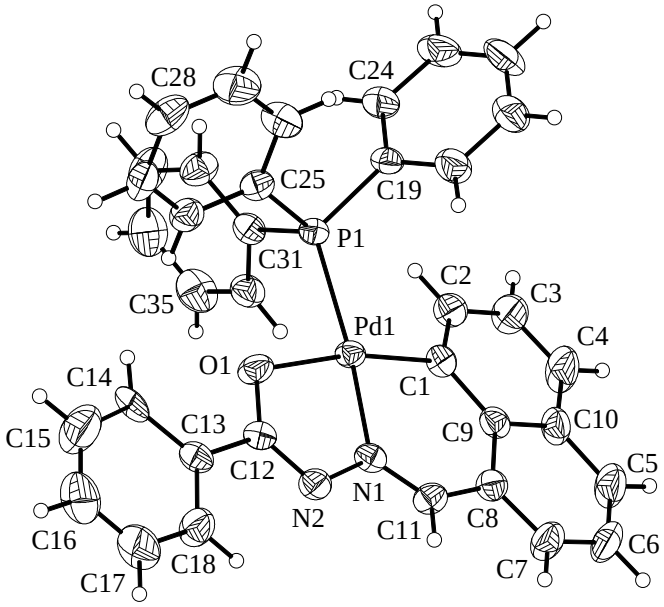

(a)

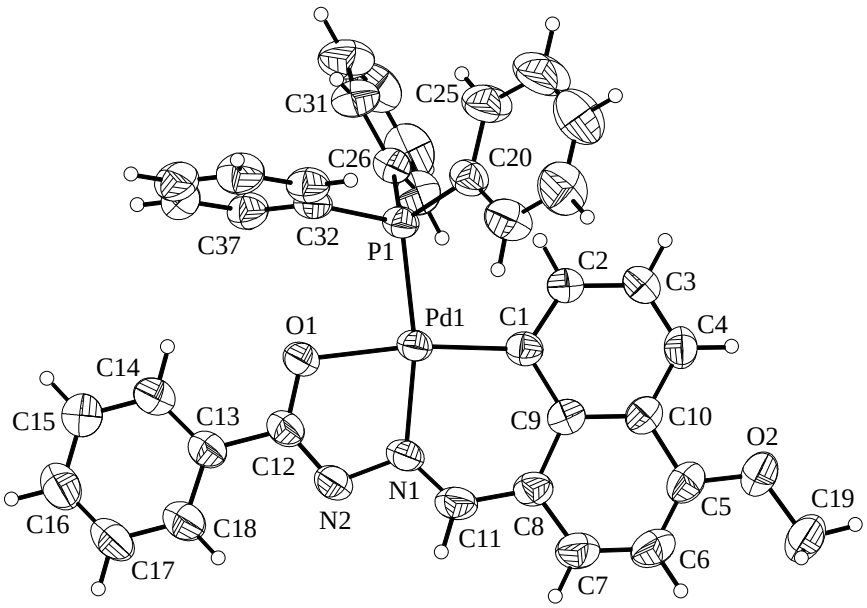

(b)

Figure 4.7. Molecular structures of (a) **3** and (b) **4** with the atom labeling schemes. For clarity selected C-atoms of the PPh_3 in each structure are labeled. All non-hydrogen atoms are represented by their 50% probability thermal ellipsoids.

4.4. Conclusions

Cyclometallated complexes [Pd(HL^n)Cl] (**1** and **2**) and [Pd(L^n)(PPh_3)] (**3** and **4**) with the C,N,O-donor Schiff bases N′-(4-*R*-1-naphthylidene)-benzohydrazide (H_2L^n, *R* = H (n = 1) and OMe (n = 2)) have been synthesized and characterized. In each species, *peri* position in preference to the *ortho* position of 1-naphthalenyl fragment of the tridentate ligand is metallated. This regioselective metallation in **1**–**4** has been authenticated by proton NMR and single crystal X-ray crystallography.

Till now, we have described the regioselective cyclopalladation chemistry of aroylhydrazones of various polycyclic aromatic aldehydes. For a better understanding of the regioselective process, we have studied the cyclometallation of the present and analogous aroylhydrazones with other platinum group metals. The results obtained in this effort are discussed in the next chapter.

4.5. References

[1] Y. –F. Han, H. Li, P. Hu, G. –X. Jin, *Organometallics* 30 (2011) 905−911.

[2] A. J. Klaus, P. Rys, *Helv. Chim. Acta* 64 (1981) 1452−1466.

[3] M. Hugentobler, A. J. Klaus, H. Mettler, P. Rys, G. Wehrle, *Helv. Chim. Acta* 65 (1982) 1202−1211.

[4] R. Annunziata, S. Cenini, F. Demartin, G. Palmisano, S. Tollari, *J. Organomet. Chem*. 496 (1995) C1–C3.

[5] M. Crespo, M. Font-Bardía, S. Pérez, X. *J. Organomet. Chem*. 642 (2002) 171−178.

[6] Y. Li, K. -H. Ng, S. Selvaratnam, G. -K. Tan, J. J. Vittal, P. -H. Leung, *Organometallics* 22 (2003) 834−842.

[7] R. Bhawmick, P. Das, D. N. Neogi, P. Bandyopadyay, *Polyhedron* 25 (2006) 1177–1181.

[8] L. Kind, A. J. Klaus, P. Rys, V. Gramlich, *Helv. Chim. Acta* 81 (1998) 307−316.

[9] S. Lentijo, J. A. Miguel, P. Espinet, *Organometallics* 30 (2011) 1059–1066.

[10] S. Lentijo, J. A. Miguel, P. Espinet, *Dalton Trans*. 40 (2011) 7602−7609.

[11] S. Tollari, G. Palmisano, F. Dematrin, M. Grassi, S. Magnaghi, S. Cenini, *J. Organomet. Chem*. 488 (1995) 79−83.

[12] M. Crespo, E. Evangelio, *J. Organomet. Chem*. 689 (2004) 1956−1964.

[13] D. N. Neogi, P. Das, A. N. Biswas, P. Bandyopadhyay, *Polyhedron* 25 (2006) 2149−2152.

[14] D. N. Neogi, A. N. Biswas, P. Das, R. Bhawmick, P. Bandyopadhyay, *Inorg. Chim. Acta* 360 (2007) 2181–2186.

[15] A. N. Biswas, P. Das, V. Bagchi, A. Choudhury, P. Bandyopadhyay, *Eur. J. Inorg. Chem*. (2011) 3739–3748.

[16] A. N. Biswas, P. Das, S. Sengupta, A. Choudhury, P. Bandyopadhyay, *RSC Adv.* 1 (2011) 1279–1286.

[17] D. N. Neogi, A. N. Biswas, P. Das, R. Bhawmick, P. Bandyopadhyay, *J. Organomet. Chem*. 724 (2013) 147−154.

[18] A. R. B. Rao, S. Pal, *J. Organomet. Chem*. 696 (2011) 2660–2664.

[19] D. D. Perrin, W. L. F. Armarego, D. P. Perrin, *Purification of Laboratory Chemicals* 2nd ed., Pergamon, Oxford, 1983.

[20] *SMART version 5.630 and SAINT-plus version 6.45* Bruker-Nonius Analytical X-ray Systems Inc., Madison, WI, USA, 2003.

[21] G. M. Sheldrick, *SADABS, Program for Area Detector Absorption Correction* University of Göttingen, Göttingen, Germany, 1997.

[22] *CrysAlisPro version 1.171.33.55* Oxford Diffraction Ltd., Abingdon, Oxfordshire, UK, 2007.

[23] G. M. Sheldrick, *XHELX-97, Structure Determination Software* University of Göttingen, Göttingen, Germany, 1997.

[24] L. J. Farrugia, *WinGX suite for small molecule single-crystal crystallography* J. Appl. Crystallogr. 32 (1999) 837−838.

[25] A. L. Spek, Platon, A *Multipurpose Crystallographic Tool* Utrecht University, Utrecht, The Netherlands, 2002.

[26] C. F. Macrae, I. J. Bruno, J. A. Chisholm, P. R. Edgington, P. McCabe, E. Pidcock, L. Rodriguez-Monge, R. Taylor, J. van de Streek, P. A. Wood, *J. Appl. Crystallogr*. 41 (2008) 466−470.

[27] S. Das, S. Pal, *J. Organomet. Chem*. 689 (2004) 352–360.

[28] S. Das, S. Pal, *J. Organomet. Chem*. 691 (2006) 2575–2583.

[29] R. Raveendran, S. Pal, *J. Organomet. Chem*. 692 (2007) 824–830.

[30] R. Raveendran, S. Pal, *J. Organomet. Chem*. 694 (2009) 1482–1486.

[31] A. R. B. Rao, S. Pal, *J. Organomet. Chem*. 701 (2012) 62–67.

[32] J. M. Dixon, M. Taniguchi, J. S. Lindsey, *Photochem. Photobiol*. 81 (2005) 212–213.

[33] S. Suzuki, T. Fuji, T. Ishikawa, *J. Mol. Spectrosc*. 57 (1975) 490–499.

[34] L. Cuffe, R. D. A. Hudson, J. F. Gallagher, S. Jennings, C. J. McAdam, R. B. T. Connelly, A. R. Manning, B. H. Robinson, J. Simpson, *Organometallics* 24 (2005) 2051−2060.

[35] Y. –Y. Liu, M. Grzywa, M. Tonigold, G. Sastre, T. Schüttrigkeit, N. S. Leeson, D. Volkmer, *Dalton Trans*. 40 (2011) 5926–5938.

[36] J. Granell, R. Moragas, J. Sales, M. Font-Bardía, X. Solans, J. Chem. Soc., *Dalton Trans*. (1993) 1237−1244.

Chapter 5

Regioselective cyclometallation of 4-*R*-N′-(arylidene)-benzohydrazides with Rh(III), Ir(III), Pd(II) and Pt(II)[§]

Reactions of $[Rh(PPh_3)_3Cl]$, $[Ir(PPh_3)_3Cl]$, $Li_2[PdCl_4]$ and $K_2[PtCl_4]$ with the corresponding 4-*R*-N′-(arylidene)benzohydrazides (H_2L^n; n = 1 and 2 for arylidene = 1-pyrenylidene and *R* = H and Cl, respectively and n = 3 for arylidene = 1-naphthylidene and *R* = H) in presence of $CH_3COONa·3H_2O$ in methanol/toluene provide the complexes with general formula *trans*-$[Rh(L^n)(PPh_3)_2H]$ (**1** and **2**), *trans*-$[Ir(L^n)(PPh_3)_2H]$ (**3** and **4**), $[Pd(HL^n)Cl]$ (**5)** and $[Pt(HL^n)Cl]$ (**6**), respectively. Reactions of **5** and **6** with PPh_3 in acetone produce the complexes $[Pd(L^n)(PPh_3)]$ (**7)** and $[Pt(L^n)(PPh_3)]$ (**8**), respectively. All the complexes have been characterized with the help of microanalysis (CHN), spectroscopic (infrared, NMR, electronic and emission) and cyclic voltammetric measurements. Molecular structures of **1**–**5** and **8** have been confirmed with single crystal X-ray crystallography. In **5** and **6**, $(HL^1)^-$ acts as a monobasic CNO-donor ligand, whereas in each of **1**−**4**, **7** and **8**, the $(L^n)^{2-}$ acts as a dibasic CNO-donor ligand. In **1**, **2**, **5** and **7**, metallation at the *peri* position of the 1-pyrenyl moiety of the pincer like ligand leads to the formation of 6,5-membered fused chelate rings, whereas in **3**, **4**, **6** and **8** metallation takes place at *ortho* position of the 1-pyrenyl/1-naphthalenyl moiety of the ligand with the formation of 5,5-membered fused chelate rings.

5.1. Introduction

In the previous chapters we have described the regioselectivity in cyclopalladation of aroylhydrazones of some polycyclic aromatic aldehydes.

[§] This work has been published in *J. Organomet. Chem.* 762 (2014) 58–66.

However, the specific factors that control the regioselective cyclometallation processes are yet to be ascertained. Many parameters such as nature of the metal ion, steric constraints, reaction temperature, polarity of the solvent etc. may affect and hence regulate the regioselective metallation of the substrate [1,2]. A better understanding of these controlling parameters could lead to the development of new and effective synthetic strategies for designer molecules. In the present chapter, we have studied the cyclometallation chemistry of some platinum group metal (Rh, Ir, Pd and Pt) ions with 4-*R*-N′-(1-pyrenylidene/1-naphthylidene)benzohydrazides (H_2L^n, 2 H represent the amide and aryl C–H protons). The aim was to unravel whether the regioselective cyclometallation of the polycyclic aryl group of H_2L^n is a metal ion dependent process or not. In this effort, we have isolated a new group of cyclometallates with CNO-pincer like ligands (Scheme 5.1). Indeed in these cyclometallates, the 4d metal ions (Rh(III) and Pd(II)) prefer the *peri* position, while the 5d metal ions (Ir(III) and Pt(II)) prefer the *ortho* position of the polycyclic aryl group and form six- and five-membered chelate rings, respectively. Herein, we report the syntheses, characterization, properties and structures of these cyclometallates.

5.2. Experimental section

5.2.1. Materials

All chemicals used in this work were of analytical grade available commercially and were used as received. The solvents used were purified by standard methods [3]. $[Rh(PPh_3)_3Cl]$ and $[Ir(PPh_3)_3Cl]$ were synthesized by literature methods [4,5].

5.2.2. Physical measurements

Microanalyses (CHN) were carried out with a Thermo Finnigan Flash EA-1112 elemental analyzer. A Shimadzu LCMS 2010 liquid chromatograph mass spectrometer was used for the purity verification of H_2L^1–H_2L^3.

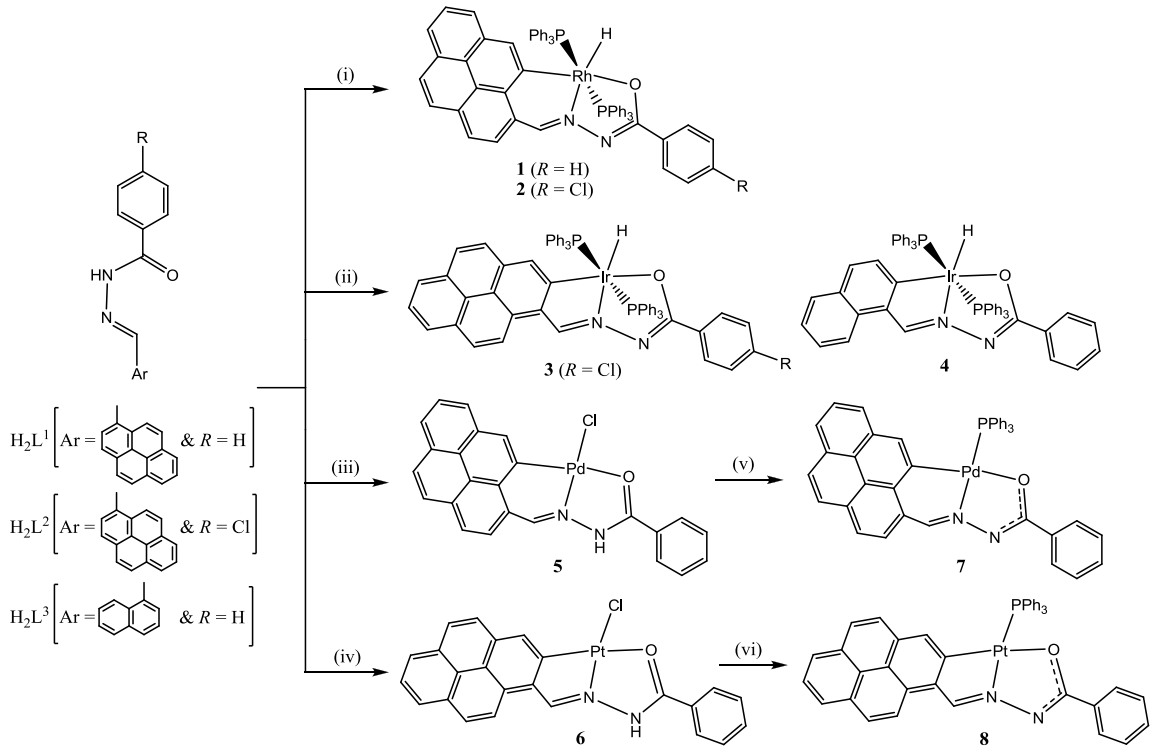

Scheme 5.1. (i) $[Rh(PPh_3)_3Cl]$ and $CH_3COONa{\cdot}3H_2O$ (1:2) in methanol, refluxing, 8 h; (ii) $[Ir(PPh_3)_3Cl]$ and $CH_3COONa{\cdot}3H_2O$ (1:2) in toluene, refluxing, 48 h; (iii) $Li_2[PdCl_4]$ and $CH_3COONa{\cdot}3H_2O$ (1:1) in methanol, stirring at room temp., 48 h; (iv) $K_2[PtCl_4]$ and $CH_3COONa{\cdot}3H_2O$ (1:1) in methanol-water, stirring at 60° C, 12 h; (v) and (vi) PPh_3 (2 mole equiv.) in acetone, stirring at room temp., 24 h.

Magnetic susceptibility measurements at room temperature (298 K) were performed with a Sherwood scientific balance. A Thermo Scientific Nicolet 380 FT-IR spectrophotometer was used to record the infrared spectra of the complexes in KBr pellets. Solution electrical conductivities were measured with a Digisun DI-909 conductivity meter. A Shimadzu UV3600 UV-Vis-NIR spectrophotometer was used to collect the electronic spectra. The emission spectra were recorded on a Horiba Jobin Yvon Fluoromax-4 spectrofluorometer. The ^{1}H (400 MHz) and ^{31}P (121 MHz for **1**–**4** and **7** and 202 MHz for **8**) NMR spectra were recorded with the help of Bruker NMR spectrometers. A CH-Instruments model 620A electrochemical analyzer was used for cyclic voltammetric experiments with dichloromethane solutions of the complexes containing tetrabutylammonium perchlorate (TBAP) as the supporting electrolyte. The measurements were carried out with a platinum disk working electrode, a platinum wire auxiliary electrode and an Ag/AgCl reference electrode at 298 K under nitrogen atmosphere. Under similar condition the $E_{1/2}$ value of the ferrocenium/ferrocene (Fc^{+}/Fc) redox couple was observed at 0.44 V.

5.2.3. Synthesis of *trans*-[Rh(L^{1})(PPh$_3$)$_2$H] (1)

[Rh(PPh$_3$)$_3$Cl] (185 mg, 0.2 mmol) and CH$_3$COONa·3H$_2$O (55 mg, 0.4 mmol) were added to a suspension of H$_2$L^{1} (69 mg, 0.2 mmol) in methanol (20 ml). The mixture was refluxed under nitrogen atmosphere for 8 h. The yellow solid formed was filtered and washed with cold methanol and dried in air. Yield was 145 mg (74%). Selected IR bands (cm^{-1}): ν_{Rh-H}, 2010; $\nu_{C=N}$, 1582. ^{31}P NMR in CDCl$_3$: δ (ppm) ($J_{(Rh-P)}$ (Hz)) = 39.54 (118) (d). Emission in CH$_2$Cl$_2$: λ_{max} (nm) (λ_{exc} (nm)) = 515, 395, 415 (320).

5.2.4. Synthesis of *trans*-[Rh(L^{2})(PPh$_3$)$_2$H] (2)

This complex was prepared in 70% yield by following the same procedure as described above for **1** using H$_2$L^{2} instead of H$_2$L^{1}. Selected IR bands (cm^{-1}): ν_{Rh-H}, 2016; $\nu_{C=N}$, 1578. ^{31}P NMR in CDCl$_3$: δ (ppm) ($J_{(Rh-P)}$

(Hz)) = 39.52 (118) (d). Emission in CH_2Cl_2: λ_{max} (nm) (λ_{exc} (nm)) = 515, 415, 395 (310).

5.2.5. Synthesis of *trans*-[Ir(L^2)(PPh_3)$_2$H] (3)

[$Ir(PPh_3)_3Cl$] (203 mg, 0.2 mmol) and $CH_3COONa{\cdot}3H_2O$ (55 mg, 0.4 mmol) were added to a suspension of H_2L^2 (72 mg, 0.2 mmol) in toluene (20 ml). The mixture was refluxed under nitrogen atmosphere for 48 h. The orange solution formed was evaporated to dryness. The solid obtained was dissolved in dichloromethane and transferred to a silica gel column packed with *n*-hexane. The elution was done with *n*-hexane-acetone mixture. The initial yellow band was discarded. The following orange band containing **3** was collected and evaporated to dryness. The yield of **3** thus obtained was 138 mg (62%). Selected IR bands (cm^{-1}): ν_{Ir-H}, 2050; $\nu_{C=N}$, 1588. ^{31}P NMR in $(CD_3)_2SO$: δ (ppm) = 14.94 (s).

5.2.6. Synthesis of *trans*-[Ir(L^3)(PPh_3)$_2$H] (4)

Complex **4** was synthesized in 65% yield by following a procedure similar to that described for **3** by using H_2L^3 instead of H_2L^2. Selected IR bands (cm^{-1}): ν_{Ir-H}, 2070; $\nu_{C=N}$, 1572. ^{31}P NMR in $CDCl_3$: δ (ppm) = 16.65 (s).

5.2.7. Synthesis of [Pd(HL^1)Cl] (5)

H_2L^1 (174 mg, 0.5 mmol) and $CH_3COONa{\cdot}3H_2O$ (68 mg, 0.5 mmol) were added to a methanol solution (40 ml) of $Li_2[PdCl_4]$ (prepared in situ using 0.5 mmol of $PdCl_2$ and 1.0 mmol of LiCl). The mixture was stirred under aerobic condition at room temperature for 48 h. The product precipitated as a yellow solid was filtered and washed with cold methanol and dried in air. Yield was 221 mg (90%). Selected IR bands (cm^{-1}): ν_{N-H}, 3144; $\nu_{C=O}$, 1643; $\nu_{C=N}$, 1604. Emission in Me_2NCHO: λ_{max} (nm) (λ_{exc} (nm)) = 510, 390, 410 (317).

5.2.8. Synthesis of [Pt(HL^1)Cl (6)

H_2L^1 (174 mg, 0.5 mmol) and $CH_3COONa{\cdot}3H_2O$ (68 mg, 0.5 mmol) were added to a solution of $K_2[PtCl_4]$ (208 mg, 0.5 mmol) in a solvent mixture of methanol (20 ml) and H_2O (1 ml). The reaction mixture was stirred under aerobic condition at 60º C for 12 h. The complex [Pt(HL^1)Cl] precipitated as a brown solid collected by filtration, washed with methanol and dried in air. Yield was 235 mg (80%). Selected IR bands (cm^{-1}): ν_{N-H}, 3205; $\nu_{C=O}$, 1637; $\nu_{C=N}$, 1582. Emission in Me_2NCHO: λ_{max} (nm) (λ_{exc} (nm)) = 600, 645, 405, 390 (350).

5.2.9. Synthesis of [Pd(L^1)(PPh$_3$)] (7)

[Pd(HL^1)Cl] (98 mg, 0.2 mmol) and PPh_3 (105 mg, 0.4 mmol) were taken in acetone (30 ml) and the mixture was stirred under aerobic condition at room temperature for 24 h. The complex precipitated as a yellow solid was filtered, washed with acetone and dried in air. Yield was 121 mg (85%). Selected IR bands (cm^{-1}): $\nu_{C=N}$, 1561. ^{31}P NMR in $(CD_3)_2SO$: δ (ppm) = 37.31 (s). Emission in Me_2NCHO: λ_{max} (nm) (λ_{exc} (nm)) = 510, 390, 410 (317).

5.2.10. Synthesis of [Pt(L^1)(PPh$_3$)] (8)

A mixture of [Pt(HL^1)Cl] (116 mg, 0.2 mmol) and PPh_3 (105 mg, 0.4 mmol) in acetone (30 ml) was stirred under aerobic condition at room temperature for 24 h. The resulting red solution was evaporated to dryness. The red solid so obtained was dissolved in minimum amount of dichloromethane and transferred to a silica gel column packed with *n*-hexane. The yellow band obtained first by elution with *n*-hexane-acetone mixture was discarded. The next red band containing **8** was collected and evaporated to dryness. The yield of **8** thus obtained was 80 mg (50%). Selected IR bands (cm^{-1}): $\nu_{C=N}$, 1582. ^{31}P NMR in $(CD_3)_2SO$: δ (ppm) = 22.96 (s, with ^{195}Pt satellites, $^1J_{(Pt-P)}$ = 3780 Hz). Emission in Me_2NCHO: λ_{max} (nm) (λ_{exc} (nm)) = 645, 600, 405, 390 (350).

5.2.11. X-ray crystallography

Single crystals of **1** and **2** were obtained by slow evaporation of the corresponding dichloromethane-*n*-hexane (1:1) solutions, while single crystals of **4** were grown by slow evaporation of its dichloromethane-acetonitrile (1:1) solution. Diethyl ether vapour diffusion into the dimethylformamide solution of **5** provided its single crystals as **5**·Me_2NCHO. Unit cell determination and intensity data collection of **1**, **2** and **4** were performed on a Bruker-Nonius SMART APEX CCD single crystal diffractometer (Mo $K\alpha$ radiation, λ = 0.71073 Å). An Oxford Diffraction Xcalibur Gemini single crystal X-ray diffractometer (Mo $K\alpha$ radiation, λ = 0.71073 Å) was used to obtain the unit cell parameters and intensity data for **5**·Me_2NCHO. The SMART and the SAINT-Plus packages [6] were used for data acquisition and data extraction, respectively for **1**, **2** and **4**. The absorption corrections were performed with the help of SADABS program [7]. The CrysAlisPro software [8] was used for data collection, reduction and absorption correction for **5**·Me_2NCHO. In each case, the structure was solved by direct method and refined on F^2 by full-matrix least-squares procedures. All non-hydrogen atoms were refined anisotropically. The metal bound hydrogen atoms located in the corresponding difference maps were refined isotropically for **1** and **2**, while for **4** it was refined with geometric and thermal restraints. In case of **5**·Me_2NCHO, the hydrogen atom of the amide fragment (–NHC(=O)–) of the ligand was located in a difference map and refined isotropically. The O-atom of the solvent molecule Me_2NCHO is hydrogen bonded with this amide N–H of the ligand (N···O, 2.770(5) Å; N–H···O 165(4)º). All the remaining hydrogen atoms in each structure were included in the structure factor calculation at idealized positions by using a riding model. The SHELX-97

Table 5.1. Selected crystallographic data.

Complex	**1**	**2**	**4**	**5**·Me_2NCHO
Chemical formula	$C_{60}H_{45}N_2OP_2Rh$	$C_{60}H_{44}N_2OP_2ClRh$	$C_{54}H_{43}N_2OP_2Ir$	$C_{27}H_{22}N_3O_2ClPd$
Formula weight	974.83	1009.27	990.04	562.36
Crystal system	Tetragonal	Monoclinic	Triclinic	Monoclinic
Space group	$P\bar{4}2_1c$	$P2_1/n$	$P\bar{1}$	$P2_1/n$
Temp. (K)	298	100	298	298
a (Å)	24.0598(8)	12.0869(14)	11.821(2)	10.5779(12)
b (Å)	24.0598(8)	16.2496(19)	11.851(2)	9.3644(10)
c (Å)	16.2146(7)	23.833(3)	18.726(3)	23.157(3)
α (°)	90	90	100.320(2)	90
β (°)	90	99.508(2)	93.214(3)	93.803(10)
γ (°)	90	90	119.778(2)	90
V (Å^3), Z	9386.2(6), 8	4616.7(9), 4	2207.5(7), 2	2288.8(4), 4
ρ (g cm^{-3})	1.380	1.452	1.489	1.632
μ (mm^{-1})	0.477	0.544	3.138	0.959
Reflections collected	89085	32708	21179	9396
Reflections unique	8266	8136	7727	4031
Reflections [$I \geq 2\sigma(I)$]	7074	5918	7384	2950
Parameters	599	608	544	311
$R1$, $wR2$ [$I \geq 2\sigma(I)$]	0.0527, 0.0974	0.0421, 0.0824	0.0199, 0.0499	0.0415, 0.0809
$R1$, $wR2$ [all data]	0.0646, 0.1015	0.0696, 0.0902	0.0211, 0.0503	0.0667, 0.0914
GOF on F^2	1.142	0.980	1.063	1.024
Max. / Min. peaks (e Å^{-3})	0.640 / –0.211	0.623 / –0.322	1.313 / –0.352	0.440, –0.397

programs [9] available in the WinGX package [10] were used for structure solution and refinement. The Platon [11] and the Mercury [12] software packages were used for molecular graphics. All the crystallographic data (except for the structure factors) have been deposited with the Cambridge Crystallographic Data Centre. The deposition numbers are CCDC 991421–991424 for **1**, **2**, **4** and **5**·Me_2NCHO respectively. Selected crystal data and refinement summary for all four structures are listed in Table 5.1.

5.3. Results and discussion

5.3.1. Synthesis and some properties

The 4-*R*-N′-(arylidene)benzohydrazides (H_2L^1–H_2L^3) were prepared in ~90% yields by condensation reactions of equimolar amounts of 4-*R*-benzohydrazide and the corresponding polycyclic aromatic aldehydes in ethanol [13–16]. The identities of these three compounds were authenticated by microanalysis (CHN) and spectroscopic (LC-MS, IR, ^{1}H NMR and UV-Vis) measurements. Complexes **1**–**4** were synthesized in good yields (62–74%) by reacting the monovalent metal ion starting materials [$M(PPh_3)_3Cl$] (M = Rh(I) and Ir(I)) with H_2L^n and $CH_3COONa·3H_2O$ in 1:1:2 mole ratio in methanol (for Rh(I)) or in toluene (for Ir(I)) under nitrogen atmosphere (Scheme 5.1). On the other hand, reactions of $[MCl_4]^{2-}$ (M = Pd(II) and Pt(II)) salts, H_2L^1 and $CH_3COONa·3H_2O$ in 1:1:1 mole ratio in methanol (for Pd(II)) or in methanol-water mixture (for Pt(II)) under aerobic conditions provided complexes **5** and **6** in very good yields (80–85%). Treatment of each of **5** and **6** with two mole equivalents of PPh_3 in acetone produces complexes **7** and **8** in 80 and 50% yields, respectively (Scheme 5.1). The microanalysis (CHN) data (Table 5.2) of **1**–**8** are consistent with the corresponding general formulas [$M(L^n)(PPh_3)_2H$] (M = Rh(III) (**1** and **2**) and Ir(III) (**3** and **4**)), [$M(HL^n)Cl$] (M = Pd(II) (**5**) and Pt(II) (**6**)) and [$M(L^n)(PPh_3)$] (M = Pd(II) (**7**) and Pt(II) (**8**)). In the synthesis reactions, protic methanol was used as solvent for the rhodium(III) complexes (**1** and **2**), while

Table 5.2. Elemental analysis data.

Compound	Found (calc) (%)		
	C	H	N
trans- [Rh(L^1)(PPh_3)$_2$H] (**1**)	73.81 (73.92)	4.61 (4.65)	2.78 (2.87)
trans- [Rh(L^2)(PPh_3)$_2$H] (**2**)	71.32 (71.40)	4.32 (4.39)	2.71 (2.78)
trans- [Ir(L^2)(PPh_3)$_2$H] (**3**)	65.51 (65.60)	4.12 (4.04)	2.48 (2.55)
trans- [Ir(L^3)(PPh_3)$_2$H] (**4**)	65.46 (65.51)	4.31 (4.38)	2.89 (2.83)
[Pd(HL^1)Cl] (**5**)	58.83(58.92)	3.16(3.09)	5.65(5.73)
[Pt(HL^1)Cl] (**6**)	49.72(49.88)	2.68(2.62)	4.75(4.85)
[Pd(L^1)(PPh_3)] (**7**)	70.36 (70.54)	4.31 (4.09)	3.85 (3.92)
[Pt(L^1)(PPh_3)] (**8**)	62.85 (62.76)	3.72 (3.64)	3.41 (3.49)

a non-protic solvent toluene was used for the iridium(III) complexes (**3** and **4**). **1** and **2** can also be synthesized using toluene as solvent and the same reaction conditions as applied for **3** and **4**, but attempts to synthesize any of **3** and **4** from methanol were unsuccessful. However, from ethanol instead of **3** an iridium(III) dihydride complex [Ir(HL^2)(PPh_3)$_2$$H_2$] was isolated. In this complex, $(HL^2)^-$ acts as N,O-chelating ligand. The molecular structure of this complex as obtained by preliminary X-ray crystallographic experiments is shown in Figure 5.1. Considering the formation of the dihydride complex, synthetic conditions used for **1**–**4** and the mechanisms reported in literature for the synthesis of similar cyclometallates and dihydride complexes with thosemicarbazones under comparable reaction conditions [17], we propose the following steps for the formation of **1**–**4**: oxidative addition of O–H (from the iminol form of azomethine-N coordinated H_2L^n) leading to two electron oxidation of the metal centre, formation of the five-membered N,O-chelate ring and coordination of the hydride and finally cyclometallation via activation

of aryl C–H situated in close proximity (Scheme 5.2). Solid state magnetic susceptibility measurements made at room temperature indicate the diamagnetic nature of all the complexes. Thus the metal centres (Rh and Ir) in **1**−**4** are trivalent and in low-spin state, while that (Pd and Pt) in **5**−**8** are bivalent and in square-based coordination geometry. In chloroform, dichloromethane, dimethylsulfoxide and dimethylformamide, **1**−**4** are highly soluble, while **5**–**8** are moderately soluble. In solution, each of **1**−**8** behaves as nonelectrolyte.

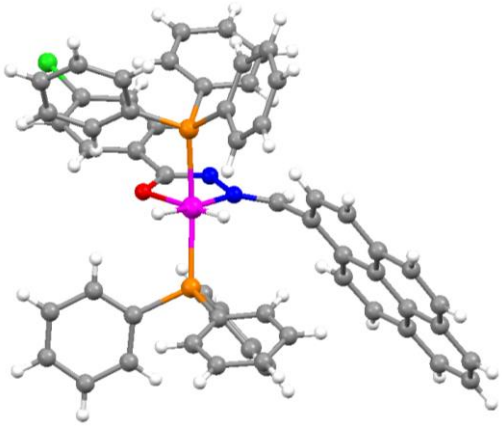

Figure 5.1. Ball and stick diagram of $[Ir(HL^2)(PPh_3)_2H_2]$.

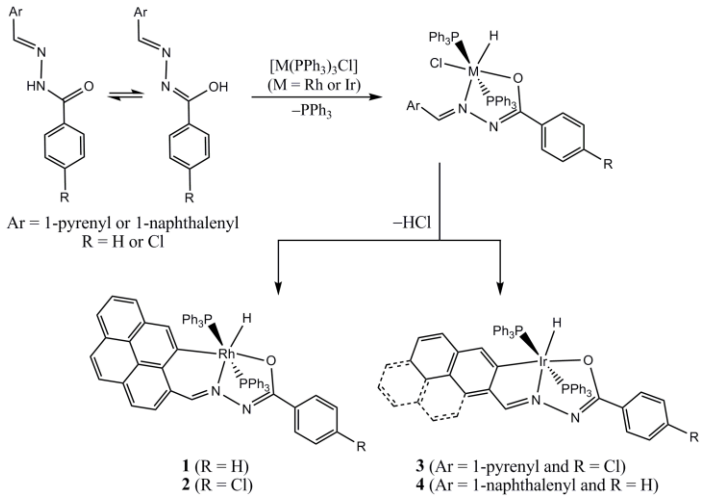

Scheme 5.2. Possible steps involved in the formation of **1**–**4**.

5.3.2. Description of X-ray structures

The molecular structures of **1**, **2**, **4** and **5** have been determined by single crystal X-ray crystallography. The bond parameters associated with the metal centres in **1**, **2** and **4** are listed in Table 5.3 and those for **5** are summarized in Table 5.4. The structures of the rhodium(III) complexes (**1** and **2**) are depicted in Figure 5.2 and the structures of the iridium(III) (**4**) and the palladium(II) (**5**) complexes are illustrated in Figure 5.3. Attempts to grow single crystals of the remaining complexes were partially successful. Crystals of **6** and **7** could not be grown, while that of **3** and **8** obtained by slow evaporation of the corresponding dichloromethane-acetonitrile (1:1) solutions were very weakly diffracting. As a result, the X-ray data obtained for the latter two complexes were of very poor quality. Nonetheless, structures for both could be solved but refinement failed to reduce the *R*-factors to a satisfactory level. The molecular structures of **3** and **8** with the selected crystal data are shown in Figure 5.4. In each of the rhodium(III) (**1** and **2**) and the iridium(III) (**3** and **4**) complexes, the metal centre is in distorted octahedral $CNOHP_2$ coordination sphere constituted by the meridional $(L^n)^{2-}$, a hydride and two mutually *trans*-oriented PPh_3 ligands. In the palladium(II) complex (**5**), $(HL^1)^-$ and the chloride, while in the platinum(II) complex (**8**), $(L^n)^{2-}$ and the PPh_3 provide satisfactory CNOCl and CNOP square-planar coordination geometries, respectively. In **1** and **2**, $(L^n)^{2-}$ coordinates the metal centre through the 1-pyrenyl *peri*-C, the azomethine-N and the amidate-O atoms and forms 6,5-membered fused chelate rings. Similarly $(HL^1)^-$ acts as the 1-pyrenyl *peri*-C, the azomethine-N and the amide-O donor to form 6,5-membered fused chelate rings in **5**. On the other hand, $(L^n)^{2-}$ uses the polycyclic aryl *ortho*-C, the azomethine-N and the amidate-O to coordinate the metal centre in each of **3**, **4** and **8** and creates 5,5-membered fused chelate rings. The C–O (1.287(4)–1.303(6) Å) and the C–N (1.306(6)–1.323(3) Å) bond lengths

Table 5.3. Selected bond lengths (Å) and angles (º) for *trans*-[Rh($L^{1/2}$)(PPh_3)$_2$H] (**1** and **2**) and *trans*-[Ir(L^3)(PPh_3)$_2$H] (**4**).

Complex	**1** (M = Rh)	**2** (M = Rh)	**4** (M = Ir)
M(1)–C(1)	2.020(4)	2.030(3)	2.040(2)
M(1)–H(1)	1.24(5)	1.48(3)	1.575(10)
M(1)–N(1)	2.049(4)	2.055(3)	2.0268(19)
M(1)–O(1)	2.128(3)	2.115(2)	2.1857(18)
M(1)–P(1)	2.3235(12)	2.3126(9)	2.2982(8)
M(1)–P(2)	2.3240(12)	2.3107(9)	2.3066(8)
C(1)–M(1)–H(1)	91(2)	94.4(12)	99.3(12)
C(1)–M(1)–N(1)	93.72(17)	93.77(12)	79.58(9)
C(1)–M(1)–O(1)	170.50(18)	170.40(11)	154.77(9)
C(1)–M(1)–P(1)	84.14(12)	88.00(9)	90.25(7)
C(1)–M(1)–P(2)	89.81(12)	89.39(9)	90.78(7)
N(1)–M(1)–H(1)	176(2)	171.7(12)	174.1(12)
N(1)–M(1)–O(1)	77.07(16)	76.70(10)	75.19(7)
N(1)–M(1)–P(1)	96.79(11)	94.24(7)	94.52(6)
N(1)–M(1)–P(2)	93.62(11)	96.64(7)	100.98(6)
O(1)–M(1)–H(1)	99(2)	95.1(12)	105.7(12)
O(1)–M(1)–P(1)	94.56(9)	91.49(6)	91.35(5)
O(1)–M(1)–P(2)	93.03(9)	92.86(6)	94.33(5)
P(1)–M(1)–H(1)	83(2)	87.5(12)	79.6(12)
P(1)–M(1)–P(2)	168.27(5)	168.95(3)	164.39(2)
P(2)–M(1)–H(1)	87(2)	82.0(12)	84.8(12)

of the amidate fragment (–C(O$^-$)=N–) of $(L^n)^{2-}$ in **1**, **2** and **4** are consistent with its deprotonated state [13–16]. In comparison, the corresponding C–O (1.246(5) Å) and C–N (1.335(5) Å) bond lengths are significantly shorter and longer, respectively due to the protonated form of the amide functionality of the ligand $(HL^1)^-$ in **5**. The M–C, M–N, M–O, M–P and M–H bond lengths in **1**–**4** are comparable with the corresponding bond lengths reported for complexes of trivalent metal ions having similar coordinating atoms [4,17–19]. The Pd–C, Pd–N, Pd–O and Pd–Cl bond lengths in **5** are unexceptional [16,17].

Table 5.4. Selected bond lengths (Å) and angles (º) for [Pd(HL^1)Cl]·Me$_2$NCHO (**5**·Me$_2$NCHO).

Complex	**5**·Me$_2$NCHO
Pd(1)–C(1)	2.001(4)
Pd(1)–N(1)	1.961(3)
Pd(1)–O(1)	2.145(3)
Pd(1)–Cl(1)	2.3227(12)
C(1)–Pd(1)–N(1)	92.45(15)
C(1)–Pd(1)–O(1)	170.97(14)
C(1)–Pd(1)–Cl(1)	98.42(12)
N(1)–Pd(1)–O(1)	79.41(12)
N(1)–Pd(1)–Cl(1)	168.04(10)
O(1)–Pd(1)–Cl(1)	90.05(9)

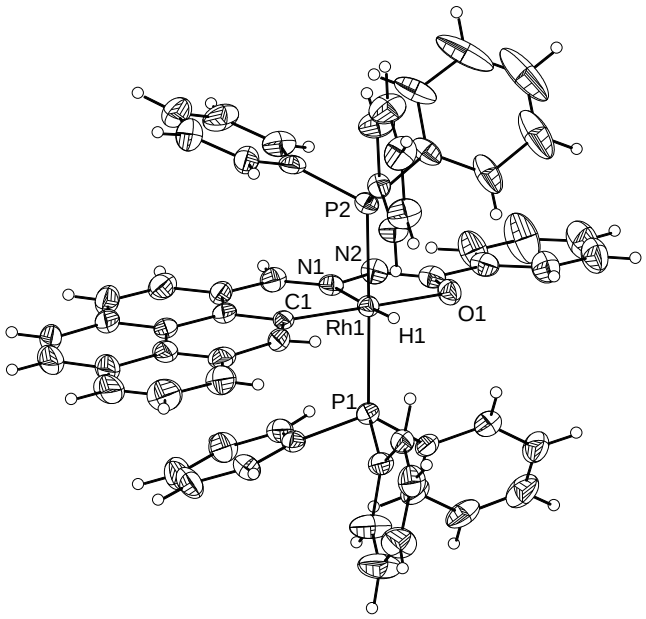

(a)

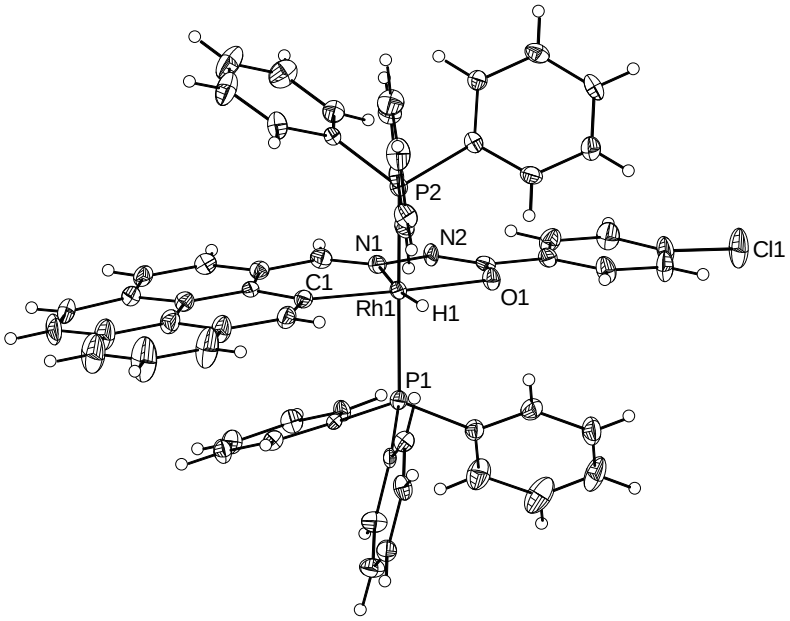

(b)

Figure 5.2. Thermal ellipsoid plots of (a) *trans*-[Rh(L^1)(PPh_3)$_2$H] (**1**) (30% probablity) and (b) *trans*-[Rh(L^2)(PPh_3)$_2$H] (**2**) (50% probablity). In both plots, for clarity none of the carbon atoms are labelled except for the metal coordinated one.

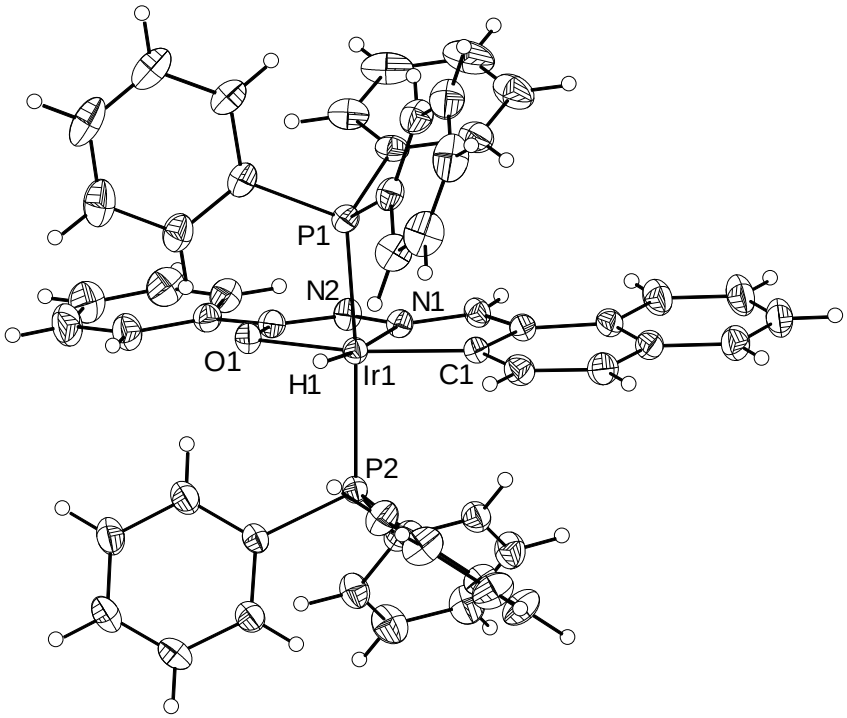

(a)

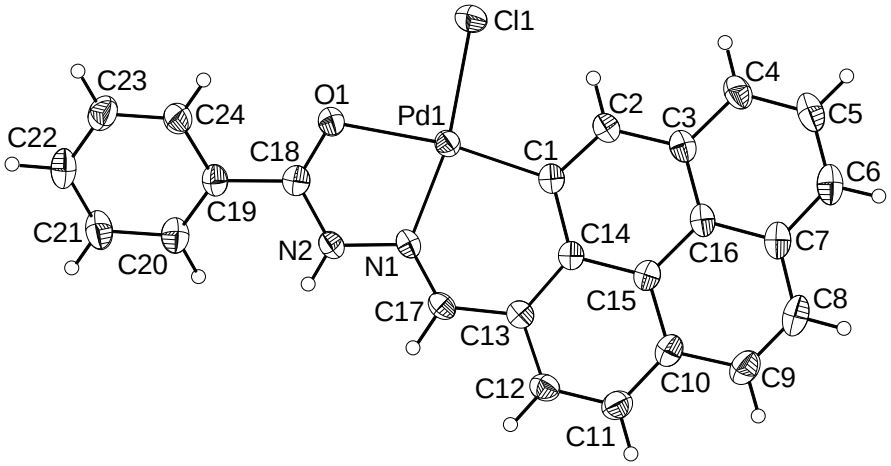

(b)

Figure 5.3. Thermal ellipsoid plots of (a) *trans*-[Ir(L^3)(PPh_3)$_2$H] (**4**) (25% probablity) and (b) [Pd(HL^1)Cl] (**5**) (30% probablity). In the plot of **4**, for clarity none of the carbon atoms are labelled except for the metal coordinated one.

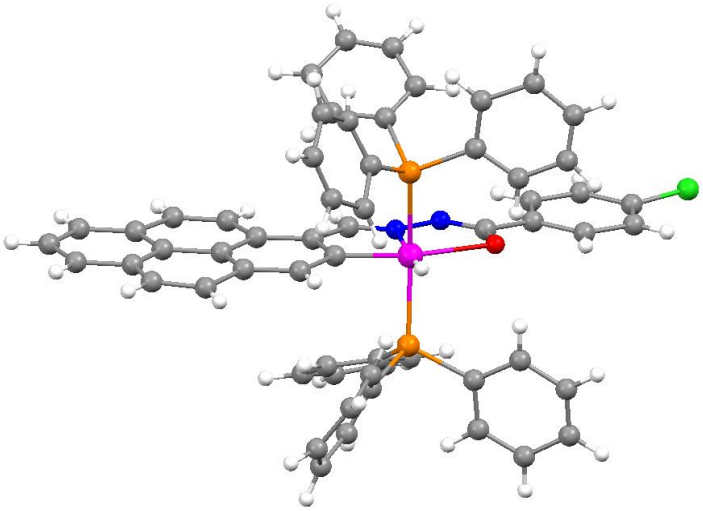

(a)

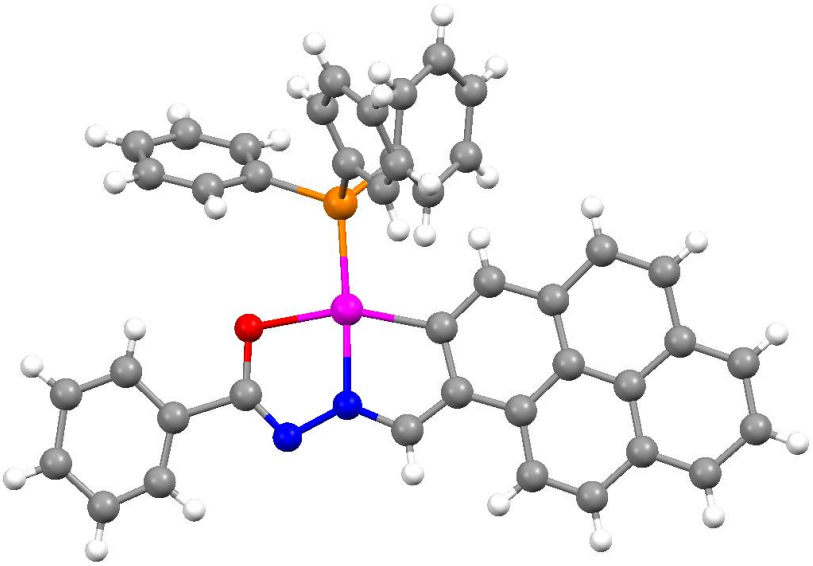

(b)

Figure 5.4. Ball and stick diagrams of (a) [Ir(L^2)(PPh_3)$_2$H] (**3**) (one of the two very similar molecules present in the asymmetric unit is shown); crystal data: space group = $P2_1/c$, a = 23.4109(17) Å, b = 17.1468(9) Å, c = 26.057(2) Å, β = 111.665(9)º, V = 9721.0(1) Å^3, Z = 8 and (b) [Pt(L^1)(PPh_3)] (**8**); crystal data: space group = $P2_1/n$, a = 14.001(5) Å, b = 9.360(2) Å, c = 24.691(6) Å, β = 94.11(3)º, V = 3227.7(2) Å^3, Z = 4.

5.3.3. Infrared spectral properties

Infrared spectra of **1**−**4**, **7** and **8** do not display any band assignable to the N–H and C=O stretches of the free H_2L^n [13–16]. Absence of these bands indicates the deprotonated state of the amide functionality in the corresponding ligands. In contrast, both **5** and **6** display a broad band at ~3175 cm^{-1} (ν_{N-H}) and a moderately strong band at ~1640 cm^{-1} ($\nu_{C=O}$) due to the protonated amide functionality of the ligands in them. A medium intensity band for the M–H stretch appears at 2010 and 2016 cm^{-1} for the rhodium(III) complexes **1** and **2**, respectively, while that appears at 2050 and 2070 cm^{-1} for the iridium(III) complexes **3** and **4**, respectively (Figure 5.5). These M–H stretching band positions are comparable with the literature values [4,17,18]. A moderate to strong band in the range 1570–1604 cm^{-1} observed for all the complexes is attributed to the metal coordinated azomethine C=N stretch [13–16]. Three strong bands in the ranges 740−755, 690−696 and 510−525 cm^{-1} in the spectra of **1**−**4**, **7** and **8** correspond to the coordinated PPh_3 in each of them [15,16,17,19].

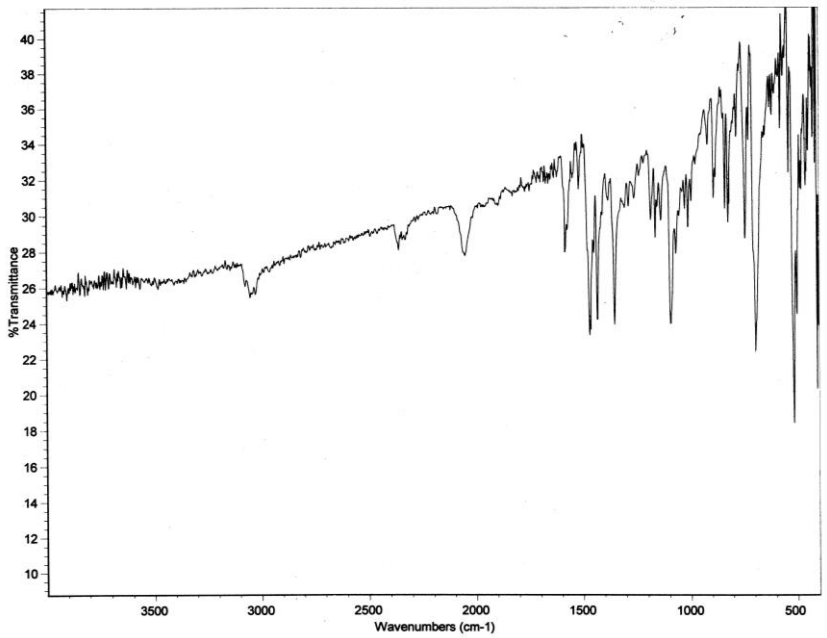

Figure 5.5. Infrared spectrum of *trans*-[Ir(L^2)(PPh_3)$_2$H] (**3**).

5.3.4. NMR spectral properties

The NMR spectra of all the complexes except **1**, **2** and **4** were recorded in $(CD_3)_2SO$. The spectra of **1**, **2** and **4** were recorded in $CDCl_3$. Proton-labeling schemes used for ^1H NMR signals assignment are shown in Figure 5.6. Representative spectra are shown in Figures 5.7 and 5.8. Chemical shift values for **1**–**8** are summarized in Tables 5.5 and 5.6.

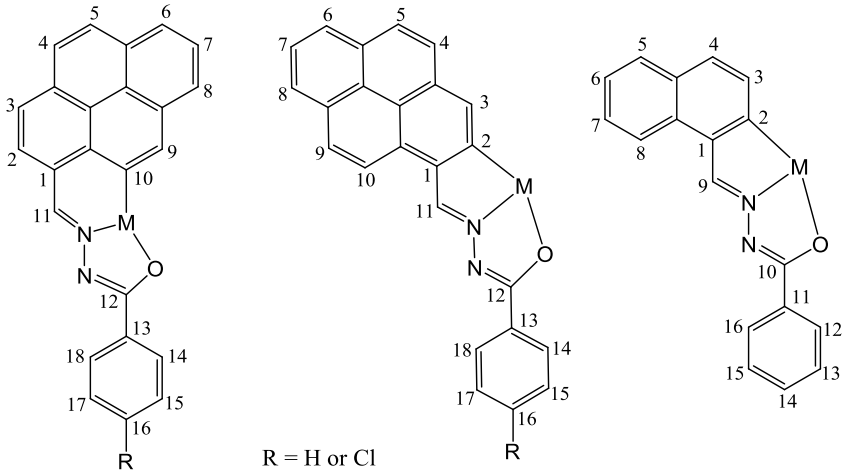

Figure 5.6. Tridentate ligand proton-labeling schemes used for ^1H NMR signals assignment.

The amide functionality N–H proton of $(HL^1)^-$ in **5** and **6** appears as a singlet at δ 11.38 and 11.95, respectively. As expected no such resonance is observed for **1**–**4**, **7** and **8** due to the deprotonation of the amide functionality in the corresponding ligands. The azomethine (CH=N) proton resonates in the ranges δ 7.75–8.29 for **1**–**4** and δ 9.05–9.54 for **5**–**8**. It appears as a rather broad singlet for all the complexes except **8** where it is observed as a doublet. Similar doublet reported for analogous complexes has been suggested to be due to the coupling of the azomethine proton with the phosphorus atom of the PPh_3 [22,23]. The ^{31}P NMR spectra of all the triphenylphosphine coordinated complexes have been recorded. The rhodium(III) complexes display a doublet

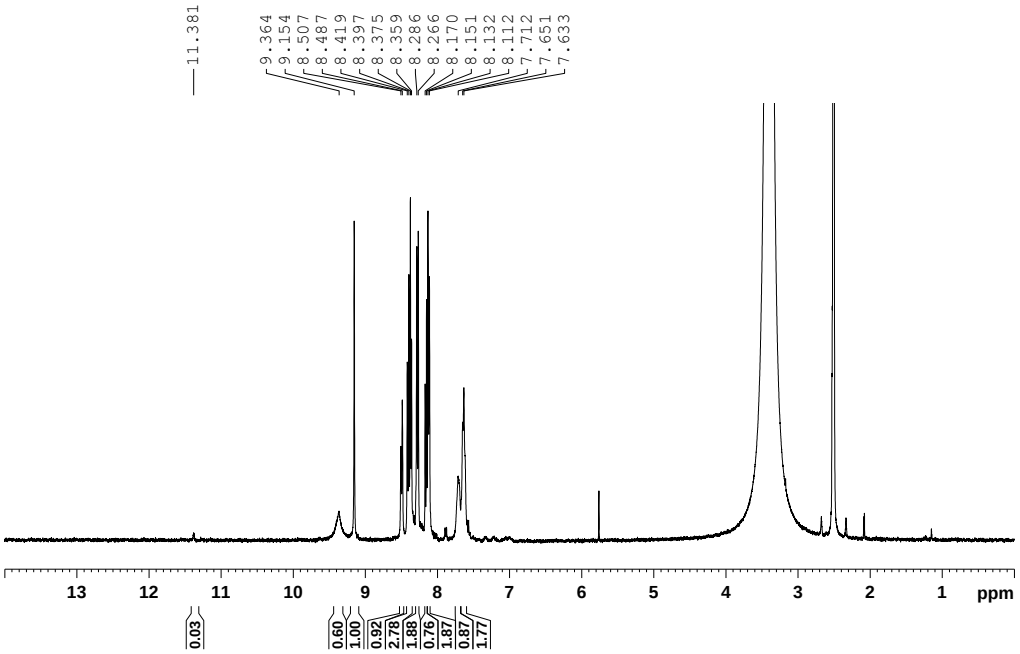

Figure 5.7. ^{1}H NMR spectrum of [Pd(HL^{1})Cl] (**5**).

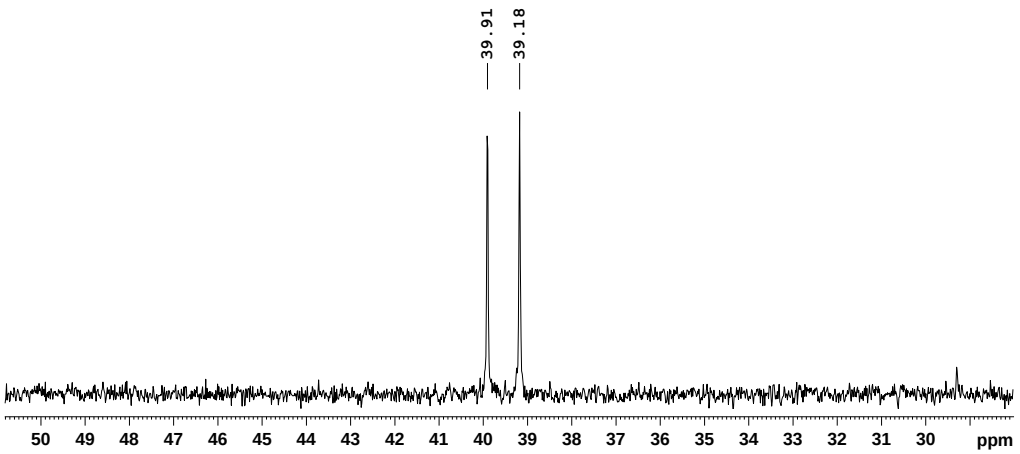

Figure 5.8. ^{31}P NMR spectrum of *trans*- [Rh(L^{1})(PPh$_3$)$_2$H]^{a} (**1**).

Table 5.5. ^{1}H NMR data of **1**–**4**.

Complex	δ (ppm) (J (Hz))
trans- [Rh(L^1)(PPh_3)$_2$H][a] (**1**)	8.26 (br, s, 1H, H^{11}), 7.93 (9) (d, 1H, H^2), 7.88 (m, 2H, H^6, H^8), 7.82 (7) (d, 1H, H^3), 7.67 (m, 3H, H^4, H^5, H^7), 7.53 (br, s, 1H, H^9), 7.50 (8) (d, 2H, H^{14}, H^{18}), 7.32–6.91 (m, 33H, H^{15}, H^{16}, H^{17} and 2 PPh_3 protons), −10.13 (qd, 1H, Rh−H).
trans- [Rh(L^2)(PPh_3)$_2$H][a] (**2**)	8.24 (br, s, 1H, H^{11}), 7.94 (9) (d, 1H, H^2), 7.88 (m, 2H, H^6, H^8), 7.82 (8) (d, 1H, H^3), 7.68 (8) (t, 1H, H^7), 7.62 (8) (d, 2H, H^4, H^5), 7.56 (br, s, 1H, H^9), 7.49 (8) (d, 2H, H^{14}, H^{18}), 7.31–6.91 (m, 32H, H^{15}, H^{17} and 2 PPh_3 protons), −10.13 (qd, 1H, Rh−H).
trans- [Ir(L^2)(PPh_3)$_2$H][b] (**3**)	8.29 (br, s, 1H, H^{11}), 8.04 (m, 2H, H^6, H^8), 7.98 (7) (d, 1H, H^9), 7.85 (m, 2H, H^{10}, H^7), 7.72 (9) (d,1H, H^5), 7.55 (9) (d, 2H, H^{14}, H^{18}), 7.41−7.24 (m, 32H, H^{15}, H^{17} and 2 PPh_3 protons), 7.20 (9) (d, 1H, H^4), 7.10 (s, 1H, H^3), −12.56 (td, 1H, Ir−H).
trans- [Ir(L^3)(PPh_3)$_2$H][a] (**4**)	7.75 (br, s, 1H, H^9), 7.54–7.07 (m, 39H, H^5–H^8, H^{12}–H^{16} and 2 PPh_3 protons), 6.69 (8) (d, 1H, H^4), 6.59 (8) (d, 1H, H^3), −12.66 (t, 1H).

[a] In $CDCl_3$.

[b] In dmso-d6.

Table 5.6. ^{1}H NMR data[a] of **5**–**8**.

Complex	δ (ppm) (J (Hz))
[Pd(HL^{1})Cl] (**5**)	11.38 (s, 1H, NH), 9.36 (br, s, 1H, H^{11}), 9.15 (s, 1H, H^{9}), 8.50 (8) (d, 1H, H^{3}), 8.39 (m, 3H, H^{2}, H^{6}, H^{8}), 8.27 (8) (d, 2H, H^{4}, H^{5}), 8.14 (m, 3H, H^{7}, H^{14}, H^{18}), 7.71 (br, s, 1H, H^{16}), 7.64 (m, 2H, H^{15}, H^{17}).
[Pt(HL^{1})Cl] (**6**)	12.06 (s, 1H, NH), 9.54 (s, 1H, H^{11}), 8.84 (m, 1H, H^{3}), 8.60 (8) (d, 1H, H^{4}), 8.39 (m, 3H, H^{5}, H^{9}, H^{10}), 8.27 (8) (d, 2H, H^{6}, H^{8}), 8.14 (8) (t, 1H, H^{7}), 8.02 (7) (d, 2H, H^{14}, H^{18}), 7.62 (m, 3H, H^{15}, H^{16}, H^{17})
[Pd(L^{1})(PPh$_3$)] (**7**)	9.22 (br, s, 1H, H^{11}), 8.58 (8) (d, 1H, H^{2}), 8.41 (8) (d, 1H, H^{3}), 8.24 (m, 4H, H^{4}, H^{5}, H^{6}, H^{8}), 8.11 (br, s, 1H, H^{7}), 7.87 –7.32 (m, 20H, H^{14}, H^{15}, H^{16}, H^{17}, H^{18} and PPh$_3$ protons), 7.12 (br, s, 1H, H^{9}).
[Pt(L^{1})(PPh$_3$)] (**8**)	9.05 (10) (d, 1H, H^{11}), 8.41 (9) (d, 1H, H^{9}), 8.13 (m, 2H, H^{6}, H^{8}), 8.02 (9) (d, 1H, H^{10}), 7.91 (m, 4H, H^{5}, H^{7}, H^{14}, H^{18}), 7.73–7.44 (m, 18H, H^{15}, H^{16}, H^{17} and PPh$_3$ protons), 6.99 (9) (d, 1H, H^{4}), 6.67 (br, s, 1H, H^{3}) .

[a] In dmso-d6.

(Figure 5.8) due to ^{103}Rh and ^{31}P coupling at δ ~39.53 ($^{1}J_{(Rh–P)}$ = 118 Hz for **1** and **2**). In contrast, a singlet was observed in the spectra of the iridium(III) complexes (at δ 14.94 and 16.65 for **3** and **4**, respectively) and the palladium(II) and platinum(II) complexes (at δ 37.31 and 22.96 for **7** and **8**, respectively).

In the ^{1}H NMR spectra of both **1** and **2**, the hydride resonates as a quartet of doublets centred at δ −10.12 (Figure 5.9). The quartet indicates coupling of the hydride with both ^{103}Rh and ^{31}P nuclei and comparable $^{1}J_{(Rh–H)}$ and $^{2}J_{(P–Rh–H/\textit{cis})}$ coupling constants (12.8 Hz) [20]. Further splitting of each peak to doublet is very likely due to weak coupling of the hydride with a nearby ligand H-atom ($J_{(H–H)}$ = 3.1 Hz for **1** and 3.4 Hz for **2**). On the other hand, the metal coordinated hydride in the iridium(III) complexes **3** and **4** appears as a triplet at δ −12.56 ($^{2}J_{(P–Ir–H/\textit{cis})}$ = 18.6 Hz) and −12.66 ($^{2}J_{(P–Ir–H/\textit{cis})}$ = 18.2 Hz), respectively (Figure 5.9). Interestingly for **3** each peak of the triplet again splits into a doublet due to weak H–H coupling ($J_{(H–H)}$ ≈ 1.2 Hz) as observed for the rhodium(III) complexes, but for **4** there is no such splitting (Figure 5.9). Appearance of triplet with no further splitting suggests that coupling of hydride occurs only with the two mutually *cis* oriented ^{31}P nuclei in **4**. The X-ray structures (*vide supra*) of both **1** and **2** show that the rhodium coordinated hydride is within 2.1–2.4 Å from one pyrenyl C–H (*ortho* to the metallated-C) and two phosphine phenyl-H atoms. Between these three H-atoms, it is expected that due to the rigidity of the tridentate ligand only the pyrenyl-H can not alter its relative position with respect to the hydride. Thus, it is very likely that in solution the pyrenyl-H is involved in a hydrogen bonding interaction with the rhodium bound hydride (Figure 5.9). Such C–H···H–Rh hydrogen bonding and similar NMR behaviour of metal bound hydride have been observed before [21]. In the iridium(III) species, the pyrenyl-H (in **3**) or the naphthalenyl-H (in **4**) is at a longer distance (~2.9 Å) from the metal coordinated hydride compared to the corresponding distances

in the rhodium(III) complexes (**1** and **2**). Perhaps for this reason C–H···H–Ir hydrogen bonding and hence the H–H NMR coupling is weaker in **3** than in **1** and **2** and the coupling could not be observed in **4** at all.

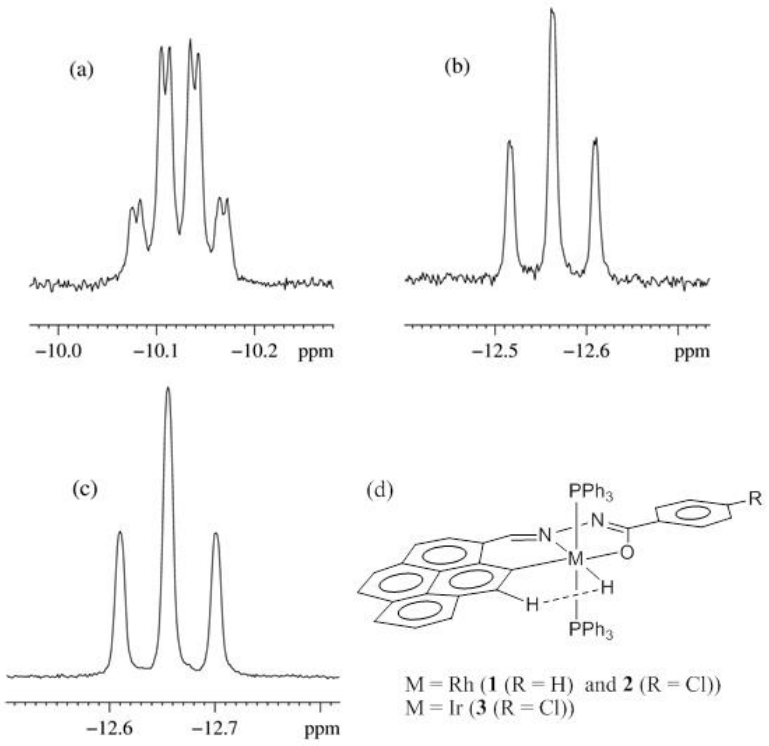

Figure. 5.9. Metal hydride ^{1}H NMR resonances in (a) *trans*-[Rh(L^2)(PPh_3)$_2$H] (**2**), (b) *trans*-[Ir(L^2)(PPh_3)$_2$H] (**3**) and (c) *trans*-[Ir(L^3)(PPh_3)$_2$H] (**4**) and (d) C–H···H–M interaction in **1**–**3**.

5.3.5. Electronic and emission spectral properties

The room temperature electronic absorption spectra of the rhodium(III) and the iridium(III) complexes (**1**−**4**) were collected in dichloromethane, while that of the palladium(II) and the platinum(II) complexes (**5**−**8**) were recorded in dimethylformamide. Spectroscopic data are listed in Table 5.7. Each complex shows multiple strong to very strong absorption bands in the visible and ultraviolet regions. Representative spectra are illustrated in Figure 5.10. H_2L^1 and H_2L^2 display two strong bands at ~370 and ~285 nm [15], while H_2L^3 shows only one strong band at ~340 nm [14]. Each of these bands is flanked by several shoulders. This type of spectra are very similar to that of pure polycyclic aromatic hydrocarbon except for the red-shift and poorly resolved vibrational structure [14–16,24–26]. The spectra of **1**−**8** are somewhat comparable and display a group of absorptions in the visible region (within ~390–510 nm) and one or two bands in the ultra-violet region (< 390 nm). In general the spectral profiles particularly in the visible range are similar to the profiles of free H_2L^n except for the further red-shift and more pronounced vibrational structure. Thus the absorption bands displayed by **1**−**8** are attributed to the transitions primarily centred at the polycyclic aryl group of the corresponding ligands ($(HL^n)^-$ or $(L^n)^{2-}$) [14–16,25,26]. Above 510 nm only the platinum(II) complexes (**6** and **8**) show two weak shoulders at ~535 and ~580 nm at the tail of the adjoining shorter wavelength strong band. It is very likely that these shoulders are due to spin-forbidden transitions involving the metal centre having high spin-orbit coupling constant [27–29].

Table 5.7. Electronic spectroscopic data

Complex	Absorption λ_{max} (nm) ($10^{-4} \times \varepsilon$ (M^{-1} cm^{-1}))
trans- $[Rh(L^1)(PPh_3)_2H]$[a] (**1**)	478 (6.29), 448 (5.54), 423 (3.42), 400 (2.51), 318 (6.95), 310[c] (6.80), 230 (20.55).
trans- $[Rh(L^2)(PPh_3)_2H]$[a] (**2**)	483 (1.91), 451 (1.93), 425 (1.56), 400[c] (1.42), 313 (3.19) 230 (9.53).
trans- $[Ir(L^2)(PPh_3)_2H]$[a] (**3**)	510[c] (2.23), 476 (2.91), 435 (6.91), 418 (6.71), 395[c] (4.44), 356 (4.25), 340 (3.69), 265 (12.71), 229 (19.17).
trans- $[Ir(L^3)(PPh_3)_2H]$[a] (**4**)	495[c] (0.34), 468 (0.41), 434 (0.40), 415 (0.39), 395[c] (0.38), 360[c] (0.64), 346 (0.73).
$[Pd(HL^1)Cl]$[b] (**5**)	480 (2.39), 450 (2.78), 426 (1.93), 400[c] (1.12), 317 (2.57), 307 (2.48), 290[c] (1.64)
$[Pt(HL^1)Cl]$[b] (**6**)	590[c] (0.10), 547 (0.18), 497 (0.81), 464 (1.24), 437 (1.11), 423 (1.06), 400 (1.43), 385[c] (1.63), 372 (1.81), 350[c] (1.37), 280 (2.42)
$[Pd(L^1)(PPh_3)]$[b] (**7**)	480 (2.72), 450 (3.17), 426 (2.16), 400[c] (1.23), 317 (2.88), 307 (2.81), 290[c] (1.80)
$[Pt(L^1)(PPh_3)]$[b] (**8**)	570[c] (0.24), 530[c] (0.39), 491 (1.76), 462 (3.12), 437 (2.27), 410[c] (1.15), 368 (1.61), 350[c] (1.13), 317 (2.74), 310 (2.70), 290[c] (2.64), 274 (2.91)

[a] In dimethylformamide

[b] Shoulder.

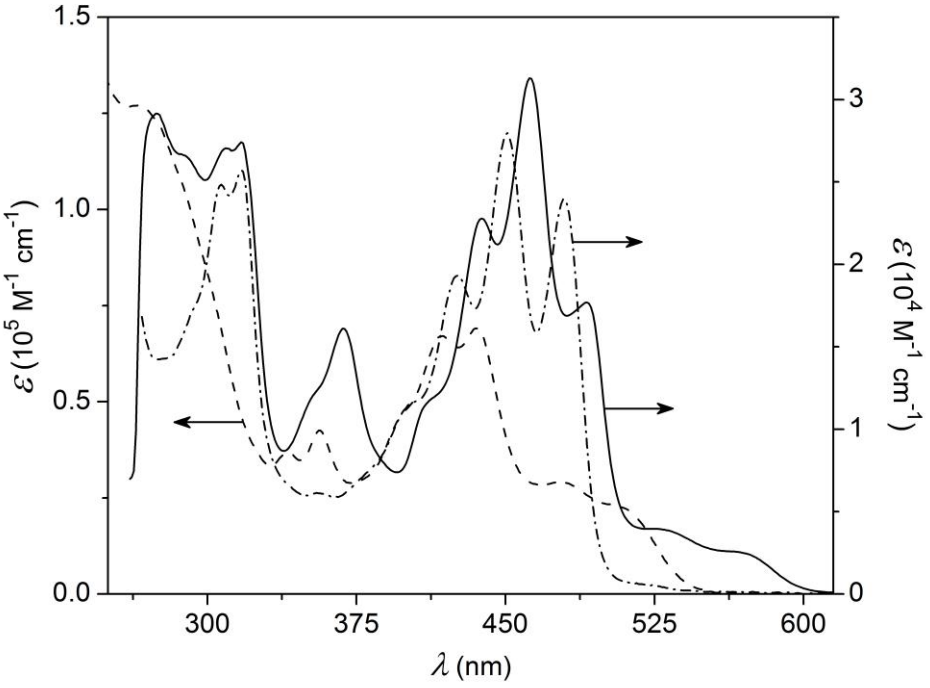

Figure 5.10. Electronic spectra of *trans*-[Ir(L^2)(PPh_3)$_2$H] (**3**) (------), [Pd(HL^1)Cl] (**5**) (-·-·-·-) and [Pt(L^1)(PPh_3)] (**8**) (——).

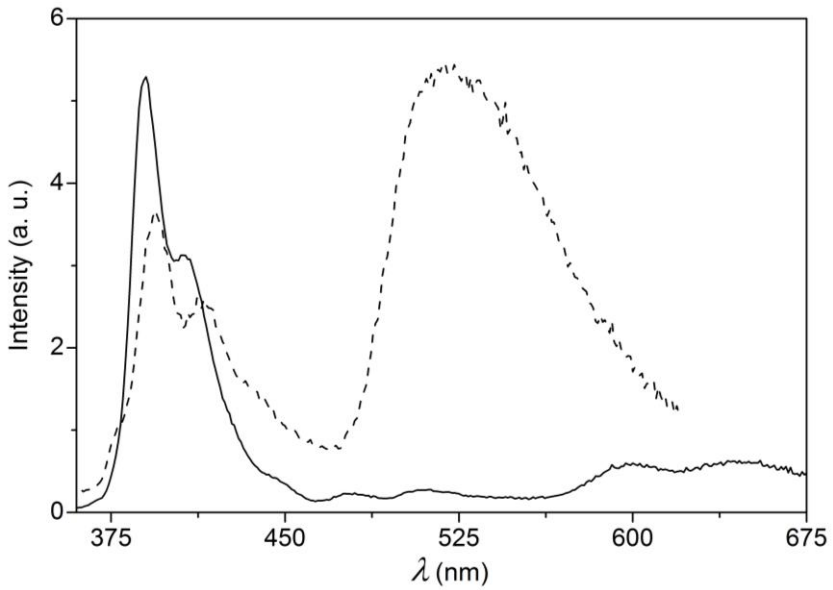

Figure 5.11. Emission spectra of *trans*-[Rh(L^1)(PPh_3)$_2$H] (**1**) (-----) and [Pt(L^1)(PPh_3)] (**8**) (——).

Room temperature emission spectral measurements were performed with dichloromethane solutions of **1**−**4** and dimethylformamide solutions of **5**–**8**. All the complexes are emissive in nature except the iridium(III) complexes (**3** and **4**). Below 450 nm, the emission spectral profiles of all the complexes (λ_{exc} = 315 nm for **1**, **2**, **5** and **7** and λ_{exc} = 350 nm for **6** and **8**) are very similar and display two closely spaced bands at ~410 and ~390 nm (Figure 5.11). In addition to these two bands, rhodium(III) complexes (**1** and **2**) display a third relatively stronger band at ~515 nm. This same third band is also observed on excitation at 470 nm. On the other hand, the palladium(II) (**5** and **7**) complexes display a similar band at ~510 nm only on excitation at 400 nm. Considering the electronic spectroscopic characteristics of the free H_2L^n and the corresponding complexes all these emission bands are assigned to predominantly ligand centred emissive states [14,25,26,30]. Unlike the other complexes, the platinum(II) (**6** and **8**) complexes display not one but two additional very weak bands above 450 nm at a comparatively much longer wavelengths (~600 and ~645 nm) (Figure 5.11). These two bands can also be seen on excitation at ~570 nm. Perhaps these weak emissions are due to the spin-forbidden optical transitions observed for the platinum(II) complexes (**6** and **8**) [27–29].

5.3.6. Redox properties

Redox characteristics of all the complexes in dichloromethane solutions have been examined by cyclic voltammetric measurements at room temperature. The rhodium(III) and the iridium(III) complexes (**1**−**4**) display an oxidation response on the anode side of the Ag/AgCl reference electrode. The one-electron nature of this oxidation is proposed by comparing the current heights with the current heights of known one-electron redox processes under similar conditions [15,16,30]. Representative voltammograms are illustrated in Figure 5.12. The response for each of **1** and **2** is irreversible and the E_{pa} value is 0.95(±1) V. On the other hand, quasi-reversible responses are observed for both **3** and **4** at $E_{1/2}$ values of 0.92 and 0.82 V, respectively. The

peak-to-peak separations ($\Delta E_p = E_{pa} - E_{pc}$) are 240 and 260 mV for **3** and **4**, respectively. Absence of any such oxidation response in the cyclic voltammograms of the palladium(II) and the platinum(II) complexes (**5**−**8**) indicates that the oxidations observed for **1**−**4** are metal centred.

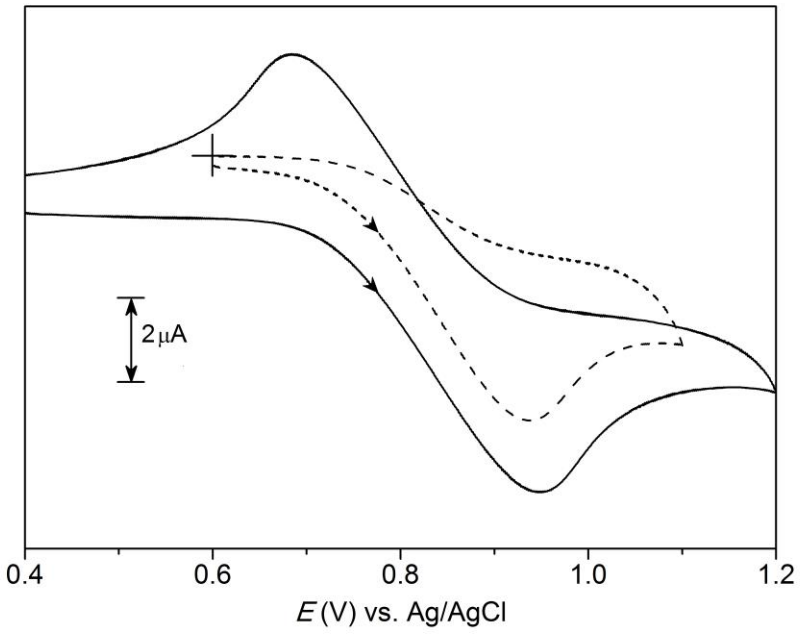

Figure 5.12. Cyclic voltammograms of *trans*-[Rh(L^1)(PPh_3)$_2$H] (**1**) (-----) and *trans*-[Ir(L^3)(PPh_3)$_2$H] (**4**) (——) in dichloromethane (0.1 M TBAP) at 298 K.

5.4. Conclusions

Synthesis, characterization and spectroscopic properties of one pair of each of rhodium(III), iridium(III), palladium(II) and platinum(II) cyclometallates with tridentate 4-*R*-N′-(1-pyrenylidene/naphthylidene) benzohydrazides are reported. Electronic spectral features correspond to primarily ligand centred transitions. Except for the iridium(III) complexes, the remaining complexes are emissive. The rhodium(III) and the iridium(III) complexes are redox active and show a metal centred oxidation. The molecular structures of the rhodium(III) and iridium(III) complexes and one

each from the palladium(II) pair and the platinum(II) pair of complexes are determined by X-ray crystallography. The similarities in the physical properties of each pair of bivalent metal ion complexes suggest that the molecular structures in the corresponding pairs are also analogous. The structures reveal that the polycyclic aryl group of the tridentate ligand undergoes *peri*-metallation in case of the 4d metal ions, while the same undergoes *ortho*-metallation in case of the 5d metal ions. With the present CNO-donor ligand system *peri*-metallation leads to 6,5-membered fused chelate rings, while *ortho*-metallation results in the formation of 5,5-membered fused chelate rings.

5.5. References

[1] E. C. Constable, R. P. G. Henney, P. R. Raithby, L. R. Sousa, *Angew. Chem. Int. Ed. Engl*. 30 (1991) 1363–1364.

[2] B. Teijido, A. Fernández, M. López-Torres, S. Castro-Juiz, A. Suárez, J. M. Ortigueira, J. M. Vila, J. J. Fernández, *J. Organomet. Chem*. 598 (2000) 71–79.

[3] D. D. Perrin, W. L. F. Armarego, D. P. Perrin, *Purification of Laboratory Chemicals* 2nd ed., Pergamon, Oxford, 1983.

[4] J. A. Osborn, F. H. Jardine, J. F. Young, G. Wilkinson, *J. Chem. Soc. A* (1966) 1711–1732.

[5] R. Acharyya, F. Basuli, R. –Z. Wang, T. C. W. Mak, S. Bhattacharya, *Inorg. Chem*. 43 (2004) 704–711.

[6] *SMART version 5.630 and SAINT-plus version 6.45* Bruker-Nonius Analytical X-ray Systems Inc., Madison, WI, USA,. 2003.

[7] G. M. Sheldrick, *SADABS, Program for Area Detector Absorption Correction* University of Göttingen, Göttingen, Germany, 1997.

[8] *CrysAlisPro, Version 1.171.34.40* Oxford Diffraction Ltd., Abingdon, Oxfordshire, UK, 2010.

[9] G. M. Sheldrick, *Acta Crystallogr., Sect. A* 64 (2008) 112–122.

[10] L. J. Farrugia, *J. Appl. Crystallogr*. 45 (2012) 849−854.

[11] A. L. Spek, *Platon, A Multipurpose Crystallographic Tool* Utrecht University, Utrecht, The Netherlands, 2002.

[12] C. F. Macrae, I. J. Bruno, J. A. Chisholm, P. R. Edgington, P. McCabe, E. Pidcock, L. Rodriguez-Monge, R. Taylor, J. van de Streek, P. A. Wood, *J. Appl. Crystallogr*. 41 (2008) 466−470.

[13] A. R. B. Rao, S. Pal, *J. Organomet. Chem.* 696 (2011) 696, 2660–2664.

[14] A. R. B. Rao, S. Pal, *J. Organomet. Chem*. 731 (2013) 67–72.

[15] K. Nagaraju, S. Pal, *J. Organomet. Chem*. 737 (2013) 7–11.

[16] K. Nagaraju, S. Pal, *J. Organomet. Chem*. 745–746 (2013) 404–408.

[17] S. Basu, R. Acharyya, F. Basuli, S. –M. Peng, G. –H. Lee, G. Mostafa, S. Bhattacharya, *Inorg. Chim. Acta* 363 (2010) 2848–2856.

[18] M. B. Ezhova, B. O. Patrick, B. R. James, M. E. Ford, F. J. Waller, *Russ. Chem. Bull., Int. Ed*. 52 (2003) 2707−2714.

[19] S. Dutta, S.–M. Peng, S. Bhattacharya, J. Chem. Soc., *Dalton Trans*. (2000) 4623−4627.

[20] M. G. Partridge, B. A. Messerle, L. D. *Organometallics* 14 (1996) 3527−3530.

[21] J. R. Krumper, M. Gerisch, A. Magistrato, U. Rothlisberger, R. G. Bergman, T. D. Tilley, *J. Am. Chem. Soc*. 126 (2004) 12492−12502.

[22] P. Kalaivani, R. Prabhakaran, E. Ramachandran, F. Dallemer, G. Paramaguru, R. Renganathan, P. Poornima, V. V. Padma, K. Natarajan, *Dalton Trans*. 41 (2012) 2486–2499.

[23] A. A. Ibrahim, H. Khaledi, P. Hassandarvish, H. M. Ali, H. Karimian, *Dalton Trans*. 43 (2014) 3850–3860.

[24] H. Du, R. –C. A. Fuh, J. Li, L. A. Corkan, J. S. Lindsey, *Photochem. Photobiol*. 68 (1998) 141−142.

[25] S. Lentijo, J. A. Miguel, P. Espinet, *Organometallics* 30 (2011) 1059−1066.

[26] S. Lentijo, J. A. Miguel, P. Espinet, *Dalton Trans.* 40 (2011) 7602–7609.

[27] A. B. Tamayo, B. D. Alleyne, P. I. Djurovich, S. Lamansky, I. Tsyba, N. N. Ho, R. Bau, M. E. Thompson, *J. Am. Chem. Soc*. 125 (2003) 7377–7387.

[28] E. V. Ivanova, M. V. Puzyk, K. P. Balashev, *Russ. J. Gen. Chem*. 79 (2009) 2096–2101.

[29] L. F. Gildea, A. S. Batsanov, J. A. G. Williams, *Dalton Trans*. 42 (2013) 10388–10393.

[30] K. Nagaraju, S. Pal, *Inorg. Chim. Acta* 413 (2014) 102–108.

Appendix

Tables for atomic coordinates (x 10^4) and equivalent isotropic displacement parameters ($Å^2$ x 10^3). U(eq) is defined as one third of the trace of the orthogonalized U_{ij} tensor.

Table A.1. For **[Pd(HL^1)Cl] (1**·Me_2NCHO**) (*Chapter 2*)**

Atom	x	y	z	U(eq)
Pd	2835(1)	2128(1)	8304(1)	17(1)
Cl	2122(1)	4391(1)	7180(1)	26(1)
O(1)	811(2)	2189(2)	9599(1)	20(1)
N(1)	3066(2)	257(2)	9434(2)	17(1)
N(2)	1866(2)	19(2)	10399(2)	18(1)
C(1)	4780(3)	1782(2)	7270(2)	20(1)
C(2)	5263(3)	2840(2)	6254(2)	23(1)
C(3)	6653(3)	2726(2)	5475(2)	27(1)
C(4)	7575(3)	1524(2)	5692(2)	24(1)
C(5)	8853(3)	-3242(2)	8035(2)	24(1)
C(6)	8545(3)	-4383(2)	8973(2)	28(1)
C(7)	7156(3)	-4356(3)	9767(2)	31(1)
C(8)	6125(3)	-3201(2)	9626(2)	27(1)
C(9)	5410(2)	-718(2)	8506(2)	18(1)
C(10)	8111(3)	-843(2)	6880(2)	23(1)
C(11)	7804(3)	-2017(2)	7845(2)	20(1)
C(12)	6415(3)	-1972(2)	8671(2)	20(1)
C(13)	5735(2)	477(2)	7516(2)	19(1)
C(14)	7148(3)	376(2)	6693(2)	21(1)
C(15)	4093(2)	-759(2)	9421(2)	19(1)
C(16)	751(2)	1066(2)	10423(2)	18(1)
C(17)	-512(2)	835(2)	11459(2)	19(1)
C(18)	-654(3)	-390(2)	12388(2)	24(1)
C(19)	-1839(3)	-518(2)	13351(2)	27(1)

Table A.1. Continued…

Atom	x	y	z	U(eq)
C(20)	-2890(3)	589(3)	13396(2)	29(1)
C(21)	-2763(3)	1812(3)	12471(2)	33(1)
C(22)	-1590(3)	1943(2)	11496(2)	27(1)
O(2)	2320(2)	-2696(2)	11706(2)	27(1)
N(3)	2484(2)	-4794(2)	13157(2)	24(1)
C(23)	1733(3)	-3600(2)	12563(2)	24(1)
C(24)	4109(3)	-5184(3)	12810(2)	32(1)
C(25)	1710(3)	-5813(2)	14149(2)	31(1)

Table A.2. For **[Pd(HL^2)Cl] (2**·Me_2NCHO**) (*Chapter 2*)**

Atom	x	y	z	U(eq)
Pd	2586(1)	4035(1)	5837(1)	41(1)
Cl	4799(2)	4127(1)	6640(3)	95(1)
O(1)	2374(3)	4650(1)	4496(5)	46(1)
N(1)	704(4)	4064(1)	4998(4)	34(1)
N(2)	305(4)	4445(1)	3987(5)	34(1)
N(3)	-47(5)	6252(1)	-453(6)	54(1)
C(1)	2507(5)	3449(2)	6953(6)	39(1)
C(2)	3636(5)	3238(2)	7727(7)	54(1)
C(3)	3688(6)	2829(2)	8582(8)	66(2)
C(4)	2614(6)	2630(2)	8694(7)	57(2)
C(5)	-2066(6)	2546(2)	7496(7)	53(1)
C(6)	-3235(6)	2707(2)	6820(8)	59(2)
C(7)	-3395(6)	3110(2)	5917(8)	54(2)
C(8)	-2361(5)	3339(2)	5719(7)	47(1)
C(9)	51(5)	3411(2)	6240(6)	34(1)
C(10)	278(5)	2613(2)	8030(6)	45(1)
C(11)	-947(5)	2773(2)	7322(6)	42(1)

Table A.2. Continued…

Atom	x	y	z	U(eq)
C(12)	-1077(5)	3183(2)	6392(6)	36(1)
C(13)	1312(5)	3238(2)	6992(6)	36(1)
C(14)	1392(5)	2819(2)	7912(6)	42(1)
C(15)	-178(5)	3816(2)	5264(6)	34(1)
C(16)	1216(5)	4729(2)	3767(6)	35(1)
C(17)	818(4)	5123(1)	2679(6)	33(1)
C(18)	-440(5)	5227(2)	1816(6)	40(1)
C(19)	-733(5)	5599(2)	800(6)	40(1)
C(20)	245(5)	5879(2)	565(6)	40(1)
C(21)	1520(5)	5769(2)	1432(7)	43(1)
C(22)	1787(5)	5404(2)	2448(6)	40(1)
C(23)	976(6)	6516(2)	-810(8)	62(2)
C(24)	-1355(6)	6385(2)	-1235(7)	60(2)
O(2)	-2340(4)	4368(1)	2781(6)	65(1)
N(4)	-4511(4)	4409(2)	1986(7)	60(1)
C(25)	-3353(6)	4572(2)	2566(8)	60(2)
C(26)	-4692(8)	3946(2)	1601(12)	106(3)
C(27)	-5655(7)	4678(3)	1766(13)	117(3)

Table A.3. For **[Pd(L^1)(PPh_3)] (3**·MeCN**) (*Chapter 2*)**

Atom	x	y	z	U(eq)
Pd	1929(1)	7503(1)	857(1)	37(1)
P	3142(1)	8490(1)	474(1)	36(1)
O(1)	1741(2)	8555(2)	1563(1)	44(1)
N(1)	1101(3)	6698(2)	1375(2)	35(1)
N(2)	720(3)	7229(2)	1847(2)	41(1)
C(1)	1780(3)	6403(3)	199(2)	38(1)
C(2)	1855(3)	6607(3)	-426(2)	47(1)
C(3)	1812(4)	5860(3)	-906(2)	54(1)

Table A.3. Continued…

Atom	x	y	z	U(eq)
C(4)	1717(4)	4881(3)	-756(2)	50(1)
C(5)	1309(4)	2202(3)	758(3)	61(1)
C(6)	1195(4)	1900(3)	1343(3)	65(2)
C(7)	1118(4)	2620(3)	1817(2)	60(1)
C(8)	1123(4)	3626(3)	1689(2)	51(1)
C(9)	1295(3)	5040(3)	931(2)	38(1)
C(10)	1466(3)	3584(3)	9(2)	50(1)
C(11)	1336(3)	3251(3)	605(2)	45(1)
C(12)	1240(3)	3987(3)	1080(2)	44(1)
C(13)	1566(3)	5358(3)	349(2)	37(1)
C(14)	1584(3)	4593(3)	-135(2)	43(1)
C(15)	991(3)	5732(3)	1381(2)	39(1)
C(16)	1098(3)	8165(3)	1894(2)	38(1)
C(17)	722(3)	8820(3)	2372(2)	38(1)
C(18)	-204(4)	8557(3)	2606(2)	50(1)
C(19)	-569(4)	9184(3)	3027(2)	61(1)
C(20)	-15(5)	10064(4)	3236(2)	63(1)
C(21)	911(4)	10332(3)	3013(2)	61(1)
C(22)	1276(4)	9713(3)	2579(2)	50(1)
C(23)	2494(3)	9489(3)	-80(2)	36(1)
C(24)	3106(4)	10289(3)	-227(2)	47(1)
C(25)	2598(4)	11066(3)	-630(2)	52(1)
C(26)	1459(4)	11045(3)	-892(2)	55(1)
C(27)	832(4)	10259(3)	-751(2)	62(1)
C(28)	1343(4)	9481(3)	-344(2)	50(1)
C(29)	4035(3)	9193(3)	1151(2)	39(1)
C(30)	5115(4)	8905(3)	1453(2)	54(1)
C(31)	5734(4)	9474(4)	1972(2)	71(2)
C(32)	5278(5)	10313(4)	2185(2)	67(2)

Table A.3. Continued…

Atom	x	y	z	U(eq)
C(33)	4202(5)	10597(3)	1897(2)	58(1)
C(34)	3581(4)	10039(3)	1382(2)	51(1)
C(35)	4127(3)	7837(3)	102(2)	35(1)
C(36)	4430(4)	8156(3)	-448(2)	45(1)
C(37)	5189(4)	7600(3)	-702(2)	58(1)
C(38)	5634(4)	6718(3)	-405(2)	58(1)
C(39)	5336(4)	6393(3)	140(2)	61(1)
C(40)	4579(4)	6934(3)	386(2)	53(1)
N(3)	7754(5)	12000(5)	3007(3)	123(2)
C(41)	7939(5)	11771(5)	2535(4)	90(2)
C(42)	8195(6)	11461(5)	1934(3)	128(3)

Table A.4. For **[Pd(L^2)(PPh_3)] (4) (*Chapter 2*)**

Atom	x	y	z	U(eq)
Pd	3302(1)	8551(1)	2242(1)	33(1)
P	5492(1)	8680(1)	2507(1)	32(1)
O(1)	2942(1)	8685(1)	3119(1)	40(1)
N(1)	1381(2)	8680(1)	2160(1)	35(1)
N(2)	825(2)	8759(1)	2691(1)	42(1)
N(3)	167(2)	8725(2)	5480(1)	62(1)
C(1)	3326(2)	8342(2)	1370(1)	39(1)
C(2)	4432(2)	8029(2)	1153(1)	52(1)
C(3)	4547(3)	7859(2)	551(1)	60(1)
C(4)	3530(3)	8015(2)	147(1)	56(1)
C(5)	-970(3)	8875(2)	-429(1)	64(1)
C(6)	-2145(3)	9136(2)	-299(1)	70(1)
C(7)	-2366(3)	9280(2)	294(1)	66(1)
C(8)	-1399(3)	9160(2)	744(1)	57(1)
C(9)	923(2)	8732(2)	1087(1)	40(1)

Table A.4. Continued…

Atom	x	y	z	U(eq)
C(10)	1288(3)	8464(2)	-105(1)	54(1)
C(11)	78(3)	8740(2)	28(1)	50(1)
C(12)	-129(2)	8880(2)	632(1)	46(1)
C(13)	2189(2)	8479(1)	942(1)	39(1)
C(14)	2335(3)	8327(2)	325(1)	47(1)
C(15)	612(2)	8806(2)	1687(1)	43(1)
C(16)	1719(2)	8737(1)	3152(1)	36(1)
C(17)	1276(2)	8767(2)	3749(1)	38(1)
C(18)	-7(2)	8624(2)	3854(1)	46(1)
C(19)	-378(3)	8623(2)	4417(1)	50(1)
C(20)	518(3)	8771(2)	4916(1)	46(1)
C(21)	1798(2)	8942(2)	4808(1)	50(1)
C(22)	2161(2)	8927(2)	4240(1)	46(1)
C(23)	-1153(3)	8545(2)	5590(1)	68(1)
C(24)	1086(3)	8921(2)	5990(1)	70(1)
C(25)	6562(2)	7701(1)	2411(1)	35(1)
C(26)	6063(2)	6817(2)	2416(1)	60(1)
C(27)	6875(3)	6059(2)	2402(2)	76(1)
C(28)	8165(3)	6167(2)	2373(2)	65(1)
C(29)	8667(3)	7042(2)	2368(1)	63(1)
C(30)	7873(2)	7805(2)	2390(1)	48(1)
C(31)	6235(2)	9699(1)	2200(1)	38(1)
C(32)	7360(3)	10098(2)	2476(1)	57(1)
C(33)	7863(3)	10887(2)	2241(2)	76(1)
C(34)	7257(4)	11285(2)	1738(2)	76(1)
C(35)	6152(3)	10896(2)	1463(1)	68(1)
C(36)	5637(2)	10107(2)	1694(1)	50(1)
C(37)	5753(2)	8875(2)	3307(1)	39(1)
C(38)	5567(2)	9744(2)	3540(1)	53(1)

Table A.4. Continued…

Atom	x	y	z	U(eq)
C(39)	5644(3)	9874(2)	4146(1)	65(1)
C(40)	5902(3)	9144(3)	4523(1)	69(1)
C(41)	6088(3)	8284(2)	4300(1)	65(1)
C(42)	6019(2)	8143(2)	3696(1)	51(1)

Table A.5. For **[Pd(HL^1)Cl] (1**·CH_3CN**) (*Chapter 3*)**

Atom	x	y	z	U(eq)
Pd	2975(1)	1853(1)	8198(1)	42(1)
Cl	1651(1)	1643(2)	6617(1)	74(1)
O(1)	939(3)	2434(3)	9319(2)	50(1)
N(1)	8699(3)	1146(3)	8234(3)	57(1)
N(2)	3847(3)	2048(3)	9752(3)	41(1)
N(3)	2708(3)	2407(3)	10632(3)	46(1)
C(1)	4962(4)	1407(3)	7313(3)	42(1)
C(2)	5252(4)	1127(4)	6132(4)	52(1)
C(3)	6706(5)	872(5)	5573(4)	63(1)
C(4)	7941(4)	865(4)	6177(4)	60(1)
C(5)	7692(4)	1116(4)	7370(4)	48(1)
C(6)	6240(4)	1390(3)	7937(3)	42(1)
C(7)	6426(4)	1568(4)	9167(3)	45(1)
C(8)	7952(4)	1412(4)	9290(4)	55(1)
C(9)	5233(4)	1872(4)	10055(3)	46(1)
C(10)	1243(4)	2625(4)	10326(3)	43(1)
C(11)	15(4)	3113(4)	11216(3)	44(1)
C(12)	340(4)	2950(4)	12535(4)	55(1)
C(13)	-873(5)	3443(5)	13285(4)	68(1)
C(14)	-2399(5)	4054(5)	12765(4)	69(1)
C(15)	-2725(4)	4204(4)	11473(4)	61(1)
C(16)	-1532(4)	3752(4)	10685(4)	51(1)

Table A.5. Continued…

Atom	x	y	z	U(eq)
N(4)	3696(4)	3620(5)	12409(4)	79(1)
C(17)	3253(5)	4200(5)	13120(4)	67(1)
C(18)	2677(8)	4960(6)	14050(5)	118(2)

Table A.6. For **[Pd(HL^2)Cl] (2**·Me_2NCHO**) (*Chapter 4*)**

Atom	x	y	z	U(eq)
Pd(1)	1089(1)	1351(1)	5510(1)	45(1)
Cl(1)	2007(1)	928(2)	6372(1)	75(1)
O(1)	1483(2)	-134(4)	5025(2)	50(1)
O(2)	-1172(2)	6065(4)	5774(2)	61(1)
N(1)	372(2)	1358(4)	4716(2)	44(1)
N(2)	505(2)	458(5)	4306(2)	50(1)
C(1)	636(2)	2848(6)	5835(2)	45(1)
C(2)	965(3)	3416(6)	6395(2)	56(2)
C(3)	691(3)	4519(7)	6651(2)	64(2)
C(4)	68(3)	5047(6)	6351(2)	57(2)
C(5)	-960(3)	5069(6)	5461(3)	51(1)
C(6)	-1325(3)	4601(6)	4901(3)	53(1)
C(7)	-1047(3)	3548(6)	4632(2)	53(2)
C(8)	-414(2)	2976(6)	4907(2)	43(1)
C(9)	-22(2)	3412(5)	5500(2)	42(1)
C(10)	-296(3)	4507(6)	5777(2)	47(1)
C(11)	-204(3)	1987(6)	4547(2)	45(1)
C(12)	1090(3)	-274(6)	4499(2)	44(1)
C(13)	1252(3)	-1241(6)	4073(2)	48(1)
C(14)	1886(3)	-1860(6)	4268(3)	55(2)
C(15)	2079(3)	-2806(7)	3907(3)	66(2)
C(16)	1627(3)	-3141(8)	3352(3)	78(2)
C(17)	995(3)	-2545(8)	3148(3)	78(2)

Table A.6. Continued…

Atom	x	y	z	U(eq)
C(18)	805(3)	-1613(7)	3512(3)	65(2)
C(19)	-1836(3)	6627(7)	5496(3)	70(2)
O(3)	-363(3)	976(5)	3176(2)	83(2)
N(3)	-1339(3)	1182(6)	2407(2)	80(2)
C(20)	-932(4)	613(9)	2909(3)	81(2)
C(21)	-1084(4)	2291(10)	2100(3)	118(3)
C(22)	-2025(4)	655(10)	2112(4)	130(3)

Table A.7. For **[Pd(L^1)(PPh$_3$)] (3) (*Chapter 4*)**

Atom	x	y	z	U(eq)
Pd(1)	3028(1)	1402(1)	1077(1)	27(1)
P(1)	2309(1)	1395(1)	1826(1)	27(1)
O(1)	3035(2)	2749(2)	1061(1)	37(1)
N(1)	3539(2)	1639(2)	381(1)	28(1)
N(2)	3622(2)	2518(2)	255(1)	34(1)
C(1)	3226(2)	114(2)	1037(2)	30(1)
C(2)	3147(2)	-422(2)	1496(2)	37(1)
C(3)	3317(3)	-1308(3)	1510(2)	51(1)
C(4)	3569(3)	-1686(3)	1059(2)	57(1)
C(5)	3992(3)	-1592(3)	116(2)	53(1)
C(6)	4138(3)	-1145(3)	-348(2)	55(1)
C(7)	3999(3)	-261(3)	-369(2)	45(1)
C(8)	3722(2)	182(2)	68(2)	34(1)
C(9)	3531(2)	-277(2)	566(2)	31(1)
C(10)	3695(3)	-1180(2)	576(2)	39(1)
C(11)	3708(2)	1105(2)	6(2)	33(1)
C(12)	3359(2)	3012(2)	629(2)	30(1)
C(13)	3425(2)	3963(2)	549(2)	33(1)
C(14)	3132(2)	4562(2)	954(2)	35(1)

Table A.7. Continued…

Atom	x	y	z	U(eq)
C(15)	3194(4)	5401(3)	818(2)	76(2)
C(16)	3530(3)	5729(3)	375(2)	66(2)
C(17)	3825(3)	5167(3)	18(2)	62(1)
C(18)	3774(3)	4289(3)	100(2)	49(1)
C(19)	1579(2)	504(2)	1857(2)	30(1)
C(20)	1125(2)	173(3)	1326(2)	46(1)
C(21)	552(3)	-491(3)	1314(2)	56(1)
C(22)	431(3)	-838(3)	1821(2)	62(1)
C(23)	887(3)	-534(3)	2362(2)	51(1)
C(24)	1452(2)	147(2)	2372(2)	41(1)
C(25)	1629(2)	2349(2)	1830(2)	31(1)
C(26)	746(2)	2288(3)	1747(2)	47(1)
C(27)	263(3)	3011(3)	1769(2)	57(1)
C(28)	635(3)	3811(3)	1868(2)	54(1)
C(29)	1509(3)	3883(3)	1945(2)	45(1)
C(30)	2002(2)	3159(3)	1931(2)	38(1)
C(31)	3032(2)	1463(2)	2553(2)	31(1)
C(32)	2775(2)	1777(3)	3043(2)	41(1)
C(33)	3350(3)	1862(3)	3579(2)	57(1)
C(34)	4186(3)	1621(3)	3629(2)	58(1)
C(35)	4449(3)	1309(3)	3155(2)	53(1)
C(36)	3887(2)	1230(2)	2612(2)	39(1)
Pd(2)	8100(1)	8033(1)	1093(1)	27(1)
P(2)	7426(1)	8033(1)	1863(1)	27(1)
O(2)	8081(2)	9377(2)	1053(1)	38(1)
N(3)	8593(2)	8262(2)	389(1)	28(1)
N(4)	8677(2)	9130(2)	250(1)	33(1)
C(37)	8291(2)	6743(2)	1057(2)	28(1)
C(38)	8214(2)	6203(2)	1515(2)	34(1)

Table A.7. Continued…

Atom	x	y	z	U(eq)
C(39)	8321(2)	5301(2)	1507(2)	44(1)
C(40)	8432(3)	4902(2)	1038(2)	62(2)
C(41)	8857(3)	5005(3)	69(2)	56(1)
C(42)	9028(3)	5457(3)	-384(2)	57(1)
C(43)	8973(3)	6348(2)	-382(2)	44(1)
C(44)	8740(2)	6794(2)	75(2)	29(1)
C(45)	8537(2)	6341(2)	569(2)	28(1)
C(46)	8625(2)	5412(2)	558(2)	38(1)
C(47)	8758(2)	7716(2)	18(2)	32(1)
C(48)	8411(2)	9634(2)	625(2)	32(1)
C(49)	8491(2)	10581(2)	537(2)	35(1)
C(50)	8103(3)	11158(3)	853(2)	55(1)
C(51)	8152(4)	12033(3)	764(2)	75(2)
C(52)	8601(4)	12341(3)	372(2)	70(2)
C(53)	8999(3)	11783(3)	66(2)	64(1)
C(54)	8943(3)	10913(3)	153(2)	55(1)
C(55)	6663(2)	7170(2)	1891(2)	30(1)
C(56)	6230(2)	6829(3)	1358(2)	51(1)
C(57)	5613(3)	6191(4)	1347(2)	79(2)
C(58)	5447(3)	5899(4)	1856(3)	81(2)
C(59)	5870(3)	6220(3)	2386(2)	62(1)
C(60)	6478(2)	6865(2)	2406(2)	41(1)
C(61)	6778(2)	9001(2)	1881(2)	30(1)
C(62)	5898(2)	8954(3)	1807(2)	42(1)
C(63)	5424(3)	9695(3)	1811(2)	48(1)
C(64)	5810(3)	10489(3)	1889(2)	54(1)
C(65)	6682(3)	10541(3)	1958(2)	44(1)
C(66)	7168(2)	9812(2)	1962(2)	35(1)
C(67)	8178(2)	8070(2)	2580(2)	31(1)

Table A.7. Continued…

Atom	x	y	z	U(eq)
C(68)	9015(2)	7823(2)	2627(2)	35(1)
C(69)	9596(3)	7868(3)	3166(2)	52(1)
C(70)	9345(3)	8167(3)	3653(2)	62(1)
C(71)	8519(3)	8421(3)	3613(2)	59(1)
C(72)	7931(3)	8367(3)	3081(2)	46(1)

Table A.8. For **[Pd(L^2)(PPh_3)] (4) (*Chapter 4*)**

Atom	x	y	z	U(eq)
Pd(1)	1407(1)	9084(1)	2056(1)	41(1)
P(1)	683(1)	9115(1)	2773(1)	41(1)
O(1)	1413(1)	7769(1)	2088(1)	50(1)
O(2)	2332(1)	12804(2)	869(2)	71(1)
N(1)	2094(1)	8817(2)	1620(2)	45(1)
N(2)	2216(1)	7958(2)	1566(2)	51(1)
C(1)	1453(1)	10322(2)	1796(2)	42(1)
C(2)	1015(1)	10869(2)	1813(2)	49(1)
C(3)	1017(1)	11728(2)	1609(2)	57(1)
C(4)	1463(1)	12087(2)	1388(2)	55(1)
C(5)	2388(1)	11966(2)	1063(2)	53(1)
C(6)	2843(1)	11507(2)	1019(2)	63(1)
C(7)	2844(1)	10652(2)	1188(2)	61(1)
C(8)	2407(1)	10231(2)	1419(2)	47(1)
C(9)	1924(1)	10703(2)	1526(2)	42(1)
C(10)	1923(1)	11582(2)	1330(2)	45(1)
C(11)	2459(1)	9336(2)	1469(2)	53(1)
C(12)	1838(1)	7489(2)	1811(2)	47(1)
C(13)	1892(1)	6563(2)	1714(2)	50(1)
C(14)	1472(2)	6026(2)	1820(3)	69(1)
C(15)	1509(2)	5169(3)	1702(3)	80(1)

Table A.8. Continued…

Atom	x	y	z	U(eq)
C(16)	1962(2)	4829(3)	1488(3)	80(1)
C(17)	2385(2)	5350(3)	1394(4)	112(2)
C(18)	2348(2)	6200(3)	1508(3)	93(2)
C(19)	2794(2)	13239(2)	654(3)	86(1)
C(20)	647(1)	9998(2)	3513(2)	49(1)
C(21)	1121(2)	10419(2)	3884(2)	68(1)
C(22)	1109(2)	11110(3)	4430(3)	83(1)
C(23)	630(2)	11394(3)	4591(3)	94(2)
C(24)	155(2)	10996(3)	4228(3)	98(2)
C(25)	155(2)	10301(3)	3684(2)	72(1)
C(26)	12(1)	9041(2)	2041(2)	46(1)
C(27)	-34(2)	9257(2)	1169(2)	60(1)
C(28)	-536(2)	9162(3)	599(3)	82(1)
C(29)	-970(2)	8852(3)	880(3)	82(1)
C(30)	-934(1)	8622(3)	1742(3)	81(1)
C(31)	-443(1)	8718(2)	2323(2)	62(1)
C(32)	679(1)	8172(2)	3455(2)	43(1)
C(33)	821(1)	8195(2)	4363(2)	52(1)
C(34)	824(1)	7463(3)	4850(2)	65(1)
C(35)	691(2)	6700(3)	4435(3)	70(1)
C(36)	549(1)	6668(2)	3539(3)	64(1)
C(37)	541(1)	7394(2)	3051(2)	53(1)
Pd(2)	3684(1)	9369(1)	3237(1)	43(1)
P(2)	4378(1)	9260(1)	2464(1)	44(1)
O(3)	3673(1)	10688(1)	3141(2)	53(1)
O(4)	2621(1)	5650(2)	4100(2)	77(1)
N(3)	3018(1)	9670(2)	3713(2)	47(1)
N(4)	2891(1)	10532(2)	3727(2)	50(1)
C(38)	3625(1)	8132(2)	3512(2)	45(1)

Table A.8. Continued…

Atom	x	y	z	U(eq)
C(39)	4061(1)	7575(2)	3525(2)	53(1)
C(40)	4029(1)	6711(2)	3671(2)	63(1)
C(41)	3558(1)	6357(2)	3813(2)	60(1)
C(42)	2613(1)	6505(2)	4044(2)	60(1)
C(43)	2184(1)	6995(3)	4157(2)	66(1)
C(44)	2232(1)	7862(3)	4103(2)	65(1)
C(45)	2678(1)	8270(2)	3902(2)	51(1)
C(46)	3140(1)	7773(2)	3745(2)	44(1)
C(47)	3104(1)	6881(2)	3862(2)	52(1)
C(48)	2653(1)	9169(2)	3893(2)	52(1)
C(49)	3247(1)	10984(2)	3405(2)	48(1)
C(50)	3148(1)	11904(2)	3338(2)	49(1)
C(51)	3562(1)	12452(2)	3195(2)	64(1)
C(52)	3482(2)	13314(3)	3146(3)	78(1)
C(53)	2984(2)	13648(3)	3216(3)	78(1)
C(54)	2572(2)	13118(3)	3328(3)	82(1)
C(55)	2644(1)	12255(2)	3390(2)	66(1)
C(56)	2121(2)	5236(2)	4168(3)	80(1)
C(57)	5062(1)	9388(2)	3144(2)	47(1)
C(58)	5141(1)	9203(2)	4031(2)	59(1)
C(59)	5654(2)	9319(2)	4567(2)	70(1)
C(60)	6076(1)	9632(3)	4232(3)	70(1)
C(61)	6004(1)	9838(3)	3355(3)	70(1)
C(62)	5496(1)	9711(2)	2811(2)	58(1)
C(63)	4387(1)	8308(2)	1806(2)	48(1)
C(64)	3888(1)	7920(2)	1461(2)	56(1)
C(65)	3867(2)	7214(2)	938(2)	65(1)
C(66)	4342(2)	6874(2)	763(2)	69(1)
C(67)	4837(2)	7243(2)	1100(2)	68(1)

Table A.8. Continued…

Atom	x	y	z	U(eq)
C(68)	4862(1)	7964(2)	1615(2)	58(1)
C(69)	4359(1)	10108(2)	1660(2)	48(1)
C(70)	4255(2)	9955(3)	764(2)	73(1)
C(71)	4241(2)	10613(3)	191(3)	103(2)
C(72)	4329(2)	11430(3)	466(3)	90(1)
C(73)	4434(2)	11596(3)	1350(3)	73(1)
C(74)	4450(1)	10937(2)	1944(3)	60(1)

Table A.9. For ***trans*-[Rh(L^{1})(PPh$_3$)$_2$H] (1) (*Chapter 5*)**

Atom	x	y	z	U(eq)
Rh(1)	8056(1)	6682(1)	7681(1)	37(1)
P(1)	7334(1)	7316(1)	7546(1)	41(1)
P(2)	8689(1)	5954(1)	7595(1)	40(1)
O(1)	8691(1)	7297(1)	7672(3)	49(1)
N(1)	8202(2)	6814(2)	8910(2)	42(1)
N(2)	8622(2)	7196(2)	9098(3)	50(1)
C(1)	7439(2)	6130(2)	7889(3)	38(1)
C(2)	7146(2)	5913(2)	7256(4)	45(1)
C(3)	6664(2)	5570(2)	7335(4)	55(1)
C(4)	6369(3)	5376(3)	6650(4)	70(2)
C(5)	5915(3)	5028(3)	6752(6)	93(2)
C(6)	5744(3)	4878(3)	7525(6)	92(3)
C(7)	6017(3)	5064(3)	8224(5)	69(2)
C(8)	5858(3)	4907(3)	9033(6)	85(2)
C(9)	6136(3)	5079(2)	9684(5)	78(2)
C(10)	6614(2)	5441(2)	9633(4)	61(2)
C(11)	6891(3)	5630(3)	10307(4)	72(2)
C(12)	7336(3)	5986(2)	10234(4)	65(2)
C(13)	7526(2)	6168(2)	9468(3)	50(1)

Table A.9. Continued…

Atom	x	y	z	U(eq)
C(14)	7266(2)	5979(2)	8736(3)	47(1)
C(15)	6794(2)	5612(2)	8837(3)	51(1)
C(16)	6493(2)	5422(2)	8138(4)	56(2)
C(17)	7975(2)	6568(2)	9523(3)	50(1)
C(18)	8832(2)	7413(2)	8428(3)	45(1)
C(19)	9286(2)	7837(2)	8524(4)	55(1)
C(20)	9463(3)	8013(3)	9289(4)	83(2)
C(21)	9883(3)	8399(4)	9359(5)	126(3)
C(22)	10128(3)	8605(3)	8668(6)	100(3)
C(23)	9955(3)	8449(3)	7920(5)	82(2)
C(24)	9536(2)	8060(3)	7846(4)	73(2)
C(25)	6829(2)	7250(2)	8379(3)	44(1)
C(26)	6330(2)	6968(2)	8291(3)	55(1)
C(27)	5987(2)	6895(3)	8962(4)	75(2)
C(28)	6123(3)	7091(3)	9715(4)	76(2)
C(29)	6620(3)	7369(2)	9814(4)	65(2)
C(30)	6970(2)	7439(2)	9157(3)	52(1)
C(31)	7531(2)	8051(2)	7563(3)	45(1)
C(32)	7246(3)	8457(2)	8000(3)	62(2)
C(33)	7416(3)	9006(2)	7965(4)	75(2)
C(34)	7862(3)	9146(3)	7485(5)	87(2)
C(35)	8138(3)	8756(3)	7030(4)	80(2)
C(36)	7977(2)	8209(2)	7081(3)	63(2)
C(37)	6900(2)	7302(2)	6604(3)	47(1)
C(38)	6421(3)	7612(3)	6583(4)	85(2)
C(39)	6083(3)	7618(3)	5897(5)	101(3)
C(40)	6223(3)	7310(3)	5232(4)	83(2)
C(41)	6705(3)	7017(3)	5226(3)	66(2)
C(42)	7040(2)	7008(2)	5908(3)	47(1)

Table A.9. Continued…

Atom	x	y	z	U(eq)
C(43)	8616(2)	5459(2)	8443(3)	46(1)
C(44)	8314(2)	4977(2)	8340(3)	58(1)
C(45)	8227(3)	4624(3)	8985(4)	80(2)
C(46)	8448(3)	4737(3)	9746(4)	85(2)
C(47)	8737(3)	5218(3)	9873(4)	79(2)
C(48)	8823(2)	5584(2)	9219(3)	62(2)
C(49)	9427(2)	6145(2)	7604(4)	57(1)
C(50)	9836(2)	5859(3)	8042(4)	86(2)
C(51)	10387(3)	6000(5)	7941(6)	139(5)
C(52)	10539(4)	6407(5)	7419(9)	164(7)
C(53)	10149(4)	6707(4)	7012(6)	130(4)
C(54)	9585(3)	6578(3)	7086(4)	84(2)
C(55)	8690(2)	5503(2)	6676(3)	43(1)
C(56)	8363(2)	5592(2)	6005(3)	53(1)
C(57)	8394(3)	5245(3)	5314(3)	72(2)
C(58)	8756(3)	4816(3)	5313(4)	71(2)
C(59)	9091(3)	4725(3)	5962(4)	83(2)
C(60)	9060(3)	5069(2)	6650(4)	69(2)

Table A.10. For ***trans*-[Rh(L^2)(PPh$_3$)$_2$H] (2) (*Chapter 5*)**

Atom	x	y	z	U(eq)
Rh(1)	2072(1)	9481(1)	7615(1)	13(1)
Cl(1)	7055(1)	8526(1)	5455(1)	40(1)
P(1)	3509(1)	9654(1)	8377(1)	14(1)
P(2)	533(1)	9559(1)	6899(1)	14(1)
O(1)	3217(2)	9490(1)	7033(1)	16(1)
N(1)	2402(2)	8254(2)	7515(1)	14(1)
N(2)	3173(2)	8072(2)	7153(1)	16(1)
C(1)	1029(3)	9267(2)	8185(1)	15(1)

Table A.10. Continued…

Atom	x	y	z	U(eq)
C(2)	536(3)	9904(2)	8421(2)	20(1)
C(3)	-149(3)	9819(2)	8850(2)	24(1)
C(4)	-635(3)	10498(2)	9076(2)	41(1)
C(5)	-1283(4)	10403(2)	9496(2)	49(1)
C(6)	-1458(4)	9629(2)	9706(2)	45(1)
C(7)	-994(3)	8927(2)	9495(2)	30(1)
C(8)	-1135(3)	8128(2)	9713(2)	32(1)
C(9)	-684(3)	7470(2)	9500(2)	26(1)
C(10)	-47(3)	7544(2)	9047(2)	20(1)
C(11)	403(3)	6847(2)	8823(2)	19(1)
C(12)	1040(3)	6931(2)	8405(2)	18(1)
C(13)	1274(3)	7693(2)	8178(1)	15(1)
C(14)	823(2)	8429(2)	8379(1)	14(1)
C(15)	148(3)	8328(2)	8818(2)	16(1)
C(16)	-332(3)	9023(2)	9056(2)	22(1)
C(17)	2019(3)	7641(2)	7761(1)	18(1)
C(18)	3520(3)	8751(2)	6938(1)	16(1)
C(19)	4378(3)	8667(2)	6557(1)	16(1)
C(20)	4798(3)	9377(2)	6345(2)	22(1)
C(21)	5612(3)	9339(2)	6003(2)	27(1)
C(22)	6001(3)	8582(2)	5868(2)	25(1)
C(23)	5572(3)	7868(2)	6060(2)	26(1)
C(24)	4776(3)	7915(2)	6404(2)	22(1)
C(25)	-393(3)	10464(2)	6863(1)	16(1)
C(26)	-119(3)	11166(2)	7191(2)	21(1)
C(27)	-813(3)	11853(2)	7128(2)	22(1)
C(28)	-1796(3)	11844(2)	6743(2)	28(1)
C(29)	-2077(3)	11148(2)	6407(2)	27(1)
C(30)	-1383(3)	10469(2)	6467(2)	21(1)

Table A.10. Continued…

Atom	x	y	z	U(eq)
C(31)	924(3)	9601(2)	6190(1)	14(1)
C(32)	1743(3)	10174(2)	6120(2)	19(1)
C(33)	2147(3)	10240(2)	5616(2)	24(1)
C(34)	1730(3)	9728(2)	5162(2)	22(1)
C(35)	888(3)	9180(2)	5219(2)	21(1)
C(36)	487(3)	9111(2)	5727(1)	18(1)
C(37)	-424(3)	8695(2)	6887(1)	15(1)
C(38)	-139(3)	7929(2)	6688(2)	20(1)
C(39)	-856(3)	7268(2)	6684(2)	31(1)
C(40)	-1841(3)	7353(2)	6898(2)	39(1)
C(41)	-1408(3)	8759(2)	7113(2)	24(1)
C(42)	4894(3)	9794(2)	8177(2)	18(1)
C(43)	4957(3)	10347(2)	7741(2)	23(1)
C(44)	5967(3)	10527(2)	7571(2)	30(1)
C(45)	6926(3)	10162(2)	7839(2)	37(1)
C(46)	6889(3)	9616(2)	8271(2)	42(1)
C(47)	5879(3)	9433(2)	8450(2)	32(1)
C(48)	3486(2)	10547(2)	8849(1)	14(1)
C(49)	2881(3)	11249(2)	8678(2)	17(1)
C(50)	2963(3)	11939(2)	9024(2)	20(1)
C(51)	3641(3)	11932(2)	9546(2)	20(1)
C(52)	4246(3)	11234(2)	9723(2)	24(1)
C(53)	4179(3)	10548(2)	9375(1)	21(1)
C(54)	3624(3)	8770(2)	8850(1)	13(1)
C(55)	4158(3)	8057(2)	8712(2)	17(1)
C(56)	4169(3)	7357(2)	9039(2)	19(1)
C(57)	3623(3)	7352(2)	9503(2)	20(1)
C(58)	3058(3)	8046(2)	9639(2)	21(1)
C(59)	3047(3)	8750(2)	9309(1)	16(1)
C(60)	-2111(3)	8093(2)	7117(2)	34(1)

Table A.11. For ***trans*-[Ir(L^3)(PPh$_3$)$_2$H] (4) (*Chapter 5*)**

Atom	x	y	z	U(eq)
Ir(1)	5817(1)	1592(1)	7378(1)	38(1)
P(1)	3701(1)	906(1)	6861(1)	41(1)
P(2)	7993(1)	2138(1)	7567(1)	39(1)
O(1)	6297(2)	3665(2)	7722(1)	46(1)
N(1)	5476(2)	1804(2)	8429(1)	39(1)
N(2)	5734(2)	3034(2)	8824(1)	46(1)
C(1)	5198(2)	-285(2)	7516(1)	41(1)
C(2)	5135(3)	-1398(3)	7053(2)	52(1)
C(3)	4733(3)	-2571(3)	7268(2)	58(1)
C(4)	4324(3)	-2737(3)	7950(2)	53(1)
C(5)	3899(3)	-3952(3)	8168(2)	68(1)
C(6)	3478(3)	-4098(3)	8830(2)	76(1)
C(7)	3483(4)	-3049(3)	9303(2)	75(1)
C(8)	3902(3)	-1856(3)	9114(2)	62(1)
C(9)	4341(2)	-1663(3)	8433(2)	48(1)
C(10)	4813(2)	-427(2)	8216(1)	43(1)
C(11)	4973(2)	755(2)	8697(1)	44(1)
C(12)	6159(2)	3902(2)	8404(1)	43(1)
C(13)	6512(3)	5291(3)	8752(2)	47(1)
C(14)	6290(3)	5619(3)	9460(2)	57(1)
C(15)	6572(4)	6893(3)	9766(2)	73(1)
C(16)	7111(4)	7859(3)	9379(2)	84(1)
C(17)	7356(4)	7566(3)	8688(2)	84(1)
C(18)	7045(3)	6274(3)	8362(2)	65(1)
C(19)	2577(2)	599(3)	7527(1)	48(1)
C(20)	2025(3)	-604(4)	7748(2)	62(1)
C(21)	1299(3)	-788(5)	8314(2)	83(1)
C(22)	1121(4)	212(6)	8670(2)	93(1)
C(23)	1670(4)	1399(5)	8472(2)	84(1)

Table A.11. Continued…

Atom	x	y	z	U(eq)
C(24)	2405(3)	1607(4)	7904(2)	63(1)
C(25)	2864(3)	-625(3)	6116(1)	49(1)
C(26)	3604(4)	-963(3)	5674(2)	65(1)
C(27)	2983(5)	-2083(4)	5090(2)	83(1)
C(28)	1638(5)	-2865(4)	4946(2)	84(1)
C(29)	891(4)	-2542(3)	5368(2)	76(1)
C(30)	1496(3)	-1423(3)	5953(2)	62(1)
C(31)	3528(3)	2076(3)	6413(2)	51(1)
C(32)	4627(4)	3114(3)	6245(2)	69(1)
C(33)	4483(5)	3972(4)	5872(2)	91(1)
C(34)	3249(5)	3765(5)	5670(2)	92(1)
C(35)	2150(5)	2729(4)	5833(2)	80(1)
C(36)	2281(3)	1889(3)	6205(2)	62(1)
C(37)	8212(2)	819(3)	7041(1)	43(1)
C(38)	8629(3)	95(3)	7361(2)	54(1)
C(39)	8702(4)	-937(4)	6924(2)	72(1)
C(40)	8377(4)	-1242(4)	6178(2)	75(1)
C(41)	7976(4)	-515(4)	5850(2)	72(1)
C(42)	7894(3)	505(3)	6279(2)	59(1)
C(43)	9169(2)	3590(3)	7240(1)	44(1)
C(44)	10341(3)	3714(3)	7068(2)	55(1)
C(45)	11236(3)	4824(3)	6836(2)	59(1)
C(46)	10981(3)	5791(3)	6769(2)	66(1)
C(47)	9817(4)	5674(3)	6924(2)	79(1)
C(48)	8904(3)	4572(3)	7160(2)	65(1)
C(49)	8772(2)	2476(3)	8517(1)	43(1)
C(50)	8163(3)	1523(3)	8923(2)	52(1)
C(51)	8707(3)	1751(3)	9642(2)	63(1)
C(52)	9862(4)	2920(3)	9968(2)	70(1)

Table A.11. Continued…

Atom	x	y	z	U(eq)
C(53)	10458(3)	3876(3)	9583(2)	71(1)
C(54)	9920(3)	3662(3)	8857(2)	57(1)

Table A.12. For **[Pd(HL^1)Cl] (5**·Me_2NCHO**) (*Chapter 5*)**

Atom	x	y	z	U(eq)
Pd(1)	8659(1)	3604(1)	846(1)	40(1)
Cl(1)	6985(1)	4292(2)	1383(1)	73(1)
O(1)	7500(3)	1962(3)	438(1)	49(1)
N(1)	9792(3)	2892(3)	274(1)	38(1)
N(2)	9217(4)	1835(4)	-79(2)	42(1)
C(1)	9970(4)	4954(4)	1187(2)	37(1)
C(2)	9679(4)	5773(4)	1644(2)	44(1)
C(3)	10556(4)	6732(4)	1939(2)	44(1)
C(4)	10218(5)	7573(4)	2405(2)	55(1)
C(5)	11088(6)	8488(5)	2676(2)	63(1)
C(6)	12304(5)	8551(4)	2509(2)	61(1)
C(7)	12699(5)	7738(4)	2052(2)	52(1)
C(8)	13941(5)	7795(5)	1862(2)	66(1)
C(9)	14259(5)	7071(5)	1403(2)	60(1)
C(10)	13367(4)	6188(4)	1076(2)	47(1)
C(11)	13689(4)	5493(5)	581(2)	55(1)
C(12)	12828(4)	4631(4)	283(2)	47(1)
C(13)	11624(4)	4373(4)	477(2)	37(1)
C(14)	11216(4)	5095(4)	970(2)	34(1)
C(15)	12120(4)	6031(4)	1266(2)	40(1)
C(16)	11787(4)	6834(4)	1755(2)	41(1)
C(17)	10891(4)	3329(4)	148(2)	39(1)
C(18)	8055(4)	1410(4)	36(2)	42(1)
C(19)	7436(4)	278(4)	-324(2)	44(1)

Table A.12. Continued…

Atom	x	y	z	U(eq)
C(20)	7705(5)	43(4)	-884(2)	57(1)
C(21)	7031(5)	-965(5)	-1217(2)	66(1)
C(22)	6073(5)	-1720(5)	-989(2)	63(1)
C(23)	5803(5)	-1503(5)	-429(3)	64(1)
C(24)	6473(4)	-518(4)	-96(2)	53(1)
O(2)	10831(3)	881(4)	-891(1)	63(1)
N(3)	11641(4)	-109(5)	-1680(2)	69(1)
C(25)	10781(5)	57(6)	-1302(2)	73(2)
C(26)	11441(7)	-1146(6)	-2143(3)	110(2)
C(27)	12783(6)	649(9)	-1639(3)	139(3)

List of Publications

1. Cyclopalladated complexes with 9-anthraldehyde aroylhydrazones: Synthesis, properties and structures.

   A.R. Balavardhana Rao, Samudranil Pal.

   J. Organomet. Chem. 701 (2012) 62–67.

2. Cyclopalladation of indole-3-carboxaldehyde aroylhydrazones**.**

   A.R. Balavardhana Rao, Samudranil Pal.

   J. Organomet. Chem. 696 (2011) 2660–2664.

3. Regioselective cyclometallation of 4-R-1-naphthaldehyde benzoylhydrazones: Palladium(II) complexes with CNO pincer like ligands.

   A.R. Balavardhana Rao, Samudranil Pal.

   J. Organomet. Chem. 696 (2013) 67–72.

4. Regioselective Cyclometallation with Some Platinum group Metals ions.

   A.R. Balavardhana Rao, Samudranil Pal.

   J. Organomet. Chem. 762 (2014) 58–66.

Posters and Presentations

1. Cyclopalladated complexes with aroylhydrazones of polycyclic aromatic aldehydes.
   Poster Presentation

   Modern Trends in Inorganic Chemistry, MTIC- XIV, 2011,
   University of Hyderabad, India.

2. Regioselective cyclometallation of aroylhydrazones of polycyclic aromatic aldehydes.
   Poster Presentation
   CHEMFEST-2013, University of Hyderabad, Hederabad.

3. Cyclometallates of aroylhydrazones of polycyclic aromatic aldehydes: regioselective metallation of the aryl.
   Poster Presentation
   Modern Trends in Inorganic Chemistry, MTIC- XV, 2013, IIT Roorkee, India.

4. Cyclometallates of aroylhydrazones of polycyclic aromatic aldehydes: regioselective metallation of the aryl.
   Oral Presentation
   CHEMFEST-2014, University of Hyderabad, Hederabad.